Eirik Glimsdal

Spectroscopic characterization of some platinum acetylide molecules for optical power limiting applications

Thesis for the degree of Philosophiae Doctor

Trondheim, August 2009

Norwegian University of Science and Technology
Faculty of Natural Sciences and Technology
Department of Physics

NTNU
Norwegian University of
Science and Technology

NTNU

Norwegian University of Science and Technology

Doctoral thesis
for the degree of philosophiae doctor

Faculty of Natural Sciences and Technology
Department of Physics

© 2009 Eirik Glimsdal.

ISBN 978-82-471-1723-1 (printed version)
ISBN 978-82-471-1725-5 (electronic version)
ISSN 1503-8181

Doctoral theses at NTNU, 2009:165

Printed by NTNU-trykk

To my family,

and in the memory of my father

Where then does wisdom come from?
And where is the place of understanding?
Thus it is hidden from the eyes of all living
and concealed from the birds of the sky. [...]
God understands its way, and He knows its place.
For He looks to the ends of the earth
and sees everything under the heaven.

Book of Job 28; 20-24.

Abstract

The rapid development of laser technology results in new and powerful lasers operating at a variety of wavelengths. At the same time lasers have found its use in many electronic devices and instruments used in both civilian and military applications. However, lasers are also found to be an effective threat for blinding and destroying optical sensors. Therefore, the need for useful protection devices has increased. A protective device, constructed from nonlinear absorbing materials, can absorb the high intensity light, while at the same time keeping the device transparent for normal operation of the sensor. In this thesis, a series of square planar *trans*-diarylalkynyl-bis(tributyl-phosphine) platinum(II) complexes have been investigated for their photo-physical properties and optical power limiting (OPL) capabilities. The main objectives have been to establish methodologies for characterization of quantum efficiency, two-photon absorption cross section and excited state absorption of triplet states. These methods were applied along with absorption and time-resolved luminescence spectroscopy and OPL to characterize new materials. Also, the photo-physical characterization of a series of three Coumarin molecules suitable for reference purposes in the determination of quantum efficiencies and two-photon absorption cross sections of new samples are presented (Paper VI).

For the compounds investigated in Paper I and II, thiophene groups and methoxy substituents were inserted into the structure in an attempt to increase the nonlinear properties and OPL capabilities compared to a pure phenyl-containing analogue. In Paper III, a new synthetic route was developed for the compounds utilizing the click chemistry method through triazole formation. The introduced thiophene and triazole units were placed at different positions in the structure to investigate its effect on the photo-physical properties. Placed at different positions in the structure, the new rings were found to affect the conjugation of the ligands. Spectral shifts and shorter phosphorescence lifetimes were observed as the rings were placed closer to the Pt-atom.

In Paper IV the important triplet state absorption and relaxation processes were investigated for all compounds in Paper I − III, together with four new molecules. Methyl substituents were inserted as a means to control the ligand rotation, and a molecule with two different ligands were prepared to investigate the effect on the optical properties from a non-symmetric compound. Excited state absorption from the triplet state was found to be strong for all molecules, with extinction coefficients in the range $1 - 10 \cdot 10^4$ $M^{-1}cm^{-1}$. In Paper V, some of the molecules were incorporated into solid PMMA glasses. The photo-physical properties of the compounds in both low and high concentrated PMMA glasses were investigated and compared to similar samples prepared in solution. New excitation bands were observed at high concentrations both in liquid and solid state. Finally, using a pulse-propagation simulation method, the OPL performance of materials with photo-physical parameters typical for the investigated molecules, were examined. It was found that the triplet excited state absorption is the dominating process in operation around 532 nm for 5 ns pulses.

Populærvitenskapelig sammendrag på norsk

Forskning på laserteknologi har de siste tiårene resultert i en utvikling av mange ulike lasere til ulike formål. Lasere har et stort anvendelsesområde i mange typer instrumenter og på mange områder, både sivilt og i det militære. Samtidig som lasere med høy effekt har blitt utviklet er det blitt åpenbart at disse effektivt kan ødelegge optiske måleinstrumenter, deriblant også vårt eget øye. Det har derfor utviklet seg et behov for å kunne beskytte disse måleinstrumentene mot skadelige laserstråler med høy intensitet. En beskyttende innretning må kunne absorbere eller reflektere den skadelige strålingen samtidig som den slipper gjennom det vanlige lyset sensoren er ment å skulle oppdage. En slik innretning kan konstrueres fra såkalte ikke-lineære absorberende molekyler, som på grunn av sine egenskaper vil slippe gjennom lys med lav intensitet, men absorbere det meste av en laserpuls med høy intensitet, slik at det laserlyset som slipper igjennom ikke kan skade sensoren. En type molekyler som har disse spesielle absorberende egenskapene kalles platina(II)-acetylider, og består av et tungt platina-atom bundet til to hydrokarbonkjeder med spesiell elektronstruktur. I denne avhandligen har vi studert de foto-fysiske egenskapene til disse molekylene, for å bedre forstå de prosessene som gir opphav til den spesielle absorberende effekten og for å finne nye modifiseringer av dette molekylet som kan gi bedre absorpsjon av den skadelige laserpulsen.

Preface

This thesis is published as a partial fulfillment of the requirements for the degree of philosophiae doctor (PhD) at the Norwegian University of Science and Technology (NTNU). The presented work has been carried out during a four year period from August 2005 to September 2009 at the Department of Physics, under the supervision of Professor Mikael Lindgren. The employment as a PhD-student at the department was financed by the Faculty of Natural Sciences and Technology.

The PhD-education programme has a standard duration of three years full time study (180 credits).[†] One of the four years of employment was devoted to additional teaching duties at the department, teaching lab-courses in Mechanical Physics and Optics on the Bachelor and Master level. The teaching duties were spread out as a 25% teaching load over all four years. The fulfillment of the PhD-educational programme also requires an amount of approved organized academic training. The training covered a total of 30 credits, equivalent to six months of full time study. The academic training covered the subjects of spectroscopy, computational chemistry, optical waveguides and quantum optics.

The Swedish Defence Research Agency (FOI) has provided additional funding for scientific equipment and for travelling, within the working project – Swedish Nanohybrid Optical Protection Initiative (SNOPI). The project is a part of the Swedish Defense Nano Technology Programme, managed by the Swedish Defense Research Agency (FOI) and the Defense Material Administration (FMV).

This thesis consists of two parts; an introduction to the subject and a collection of the six published papers and manuscripts. The introductory part is divided

[†]According to the 'Regulations concerning the philosophiae doctor degree (PhD) at the Norwegian University of Science and Technology (NTNU)'.

into six chapters. After a short general introduction in Chapter 1, the basic photo-physical properties of molecules are introduced in Chapter 2. In Chapter 3, the subject of nonlinear absorption in organometallic molecules are treated, with an introduction to the studied chromophores in this thesis. In Chapter 4, all the methods of spectroscopic characterization are introduced and explained in some detail, with some examples of results. A summary and discussion on some of the results are given in Chapter 5, together with results on numerical simulations of OPL properties. Conclusions and further perspectives are discussed in Chapter 6.

Acknowledgements

Four years as a doctoral student have passed by. A lot has been said − much have been planned − and some have also been done. I thank those who gave me the opportunity to work as a PhD student; the faculty, the department and the research group, and for setting the environment around it.

Although, working with a PhD-thesis sometimes seems quite lonely, none of this would have been possible if it were not for a large number of people. They all deserve a large gratitude.

First of all, my supervisor, Professor Mikael Lindgren, is greatly acknowledged for the invaluable amount of involvement, time and guidance, the countless discussions, and the great support during the entire work. You always had new ideas and solutions when I was stuck with some problems. Working with you have been a great pleasure for me, and I have learned a lot from you. Importantly, you also never forget the most important; "First of all, we are supposed to have fun." And it certainly has been. Thank you very much!

Thanks to everyone in the SNOPI project, especially Dr. Cesar Lopes and Dr. Anders Eriksson at the Swedish Defence Research Agency (FOI) in Linköping, for discussions, help with OPL measurements and two nice visits in Linköping. The FOI is also thanked for providing funding for laboratory equipment and travelling.

Professor Bertil Eliasson, Dr. Marcus Carlsson and doctoral student Tomas Kindahl at Department of Chemistry, Umeå University, and Dr. Robert Westlund at the Royal Institute of Technology (KTH) in Stockholm, are thanked for many discussions and for synthesizing the materials. Bertil Eliasson, Robert Westlund and Dr. Patrick Norman, Linköping University, are also thanked for co-writing some of the manuscripts, and Robert also for preparing the solid PMMA glass materials. Bertil Eliasson, Patrick Norman and Professor Boris Minaev (KTH) are thanked for the theoretical and computational work on the

compounds, and for many discussions regarding that.

Professor Thor Bernt Melø at the Department of Physics, NTNU, is thanked for many helpful discussions and guidance with some of the experiments. Thanks for letting me use your sample preparation and photo-physics lab, and for your interest in my work.

All co-authors and contributors to the papers and related publications, are greatly acknowledged for their contributions and for many helpful discussions throughout the entire work. Everyone that spent the time proofreading and reviewing the English language in this thesis are also greatly acknowledged.

Everyone in the theoretical and experimental optics groups at the department; Professor Irina Sorokina, Professor Ingve Simonsen, Associate Professor Morten Kildemo, my fellow PhD-students Dr. Lars O. Løseth, Dr. Frantz Stabo-Eeg, Ingar Stian Nerbø, Paul Anton Letnes and Tor Nordam are all thanked for making the group a nice place to work. Special thanks to Frantz for co-working with me with some of the experiments in the early stages, and for help and discussions with instrumentation, LaTeX, Matlab and LabView programming.

Also, thanks to my mathematics, natural science and physics teachers on the junior high-school and high-school levels for teaching mathematics and physics in an interesting way. This became the basis for my general interest in these subjects.

Thanks to all my good friends from TKS (Laget) and Con Anima for a good fellowship. You have made my life richer.

Thanks to my mom and dad for who you are and for all great support, my brother for always being a good friend, and Jørgen for all good times and talks. Thanks to my grandparents for who you are and for all great care. Thanks also to my parents-in-law and sister-in-law, for taking me into your hearts. It is good to know that you all are always there for me.

At last, and most, thanks to my lovely wife, Elin, for all the numerous visits at the office, all wonderful words, all support and help with everything, all great smiles and kisses, and for dragging me out of the office once in a while. You are the best. I love you!

Trondheim, June 2009

Eirik Glimsdal

Papers included in thesis

Paper I:

Excited states and two-photon absorption of some novel thiophenyl Pt(II)-ethynyl derivatives.

Eirik Glimsdal, Marcus Carlsson, Bertil Eliasson, Boris Minaev and Mikael Lindgren.
Journal of Physical Chemistry A 111, p. 244-250, 2007.

Paper II:

Luminescence, singlet oxygen production and optical power limiting of some novel diacetylide platinum(II) diphosphine complexes.

Eirik Glimsdal, Marcus Carlsson, Tomas Kindahl, Mikael Lindgren, Cesar Lopes and Bertil Eliasson.
Manuscript.
Submitted for publication in *Physical Chemistry Chemical Physics*, June 2009.

Paper III:

Click chemistry for photonic applications: triazole-functionalized platinum(II) acetylides for optical power limiting.

Robert Westlund, **Eirik Glimsdal**, Mikael Lindgren, Robert Vestberg, Craig Hawker, Cesar Lopes and Eva Malmström.
Journal of Materials Chemistry 18, p. 166-175, 2008.

Paper IV:

Triplet excited states of some thiophene and triazole substituted Platinum(II) acetylide chromophores.

Eirik Glimsdal, Ingunn Dragland, Marcus Carlsson, Bertil Eliasson, Thor Bernt Melø and Mikael Lindgren.
Journal of Physical Chemistry A 113, p. 3311-3320, 2009.

Paper V:

Excitation and emission properties of platinum(II) acetylides at high and low concentrations.

Eirik Glimsdal, Patrick Norman and Mikael Lindgren.
Manuscript.
Submitted for publication in *Journal of Physical Chemistry A*, June 2009.

Paper VI:

Two-photon absorption cross-section and quantum efficiency of molecular fluorophores for spectroscopic reference purposes.

Eirik Glimsdal and Mikael Lindgren.
Manuscript.
Submitted for publication in *Journal of the Optical Society of America B*, August 2009.

Contents

Background and motivation

The task of an optical sensor is to collect and detect some sort of light or other electromagnetic energy, and convert that into a meaningful signal for the observer. In our modern society we use optical sensors in a wide range of utilities to collect some sort of optical signal or image. However, the most important and most used optical sensor is still the human eye (which you are using right now to read this text). Optical sensors, including the eye, are often made to be sensitive to low intensity light, and can easily be damaged if too much power is directed onto the detector elements. Historically, and in our everyday life, all light, except from the direct radiation of the sun, is considered to be of low intensity. With the introduction of the laser in 1960 (See Chapter 1) a new source of optical and electromagnetic radiation was discovered. This new radiation source could emit light with new kinds of properties and much higher concentrated intensity than previously known. The laser radiation can have different properties with respect to wavelength and bandwidth, being continuous or pulsed, and have different pulse lengths and pulse energies. [1]

The concept of laser safety, and the need for laser protection, became an important issue when it was observed how the laser radiation could damage optical sensors and the eye. [2] (Figure 1.) The damage caused by the laser is dependent on the energy delivered by the laser and the sensors ability to resist damage. It's important to note that even relatively low output power commercially available laser pointers may blind or dazzle a persons eyes,* and can cause severe damage if the beam is intentionally or unintentionally directed into the eye. [4]

Harmful laser radiation could be directed onto a sensor head due to careless use and accidental direction of the beam, or from a source intentionally directed

*There are several reported incidents in the media, from the USA, Europe, Australia and Norway, were airplane pilots have been dazzled by a strong laser pointer directed towards the plane from the ground. [3]

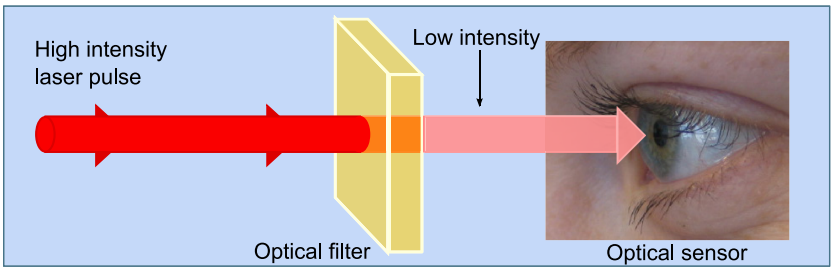

Figure 1: To prevent high laser intensities from reaching the optical sensor, a protective device, reducing the transmission of harmful radiation, is placed in front of the sensor. The optical filter must still be transparent for regular vision with low intensity light.

and made with the purpose to damage the sensor. This is especially relevant in defense and military use, due to the increasingly wide use of lasers and optical sensors in military equipment and operations. For example in range finding, missile guidance, remote sensing and laser radar systems.[5,6] Such long range applications need high power in a limited time and wavelength range, and therefore can cause severe damage to the eye and optical sensors. With the introduction of the laser in military use, came also the use of anti-sensor-lasers, that are designed to damage sensors and interrupt the collection of optical information, which could knock out strategic weapons or optical information systems.[7] It's clear that such laser 'weapons' also could be used by terrorists. Therefore, the need for laser protection has become an increasingly important issue in todays modern military equipment.

The purpose of this study has been to develop new optical protecting filter devices, based on some optical nonlinear absorbing molecules, known as platinum(II) acetylides. New molecules have been investigated and characterized for their photo-physical properties and optical power limiting abilities, both in liquid solution and incorporated into solid state glass materials. An effort has been made to explain the optical limiting performance based on the characterization of the intrinsic photo-physical properties.

Characterization of new nonlinear optical molecules could also be of general importance, and the molecules may later be found to have properties suitable for other applications. The kind of photo-active complexes studied here could for example be re-designed and developed for applications in photo-dynamic therapy, optical data-storage, light emitting diodes and solar cells.[8,9]

Chapter 1

Introduction

1.1 The laser

The word *laser* is an acronym for Light Amplification by Stimulated Emission of Radiation. The light emitted from a laser has several special properties not found for other light sources. These properties can be summarized as: highly coherent, monochromatic, low divergence and high intensity.[10] This means that all light waves are in phase (coherent), that the light has one single color or a very narrow interval of wavelength (monochromatic), that it propagates in a defined direction without spreading (low divergence) and that it has high power over a relatively small beam cross section (high intensity). These properties also allow the beam to be focused to a small spot of even higher intensities.[11]

The laser consists of three main components, as shown in Figure 1.1. First, a cavity made out of two mirrors facing each other. One highly reflecting mirror and one partially transparent (called the output coupler). Secondly, a suitable gain medium placed between the two mirrors, and finally an energy source or pumping device.[12] The gain medium is a fluorescent material emitting light after being raised to a higher energy level by the pumping device. Some of the emitted light is trapped between the two mirrors and could pass several times between the two mirrors before exiting through the output coupler. This trapped light is then capable of stimulating the gain medium to emit more light exactly equal to the stimulating light, before it is transmitted.[13] In this way, more and more light is trapped between the mirrors creating the high intensity beam.

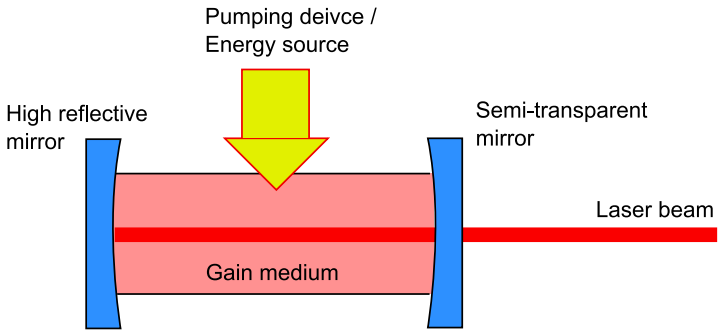

Figure 1.1: The principle components of a laser. High reflective and semi-transparent mirror, gain medium and energy/excitation source.

The laser device has become one of the most popular inventions in our modern society today. It has found a wide use of applications and has revolutionized fields such as information transmission (optical fibers), medicine (surgery), industrial materials processing (cutting, welding), data storage (CD/DVD), printing, research and defense.[11] After the theoretical development of the concept of stimulated emission and the invention of the *maser* (the microwave analogue of the laser) in the first half of the 20th century,[14,15] the first laser was demonstrated in 1960 by Theodore Maiman[16] after the proposal of Schawlow and Townes[17] of tuning the maser-wavelengths into the optical region.[18] The first laser, based on the ruby-crystal, emitted radiation at 694.3 nm.[14,16] Short after, Javan et al.[19] showed laser operation in a He-Ne gas, first in the infrared region at 1.15 μm and later in the visible region at 632.8 nm.[11] The HeNe-laser became very popular and is still one of the most widely used lasers today.[1]

1.2 Lasers and eye safety

In the 1960s the research laboratories which developed the laser was closely attached to the military research facilities,[18] and therefore the military quickly responded to this new invention, and became the first and principle market for the laser.[20] It was even expressed as early as in 1962 that "the laser may be the biggest breakthrough in the weapons area since the atomic bomb".[20] The laser was a coherent, highly directed, concentrated beam of light, and was quickly thought to have the potential use as a weapon. The military therefore became interested in laser-research for developing stronger and new types of lasers, in

addition to finding new applications for it, such as in laser ranging, missile guidance, communication and detection.[20] The idea of the laser being used as a weapon, was also soon adopted in science fiction, were laser weapons are widely used.†

The human eye is vulnerable for laser radiation for several reasons.[21] Firstly, it is the only organ that allows optical radiation to penetrate deep within it. Secondly, the cornea and lens increases the irradiance (energy per unit area) by 10,000–100,000 times, by focusing the light onto the retina.[4] Finally, the eye is often directed towards the light in a reflex action, focusing the laser onto the most sensitive part of the eye, the fovea. The laser pulse can then cause blindness, or great loss of vision, within less than 10^{-9} seconds.[21] The eye-safe energy limits for a laser pulse with picosecond to millisecond duration are usually given to be 0.2 μJ per pulse.[4,6]. However, a realistic goal for protection is more like towards $5 - 10$ times this value.[6]

Lasers pose a threat to vision in many ways in modern military operations.[22] Lasers as a weapon, using optical radiation,[23,24] have advantages of having unlimited weightless ammunition delivered silently, a huge range, and almost instantaneously delivery of energy.[21] Laser weapons have been developed for anti-personal and anti-sensor reasons, made to dazzle troops or sensors, and even designed to cause intentional blindness.[21] Even though the use of blinding laser weapons have been prohibited by international legislations, such as the Geneva convention,[25] research and development are not prohibited. Unintentional blinding from other lasers used in the battlefield, such as range-finders, missile guidance and other remote sensing equipment,[22] and lasers used to destroy electro-optical devises and sensors, are the current threat to soldiers' eyes.[26] With the development of the technology, and easy access to harmful lasers, it might also cause problems if such damaging lasers lie in the hands of terrorists, as a threat also to the civil society.

1.3 The laser protection problem

With this background it is clear that protection against harmful laser radiation is strongly needed, and that this has become essential in many military applications. Since the eye is one of the sensors that needs to be protected, the protection needs to be efficient in the whole visible region without obstructing

†For example in the Star Trek and Star Wars TV-series and movies from the 1970s and up to today.

the sensor to maintain its normal sensing abilities. Traditionally, laser protection is taken care of by using static optical filters that remove (absorb of reflect) the dangerous wavelengths from being transmitted to the sensor.[5] This is an efficient way of protection when the wavelength of the laser is known and the sensor don't need to collect data in the same wavelength range. However, when the sensors are needed to work in a wide wavelength range of the visible spectrum, and the wavelength of the hostile laser is not known, protection with static filters is not possible.

Therefore, the ideal protection filter needs to be transparent at normal conditions but still reduce or remove harmful radiation directed towards the sensor.[6] Due to the short pulses and high intensities of widely used lasers - often at picosecond to nanosecond duration - the sensor could be damaged even after one single pulse.[6] Therefore, one needs to construct protective filters that 1) work in the whole visible wavelength range, 2) is transparent at normal low intensity conditions and 3) is self-activated by the higher intensity of the harmful radiation, and subsequently removes or reduces the laser intensity below any hazard limit before it reaches the sensor. Such optical behavior can be found in certain nonlinear optical materials, and such materials therefore have the potential of presenting a solution to the laser protection problem.

1.4 Nonlinear optical absorption and OPL

For normal low intensity light, the absorbed amount of energy by any optical device is proportional to the energy of the incoming light,[10] as to be shown in Section 2.1. However, as the intensity of the light increases, some materials have the possibility to react in a non-linear way to the incoming intensity. That is, the electric polarization inside the medium, induced by the applied electric field, is no longer directly proportional to the external electric field, but contain terms being proportional to the square and cubic power of the electric field.[27] The cubic term is found to be responsible for a process called two-photon absorption, as outlined in Section 2.5. In addition, processes involving the absorption from already excited molecular states may result in the observed absorption as being nonlinear, either becoming larger or smaller depending on the excited state properties,[27] as outlined in Section 2.6.

In the view of laser protection, it is the process of increased absorption at high intensities that is of great interest, reducing the transmitted energy of a hazardous high intensity laser pulse. Some nonlinear optical (NLO) materials

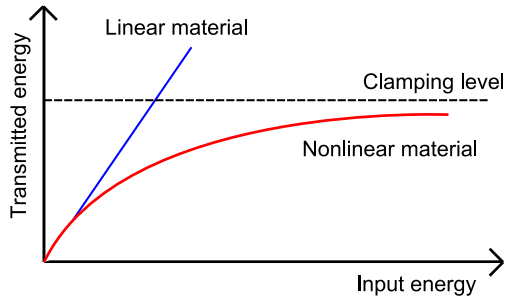

Figure 1.2: Response of linear and nonlinear absorbing optical material, clamping the transmitted energy below a certain value.

have properties that make them suitable for such applications.[28] When the material is exposed to an intense optical signal the nonlinear absorption occurs through the several NLO absorption mechanisms.

At low intensity, the absorption is low, and much light is transmitted, but at high intensities the relative absorption increases with increased laser energy. Desirable for laser protection, the nonlinear absorption increases in such a way that the transmitted power, or pulse energy, never exceeds a certain level (clamping level) independent of the incoming pulse energy, as shown in Figure 1.2. This clamping level should preferably be below the damage threshold of the sensor.

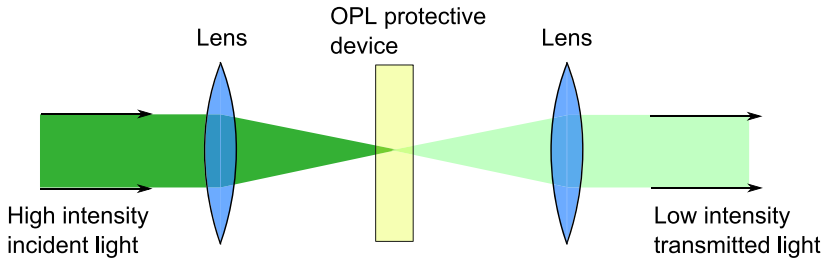

Figure 1.3: Optical power limiting is obtained from focusing the laser beam onto a nonlinear absorbing material, creating the high intensity needed for efficient nonlinear absorption.

In order to gain the high intensity needed for strong NLO absorption, the laser beam needs to be focused onto the protecting material, as shown in Figure 1.3. The nonlinear optical absorption created by these materials, and the effect of

reducing the intensity of a laser beam in this manner, is often referred to as optical power limiting, abbreviated OPL.

Chapter 2

Photo-physical processes

The interaction between electromagnetic waves (light) and matter is one of the fundamental interactions in nature. The study of how atoms and molecules react when irradiated with light, as a function of the light frequency, is called spectroscopy.[29] Depending on how the molecules changes the light with time and wavelength, information about optical, structural, dynamic and energetic properties of the molecules can be found. In this chapter a series of photo-physical properties are presented, and in Chapter 4, the use of different spectroscopic techniques for measuring these properties are outlined.

Depending on the experiment in question, light can either be seen as electromagnetic waves or energy particles (photons).[10] From classical electromagnetic theory it is found that the energy of an electron, governed by its Hamiltonian function, is dependent on the vector- and scalar potential of the corresponding radiation field.[30] In the quantum mechanical picture the radiation field is represented by a number of photons with a specific amount of energy.[31] In quantum mechanical theory any interaction (e.g. of electrons in an electromagnetic field) is only capable of producing a probability for the system (electrons and photons) to change its energy.[32] The theory also produces a set of 'rules' that controls this energy change.[33]

2.1 Optical absorption

The first and basic consequence of light-matter interaction is optical absorption. The electrons in an atom or a molecule have certain defined discrete

energies, dependent on the type of atoms, molecular structure and number of electrons in the system.[30] With no external interactions, the total energy of the molecule (sum of electron energies) is always as low as possible. There also exists a set of possible higher energy levels that the electrons may occupy if the molecule somehow was given some more energy. The molecule can gain the amount of energy needed to change its energy from one discrete level to another for instance by absorbing a photon from a light beam passing through it.[34]

The probability for the molecule to absorb one photon (and hence increasing its own energy) is from quantum mechanical electromagnetic theory given by the Fermi golden rule[33]

$$w_{i\to f} = \frac{2\pi}{\hbar}\left|H'_{fi}\right|^2 \delta(E_f - E_i - \hbar\omega_{\text{ph}}) \tag{2.1}$$

where $w_{i\to f}$ is the transition probability per unit time* for the molecule to jump from an initial state $|i\rangle$ to a higher energy final state $|f\rangle$ by absorbing a photon of energy $\hbar\omega_{\text{ph}} = E_f - E_i$, matching the energy gap. $H'_{fi} = \langle f|H'|i\rangle$ is the quantum mechanical matrix element controlling the strength of the interaction and therefore also the magnitude of the probability.†

For a molecule with energy E_i having an empty energy level at E_f, it can be found that the transition probability per unit time (averaged over molecular orientation) for absorbing a photon is[30]

$$w_{i\to f} = \frac{\pi\omega_{\text{ph}}\, n_{\text{ph}}}{3\hbar\epsilon_0 V}\left|\vec{\mu}_{fi}\right|^2. \tag{2.2}$$

Here, n_{ph} is the number of photons at the desired frequency, and $\vec{\mu}_{fi}$ is the transition dipole moment. If the radiation is a coherent state (laser) instead of a pure number state, the expression stays the same, except that n is replaced by $\overline{n}$, the average number of photons.

The transition probability is not a molecular characteristic, since it depends on the strength of the incoming light. It is therefore convenient to define a molecular property independent of this. Dividing the transition probability by the number of photons per unit area and time (number intensity), given by $I_0^N = n_{\text{ph}}\, c/V$, yields the absorption cross section[34]

$$\sigma(\omega) = \frac{w_{i\to f}}{I_0^N} = \frac{V}{n_{\text{ph}}\, c} w_{i\to f} = \frac{\pi\omega_{\text{ph}}}{3\hbar\epsilon_0 c}\left|\vec{\mu}_{fi}\right|^2. \tag{2.3}$$

*The stimulated transition probability is related to the Einstein coefficient, B_{if}, through; $w_{i\to f} = B_{if}\, u(\omega)$, where $u(\omega)$ is the energy density of the electromagnetic field.[31]

†Here, H' is the Hamiltonian perturbation originating from the incoming light.[34]

This is a fictitious area, usually measured in units of cm^2, of which the transmitted light, at a given frequency, is the same as the amount of energy/number of photons absorbed by the molecule at that frequency.

From an experimental point of view, it is desirable to relate the molecular properties, such as the absorption cross section, to the macroscopic observables. In an absorption measurement the amount of absorbed energy is found from measuring the incoming intensity I_0 and the transmitted intensity I through a sample at different light frequencies. The absorbance, or optical density, of a sample is then defined as[29]

$$A(\omega) = \log\left(\frac{I_0(\omega)}{I(\omega)}\right) = \epsilon(\omega) \cdot C \cdot l, \tag{2.4}$$

where C is the molar concentration, l the sample length in cm, and $\epsilon(\omega)$ the extinction coefficient being the molecular property. $\epsilon(\omega)$ is then given in units of $\mathrm{M}^{-1}\mathrm{cm}^{-1}$. Equation (2.4) is usually known as the Beer-Lambert law. From equation (2.3) we see that the absorbed energy per unit time is proportional to the absorption cross section and the intensity of the light itself. In a sample containing N molecules per unit volume, the beam intensity passing through a thin slice $\mathrm{d}z$ of the sample, is reduced by the amount[27]

$$\frac{\mathrm{d}I}{\mathrm{d}z} = -\sigma \cdot N \cdot I = -\alpha \cdot I, \tag{2.5}$$

where α is the absorption coefficient in units of cm^{-1}. Integrating over the sample thickness l gives[35]

$$I = I_0 \cdot e^{-\sigma N l} = I_0 \cdot e^{-\alpha l}, \tag{2.6}$$

that is, an exponential decay of the transmitted intensity. Comparing equation (2.6) with (2.4) gives the relation between the extinction coefficient and the absorption cross section[35]

$$\sigma(\omega) = \frac{\ln 10 \cdot 1000 \frac{\mathrm{cm}^3}{\mathrm{dm}^3}}{N_A} \cdot \epsilon(\omega) \tag{2.7}$$

where N_A is Avogadro's number.[‡] $\ln 10$ comes from the base-10 logarithm in eq. (2.4) and the factor 1000 must be inserted to convert to the given units. Any of the numbers $\epsilon(\omega)$, $\alpha(\omega)$ or $\sigma(\omega)$ are, as we have seen, related to the absorption probability and therefore a measure of the 'strength' of the molecular absorption at a given frequency.

[‡]Avogadro's number: $N_A = 6.022 \cdot 10^{23}\ \mathrm{mol}^{-1}$.

Typically, if a 10 μM sample is observed to have an absorption of $A = 1.0$ in a 1 cm cell at a given frequency, the extinction coefficient is $\epsilon = 10^5$ $\mathrm{M^{-1}cm^{-1}}$. The absorption coefficient is $\alpha = 2.3$ $\mathrm{cm^{-1}}$ and the absorption cross section is $\sigma = 3.8 \cdot 10^{-16}$ $\mathrm{cm^2}$.

2.2 Emission of light

Just as atoms or molecules are capable of absorbing light they are also capable of emitting light. The interaction with radiation produces a transition probability between two energy levels of the molecule. If the electron already is in an upper energy level when the radiation strikes, the interaction may cause the electron to jump to the available lower level emitting the excess energy as a photon.[32] The probability for the light to stimulate absorption or emission is the same.[30] Stimulated emission is the origin for the laser operation as seen in Section 1.1. In addition to stimulated emission, it is also observed that the electron may spontaneously jump back to the lower electronic energy level emitting a photon without the presence of the radiation field.[34] The probability for emission is given by eq. (2.2), replacing n_{ph} with $n_{\mathrm{ph}} + 1$. The two terms then account for the stimulated and spontaneous emission, respectively.

Any process responsible for the emission of light is in general called luminescence.[36] In all cases, the emission is a response to a particular form of input energy. If the input energy comes from radiation, the emission is called photo-luminescence. The two most important types of photo-luminescence are fluorescence and phosphorescence.

2.2.1 Fluorescence

After being raised to an excited state in an absorption process, the probability for spontaneous emission causes the molecule to relax to its ground state in typical time-scales of 10^{-10} to 10^{-8} seconds.[29] This rapid emission of light is from historical reasons called fluorescence.[36] Although, this relaxation time seems to be very short, it is indeed much longer than the stimulated transition time between electronic states of about 10^{-15} seconds.[36]

Usually, the fluorescent light have slightly lower energy than that of the absorbed photons.[29] This is caused by the vibrational structure in the electronic energy levels.[36] In order to visualize the different energy levels and transi-

tions possible between the states, they are often presented using a Jablonski diagram, as shown in Figure 2.1.

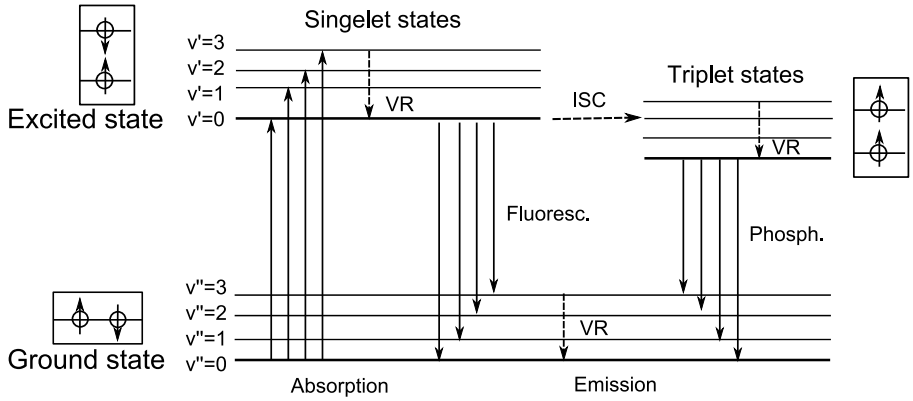

Figure 2.1: The Jablonski diagram with the triplet manifold and transitions of fluorescence, phosphorescence, vibrational relaxation (VR) and inter-system crossing (ISC). The electron spin configuration of the ground state, singlet excited state and triplet state are also shown.

The molecule can be excited into a lot of possible excited states with different energies. At room temperature the molecules will usually be in their lowest vibrational energy level.[36] Therefore excitation may occur from ground state $v'' = 0$ to any of the vibrational v'-states in Figure 2.1. After being excited, vibrational relaxation (VR) causes the molecule to quickly relax to its lowest vibrational level of that electronic state. If the molecule is excited into a higher electronic excited state (not just the first excited state), the molecule will quickly relax to the first excited state in an iso-energetic process called internal conversion (IC) followed by vibrational relaxation to this state.[36] (Figure 2.2.) In this process the molecule rapidly dissipates its vibrational excitation energy to the surroundings as heat.[35] This relaxation occur at a time scale much faster than the fluorescence, and therefore fluorescence will occur from the $v' = 0$ state of the first excited state to any of the ground state vibrational levels followed by VR to the initial $v'' = 0$ state.[29] As will be noted in upcoming sections the molecule may also relax to the ground state without emitting light, due to collisions and energy transfer to the surroundings similar to the IC process.[33]

2.2.2 Phosphorescence

Due to the electronic spin, two types of excited states exists. In most organic molecules the ground state has an even number of electrons which are paired into different molecular orbitals.[36] According to the Pauli exclusion principle all paired electrons must have opposite spin, one having spin 'up' and the other spin 'down'. The energy level is then called a singlet state.[35] When the molecule is excited due to the absorption of a photon the excited electron keeps its direction of the spin, due to the quantum mechanical selection rules, and the molecule ends up in an excited singlet state. Emission from this state is fast and called fluorescence, as described in the previous section. However, it is possible for the excited electron to change its spin into the other state after being excited, because it is no longer restricted to the Pauli principle as the electrons now are in different orbitals. The molecular excited state is now called a triplet state,[35] and the process of changing the spin state is called inter-system crossing (ISC).[29] (Figure 2.1.)

The triplet state will have a somewhat lower energy than the corresponding singlet state. The iso-energetic ISC process may occur from any of the the vibrational levels of the singlet state to a vibrational level of the corresponding triplet state, followed by vibrational relaxation in the triplet state.[29] This is shown in Figure 2.1. Spontaneous emission from the vibrationally relaxed triplet state to the ground state, is referred to as phosphorescence.[29] Due to the quantum mechanical selection rules this relaxation is much slower than from the singlet state, and usually occur in time scales of 10^2 to 10^{-3} seconds.[36] For this reason most of the molecules usually relax to the ground state by transferring its energy to the surroundings by collisions and other mechanisms. The long lifetime corresponds to a weak transition moment between the first triplet state and the ground singlet state. For this reason any absorption from the ground state directly into the triplet states is weak and usually neglected, unless under special experimental conditions.[35]

2.3 Excited state lifetime

As we have seen in the previous section, the excited state may relax to the ground state by emitting a photon. We will also see in the next section how the non-radiative processes will compete with the radiative decay and reduces the lifetime of the excited state. The radiative decay time is an important characteristic property of a molecule, and it is desirable to measure this with

great accuracy. Due to the very fast fluorescence relaxation times of about 10^{-9} seconds, this requires special techniques.

Analogous to equation (2.5), the rate of spontaneous emission is given by

$$\frac{\mathrm{d}N_f}{\mathrm{d}t} = -A_{fi} \cdot N_f, \tag{2.8}$$

where N_f is the number of excited atoms/molecules and A_{fi} is the Einstein coefficient of spontaneous emission, equal to the probability per unit time for emission.[31] This means that the number of excited molecules will have an exponential decay as

$$N_f = N_f^0 \cdot e^{-A_{fi} \cdot t} = N_f^0 \cdot e^{-t/\tau_0}, \tag{2.9}$$

where $\tau_0 = 1/A_{fi}$ is the radiative lifetime of the excited state.[§] This equation was derived on a collective basis, starting with a large number of excited molecules, and counting the number still remaining excited after time t. Looking at individual molecules the probability for a molecule to be in the excited state after time t is then[**]

$$P(t) = e^{-t/\tau_0}. \tag{2.10}$$

This is in accordance with eq. (2.9) and the statistical nature of absorption and emission.

2.4 The quantum efficiency

We have seen that a molecule may both absorb and emit light (photons), and that the emitted photons usually have a somewhat lower energy than the absorbed photons, being emitted either as fluorescence or phosphorescence from the first excited singlet or triplet states. The emitted photons are also delayed due to the lifetime of the molecular excited state. The molecule have normally only the possibility to emit one photon for each absorbed photon.[32] If the molecule emits one photon for each photon it absorbs, we say that the

[§]Relaxation time would be a more precise term being the time for the process to fall to $1/e$ of its initial value. However, lifetime is a commonly used term, representing the same phenomenon.[29]

[**]Let $k = A_{fi} = 1/\tau_0$ be the probability per unit time for spontaneous emission. The probability for no decay in the time interval Δt is then $(1 - k\Delta t)$. The probability for not making a decay in many such small time intervals is the product of such factors (independent probabilities). After time $t = \mathrm{n}\Delta t$, the probability for the molecule still being in the excited state is: $P(t) = (1 - k\Delta t)^{t/\Delta t} = [(1 - k\Delta t)^{1/k\Delta t}]^{-kt} = e^{-kt}$, when $\Delta t \to 0$.

molecule has a quantum efficiency (QE) (or quantum yield, QY) of 1.0. If, for instance, only half of the absorbed photons are emitted back as light the quantum efficiency is reduced to 0.5. In this case, the energy of the other half of the absorbed photons is transferred to heat as the molecules relaxes to its ground state through some radiationless transitions.[35]

This opens up the possibility for the molecule to have other ways of returning to the ground state, than that of emitting photons. In these radiationless transitions the energy of the excited molecule can either be redistributed within the molecule followed by vibrational relaxation, or by quenching with other surrounding molecules.[36] This intra-molecular redistribution is often referred to as internal conversion (IC). These extra relaxation channels are present both in the singlet and triplet manifolds. A more complete Jablonski diagram is then shown in Figure 2.2.

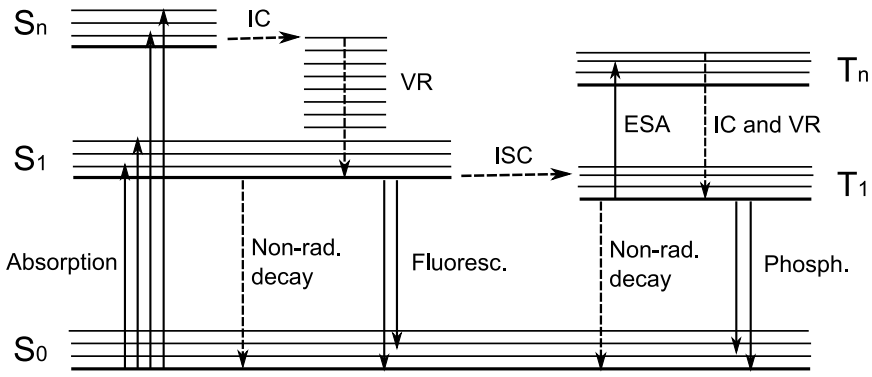

Figure 2.2: The Jablonski diagram, with possible radiative and non-radiative relaxation channels. The scheme also indicate the possibility for excited state absorption (ESA), which is particularly important in the triplet manifold for long laser pulses.

Since we are measuring the lifetime of the (singlet) excited state based on the fluorescence emitted photons, the quantum yield and relaxation lifetime are coupled.[37] If the quantum efficiency of fluorescence was 1.0 the lifetime of the state is given by the reciprocal of the emission/fluorescence probability, k_{fl} as

$$\tau = \tau_{\text{fl}} = \frac{1}{k_{\text{fl}}} \, . \tag{2.11}$$

This is the same as we found from equation (2.9) with $\tau_{\text{fl}} = \tau_0$. If other non-fluorescent relaxation paths are present with a combined probability of k_{nfl} the lifetime of the excited state would be

$$\tau = \frac{1}{k_{\text{fl}} + k_{\text{nfl}}} , \tag{2.12}$$

that is, shorter than the intrinsic fluorescence lifetime, τ_{fl}, of eq. (2.11). Any bi-molecular quenching mechanism of the singlet excited state is now included in k_{nfl}. Noting that the quantum efficiency can be given by the ratio of the transition probabilities,[37] the fluorescence quantum efficiency, Φ_F, and excited state lifetime are related as

$$\Phi_F = \frac{k_{\text{fl}}}{k_{\text{fl}} + k_{\text{nfl}}} = k_{\text{fl}} \cdot \tau = \frac{\tau}{\tau_{\text{fl}}}. \tag{2.13}$$

Therefore, by measuring both the excited state lifetime and the fluorescence quantum efficiency, k_{fl} and τ_{fl} can be calculated from equation (2.13). Then k_{nfl} is found using equation (2.12).

In the above equations we have neglected inter-system crossing (ISC) and the triplet states. In many cases the probability for ISC (k_{isc}) is close to zero, or it is not possible to distinguish it from other non-radiative processes, due to very efficient quenching of the triplet state.[37] However, when this is not the case, eq. (2.12) must be extended to

$$\Phi_F = \frac{k_{\text{fl}}}{k_{\text{fl}} + k_{\text{nfl}} + k_{\text{isc}}}. \tag{2.14}$$

Depending on the process of interest, we can in the same manner define the ISC efficiency, Φ_{ISC}, by replacing k_{fl} with k_{isc} in the numerator of eq. (2.14).[35]

From the triplet state there are also three possible relaxation paths: phosphorescence, non-phosphorescent, and quenched, with rate constants of k_{ph}, k_{nph} and k_{q}, respectively. The phosphorescence quantum efficiency will in addition also be dependent on the ISC-efficiency, and could be written as[35]

$$\Phi_{Ph} = \frac{k_{\text{isc}}}{k_{\text{fl}} + k_{\text{nfl}} + k_{\text{isc}}} \cdot \frac{k_{\text{ph}}}{k_{\text{ph}} + k_{\text{nph}} + k_{\text{q}}} = \Phi_{\text{ISC}} \cdot \tau_{\text{ph}} \cdot k_{\text{ph}}, \tag{2.15}$$

where τ_{ph} is the triplet state lifetime, measured from phosphorescence.

2.5 Two-photon absorption

In Section 2.1 we saw that a molecule can absorb a photon if the photon energy matches the molecular energy gap, and that no absorption would occur if the

energy e.g., is to low to fit the gap between the ground state and the first excited state. However, at larger intensities, the probability that a molecule can absorb more than one photon in the same quantum transition before relaxation to the ground state, increases. As early as in 1929-1931 Maria Göppert-Mayer predicted the process of two-photon absorption (TPA) and derived an expression for the two-photon transition probability in a system using second order perturbation theory.[38,39] It was not until 30 years later Kaiser and Garret[40] experimentally verified the phenomenon.*

The probability for two-photon absorption, derived from the Hamiltonian interaction in second order time-dependent perturbation theory, is much smaller than that of one-photon absorption (OPA).[34,42] Therefore, in many situations, it can be neglected. However, if the irradiation of the light is strong enough (e.g. from a focused laser beam), and the molecular properties are suitable, two-photon absorption can be observed.[27]

In this process a transition from the ground state to the excited state of the molecule occur by the simultaneous absorption of two photons from the incident radiation field.[27] Each of the two photons have only half the energy needed in the excitation process, however, the two photons 'add up' their energies and may excite the molecule. The process is illustrated in a simple energy level diagram in Figure 2.3.

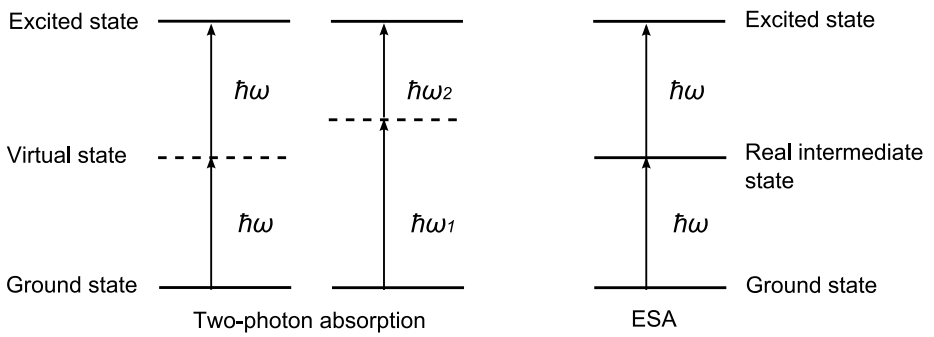

Figure 2.3: Simultaneous two-photon absorption with equal (left) and unequal (middle) photon energy, through a virtual intermediate state. Excited state absorption through a real intermediate state (right).

The process of two-photon absorption through a virtual intermediate state is

*Kaiser and Garrets experiment was the second demonstration of nonlinear optics, shortly after the experimental observation of second harmonic generation by Franken et al.[41]

called simultaneous or coherent TPA, hence the two absorbed photons must be absorbed at the same time.** The two absorbed photons may also be of different frequency in a two-beam setup, and the intermediate state can also be a real state.[27,42] The latter case, sometimes called resonant TPA, is actually more correctly referred to as excited state absorption (ESA). (Figure 2.3.)

A similar expression for the transition probability per unit time, as that found in eq. (2.1) of Section 2.1 can be found for two-photon absorption.[42] In particular, the TPA transition probability becomes proportional to the square of the number of photons, that is $w^{(2)}_{i\to f} \propto n^2_\omega \propto I^2/\omega^2$, and hence the absorption coefficient becomes intensity dependent.[27,44] This can also be seen from the equation determining the change in intensity of a beam passing through an absorbing sample, as found in eq. (2.5) for one-photon absorption. Now, this equation needs to be corrected by introducing the second order term. The equation becomes[27]

$$-\frac{\mathrm{d}I}{\mathrm{d}z} = \alpha\, I + \beta\, I^2 = (\alpha + \beta\, I)\; I = \alpha(I)\; I\;, \tag{2.16}$$

where β is the two-photon absorption coefficient, and $\alpha(I)$ is the generalized intensity dependent absorption coefficient. The two-photon absorption cross section, σ_2 is found from the two-photon absorption coefficient through[27]

$$\sigma_2 = \frac{\hbar\omega\,\beta}{N}\,, \tag{2.17}$$

where N is the volume number density of molecules in the sample. The relation in eq. (2.17) is important because it relates the macroscopic material characteristic property, β, to the single molecule property σ_2. The relation between the TPA cross section and the transition probability becomes[44]

$$w^{(2)}_{i\to f} = \frac{\sigma_2\, I^2}{(\hbar\omega)^2}\,, \tag{2.18}$$

a natural extension of the left part of equation (2.3).

The generalized $\alpha(I)$ coefficient is measured in cm^{-1} as before, but both σ_2 and β now relates to the intensity I measured in $\mathrm{W/cm}^2$.†† In the linear case it is easy to convince ourself that the absorption cross section can be treated as a physical area. That is, an area of the beam of which the number of passing

**Or within the lifetime of the virtual state of approximately $10^{-15} - 10^{-16}$ s.[43]

††First order units: $[\sigma_1]$ =cm^2, $[\alpha] = [\alpha(I)]$ =cm^{-1}.
Second order units: $[\sigma_2]$ =cm^2(# photons/s cm^2)$^{-1}$, $[\beta]$ =cm^{-1}(cm^2/W) = cm/W.

photons is the same as the ones absorbed. The two-photon absorption cross section can, by looking at the unit, be interpreted as an intensity specific area, an area which increases as the incoming intensity increases. If the intensity doubles, four times as many photons are absorbed, as seen from the square dependence of Eq. (2.18).

As known from classical optical theory, linear refraction and absorption are related to the optical permittivity (ϵ) of the material.[45] The two terms then account for the real and imaginary part of the first order complex electric susceptibility, $\chi^{(1)}$, respectively. In a similar way, the second order susceptibility, $\chi^{(2)}$, accounts for the nonlinear effect of second harmonic generation.[27,41,†] It is first due to the third order susceptibility, $\chi^{(3)}$, that nonlinear absorption and refraction occurs. The TPA coefficient β is then for instance found to be proportional to the imaginary part of $\chi^{(3)}$.[27,44]

2.6 Excited state absorption

If the incoming light intensity is strong enough, and the lifetime of the excited state is not too short, the excited states of a sample can be greatly populated. If the pulse length is long enough (> ns) compared to the lifetime of the excited state, we have the possibility for an excited molecule to be further excited into an even higher lying energy state, from absorbing yet another photon from the incident beam.[27] This is known as excited state absorption.

Two possibilities of ESA exist. If the absorption cross section of the excited state is smaller than that of the ground state, the total absorption will decrease, due to the population of the excited state.[46] This is known as saturable absorption (SA). In the opposite situation, when the absorption cross section of the excited state is larger than that of the ground state, the system will have increased absorption as the system is excited.[27] This is known as reverse saturable absorption (RSA).

If the lifetime of the excited state is much longer than the pulse length, as is the case for the triplet states, and these states are quickly populated from the singlet states, as is the case for the Platinum(II) acetylides in this study (see Section 3.3), the ESA from the triplet states can be very efficient, giving rise to the increased nonlinear absorption, needed in optical power limiting applications.

[†]It is shown that second order nonlinear effects only occur in non-centrosymmetric materials.[44]

Chapter 3

Organometallic molecules for multi-photon absorption

The main theme of this thesis is spectroscopic characterization of new molecular systems for optical power limiting by means of multi-photon absorption. In this chapter I give a brief outline of the underlining phenomena and introduce the investigated molecular systems. More experimental details and a summary of results will be given in the following chapters.

3.1 Nonlinear optical absorption

Nonlinear absorption refers to the change in transmittance of a material as a function of the intensity of the radiation.[27] Two-photon absorption is one of several multi-photon absorption (MPA) processes showing nonlinear effects in molecules.[27] It is no doubt that the invention of the laser in 1960 was the key to observing such nonlinear optical phenomena, and numerous nonlinear effects have been discovered since.[44]

Multi-photon transitions have several characteristic properties, such as intensity (I), wavelength and polarization dependence. For instance, the simultaneous n-photon transition probability is proportional to I^n, etc.[42] Further excitation of an already excited molecule, is also called MPA, since more than one photon is involved in the absorption process in each molecule.[5] For instance, simultaneous two- and three-photon absorption in combination with

excited state absorption are typical multi-photon- or nonlinear absorption processes. However, when simultaneous two-photon absorption is claimed to be measured with e.g. nanosecond pulses or longer, care should be taken so that ESA-processes are not contributing in the calculation of the TPA cross section.[5]

In addition to the absorption processes, the nonlinear polarization in molecules also have an effect on the refractive index. The linear refractive index will get an additional intensity dependent term; $n = n_0 + \Delta n$, where $\Delta n = n_2 I$, and n_2 is the nonlinear refractive index.[27] This may result in self-focusing and de-focusing effects inside a material or solution. The study of the nonlinear refractive index is not treated in this work. However, we note that nonlinear refraction effects may contribute to the optical limiting performance in the setup described in Section 4.8.

In principle, simultaneous two-photon absorption should be suitable for optical limiting of short, high intensity pulses. However, in practical studies, even materials with the largest TPA absorption coefficients are insufficient for most real applications of protecting sensors from laser pulses in the order of nanosecond duration.[47] The process of reverse saturable absorption (RSA) has the potential for improving the optical limiting behavior. Two-photon absorption is an almost instantaneous process (with a transition time in the order of 10^{-15} s), whereas any excited state absorption process exhibit certain kinetic behavior due to the lifetimes of the excited states.[47] If the absorption cross section of for instance the triplet state is large, and the lifetime of this state is sufficiently long compared to the pulse length, it is possible for several excited state absorption/relaxation processes during the laser pulse.

3.2 Nonlinear absorbing molecules

In the beginning, nonlinear optical (NLO) phenomena were investigated in inorganic materials.[48] Later, organic compounds became interesting due to their promise of having large NLO responses. Additional advantages of organic compounds were high laser damage threshold, fast NLO response, easier to synthesize and fabricate, and architectural flexibility, which allows for molecular design and engineering.[48–50] Organic molecules containing conjugated (extended) π-electron systems with charge asymmetry in a donor-acceptor structure, or in conjugated polymers, have been shown to have large second- and third-order nonlinearities.[48,49]

Like organic molecules, organometallic complexes can possess large NLO responses, due to the large molecular polarizability originating from the strong metal-ligand charge transfer in these molecules.[49,51] With an even greater flexibility in the design stage and the possibility for variation in metal-ligand environment and geometry, it became possible to tune the NLO responses in organometallic complexes in ways not possible for purely organic molecules.[47,49] Studying the nonlinear properties of a variety of metals or ligands in series of 'families' of organometallics can lead to understanding of structure to property relationships.[8,47,49]

NLO materials in general, and organometallic complexes in particular, may have a wide range of potential applications for instance in opto-electronics, optical signal processing, optical switching, frequency generation and mixing, optical data storage, optical telecommunication, image processing, liquid crystals, light-emitting diodes[9,52] and optical power limiting.[8,47,48,53] Also, a wide range of nanomaterials (carbon nanotubes,[54] nanoparticles[55]) and organic molecules, such as fullerenes,[56,57] porphyrins,[58–60] metallophthalocyanines,[61,62] thiacalixarenes,[63,64] metal acetylides,[47] polymers,[65] etc., have been studied for their NLO and optical power limiting properties.[66–68]

Metal acetylide (alkynyl) complexes have attracted significant interest, due to their extended π-conjugated systems and large NLO responses. Their properties, with metals such as Iron (Fe), Ruthenium (Ru), Nickel (Ni), Gold (Au), Titanium (Ti), Palladium (Pd) and Platinum (Pt), have been extensively reported in the literature.[8,47–49,53,69,70]

For optical power limiting applications it is desirable for the linear transmission in the visible region to be as high as possible.[6] For that reason, among the heavy metals, Platinum-complexes are preferred due to the small absorption in the visible region.[71]

3.3 Platinum(II) acetylides

The synthesis of square planar Pt(II) acetylides was first reported during the 1970s by Sonogashira et al.[72,73], and have since that time attracted much interest due to their photo-physical properties and potential as NLO chromophores for OPL applications.[28,74–79] A typical example of a square planar Pt(II) acetylide is the di((4-(phenylethynyl)phenyl)ethynyl)bis-(tributylphosphine)-platinum(II), often abbreviated Pt1, shown in Figure 3.1.

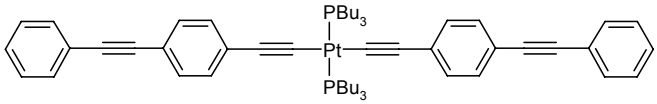

Figure 3.1: Structural formula of *trans*-Pt(P(n-Bu)$_3$)$_2$(C≡C−p-C$_6$H$_4$−C≡C−C$_6$H$_5$)$_2$, abbreviated **Pt1** in this study.

Introducing a heavy atom, in this case platinum, in an organic framework, gives rise to strong spin-orbit coupling interactions in the molecule.[35,80,81] The spin-orbit coupling (SOC) process is stronger for heavier atoms, and mixes the singlet and triplet molecular states.[27,35] This allows for more of the normally forbidden singlet to triplet transitions, and gives rise to the possibility for efficient inter-system crossing from the excited singlet to triplet states.[33]

Nonlinear absorption in platinum ethynyls has been extensively studied, and the photo-physical properties of the Pt1-molecule have been reported in several papers by Staromlynska and McKay et al.[28,75,82–85]. The strong observed nonlinear absorption in the visible region of these molecules have been interpreted as a combination of excited state absorption and two-photon absorption.[28,86,87] Later, Cooper and Rogers et al. presented a series of papers on platinum(II)-containing phenyl-ethynyl oligomers, with one, two and three phenyl rings in the ligands.[76,77,88–92] Here, their PE2-molecule is the same as our Pt1. The ISC process was found to be fast (some picoseconds)[75,83,93] and very efficient (close to 100% for Pt1)[76]. Simultaneously, similar molecules were studied also in polymer form.[79,94–97] During the last years, several studies on other similar Pt-acetylides, in modified form, have also been reported.[98–101]

3.4 The studied Pt(II)-acetylides

The results on the Platinum(II)-acetylides presented in this thesis are, in some sense, a continuation of the work presented in the theses of Anders Eriksson[5] (Linköping University, 2001), Robert Vestberg[102] (KTH, Stockholm, 2004) and Per Lind[103] (Umeå University, 2007), and carried out closely parallel to the work of Marcus Carlsson[104] (Umeå University, 2007) and Robert Westlund[105] (KTH, 2008), where the author of this thesis have contributed in their theses.

I was introduced into the project and the experimental work during the final steps of the work on the dendrimer capped Pt1 chromophores presented in the

papers by Vestberg et al.[78,106] (related paper 1) and Lindgren et al.[107] (related paper 2), following similar work on other dendrimer capped structures.[108,109] It was found that e.g. Pt1-G1 (with bis-MPA units*) had closely similar properties as Pt1, both for absorption and emission. It has therefore been natural for us to compare any following work to the Pt1 or Pt1-G1 compounds.

3.4.1 Pt-thiophenes

In Paper I, one of the two phenyl rings in each ligand of Pt1 was substituted with thiophene rings. The thiophene rings were placed at two positions in the molecular structure. For the first compound, the inner phenyl rings (closer to the Pt-atom) were replaced with thiophene rings bridging at the 2,5-positions. This structure is called T1 in Figure 3.2.† In the second compound (T2) the outer phenyl rings were replaced by thiophene rings bonded at the 2-position.

The photo-physical properties obtained for these thiophene-containing chromophores are compared with those of Pt1 and Pt1-G1. The thiophene rings were incorporated into the ligand structure in an attempt to modify the electronic structure in such a way that an increased nonlinear effect could be observed.

In Paper II, four longer thiophene containing molecules were prepared. Here, each ligand contains two phenyl rings in addition to the thiophene ring. (Figure 3.2.) In T7, the thiophene ring is placed closest to the Pt-atom (as for T1). For T3, the thiophene ring is placed between two phenyl rings, and in T4, the thiophene ring is placed at the ligand end. In all cases, all rings are linked with ethynyl triple bonds. Note that the structures of molecule T1, T3 and T7 are not straight molecules, as Figure 3.2 indicates, but actually bended at the thiophene positions, due to the bonding properties of the thiophene units. The three-ring phenyl analogue, Pt3, was synthesized and used for a comparison of the photo-physical results.

The pentyl groups in T1 and T3 were introduced in an attempt to increase the solubility of both the alkyne ligands and the final Pt complex, during the synthetic process. The solubility was probably a little better because of that group, but not much. For that reason, it was not introduced in the other compounds. We do not expect that this group would have any significant effect on the photo-physical properties, since it is not conjugated with the rest

*bis-MPA = 2,2-bis-(methylol)propionic acid

†In paper I and related papers 9 and 11, the T1, T2 compounds etc., are called ATP1, ATP2 etc.

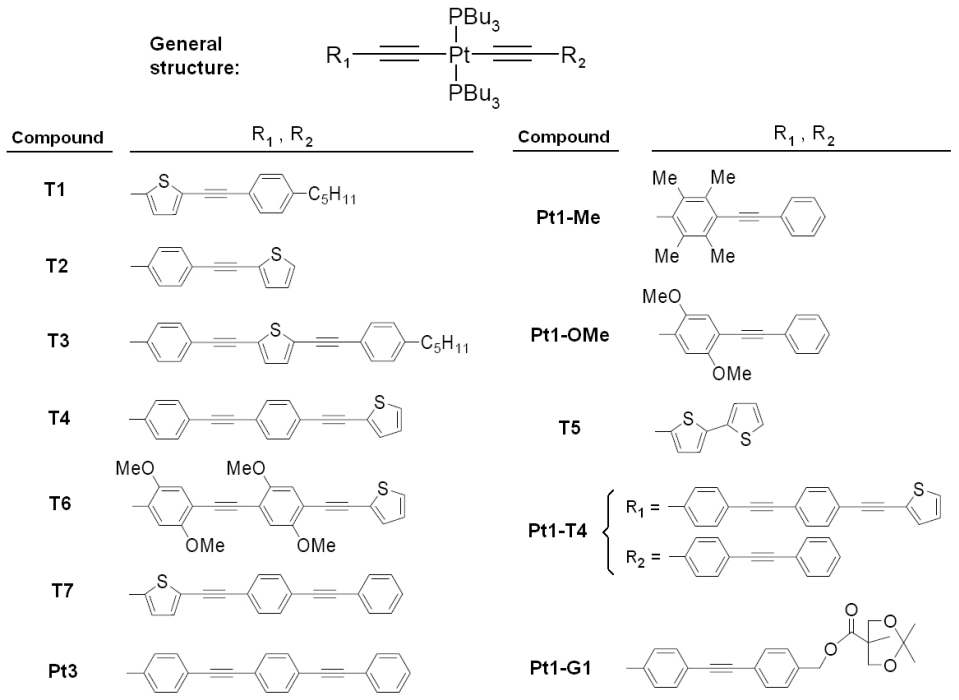

Figure 3.2: Structures of the studied Pt-acetylides with thiophene rings and methyl and methoxy substituents.

of the ligand, and has no particular electron donor/acceptor properties.

The compound T6 was synthesized for a comparison to T4, introducing electron donating methoxy substituents on the phenyl rings. These substituents have previously been found to give an increase in the third order hyperpolarizability of π-conjugated chromophores,[110]. Also, an increased solubility was expected.

In Paper IV, another four new Pt(II)-arylalkynyl compounds were investigated. (Figure 3.2.) Pt1-OMe has two methoxy groups on the inner phenyl ring of each ligand. T5 has two thiophene rings in each ligand, and Pt1-Me has four methyl substituents on each of the inner phenyl rings. The latter compound was expected to have a large preference for the rings being perpendicular to the P-Pt-P bond axis due to steric interactions between the phosphine butyl and the methyl groups. Pt1-T4 was prepared with one Pt1-like ligand and one T4-like ligand, in order to investigate the role of having a compound with two different ligands in the structure.

3.4.2 Pt-triazoles

In Paper III, a new synthetic route for the preparation of dendron decorated Pt(II)-acetylides were investigated. In this approach, the dendrons are attached to the phenyl-ethynyl arms during triazole formation through 1,3-dipolar cyclo-addition of azides and alkynes.[111] The triazole unit was placed at three different positions in the ligand structure (Figure 3.3) to investigate the effect of the triazole unit on the photo-physical properties and OPL performance of these chromophores. The Z1 molecule contains a short conjugation path of one phenyl-ethynyl group with the triazole unit at the end. The Z2 molecule has the triazole unit between two phenyl rings, and Z3 has the triazole unit at the end of a longer conjugation similar to Pt1. The Z2 molecule was prepared to investigate whether the triazole unit disturbs the conjugation between the two aromatic rings, or not.

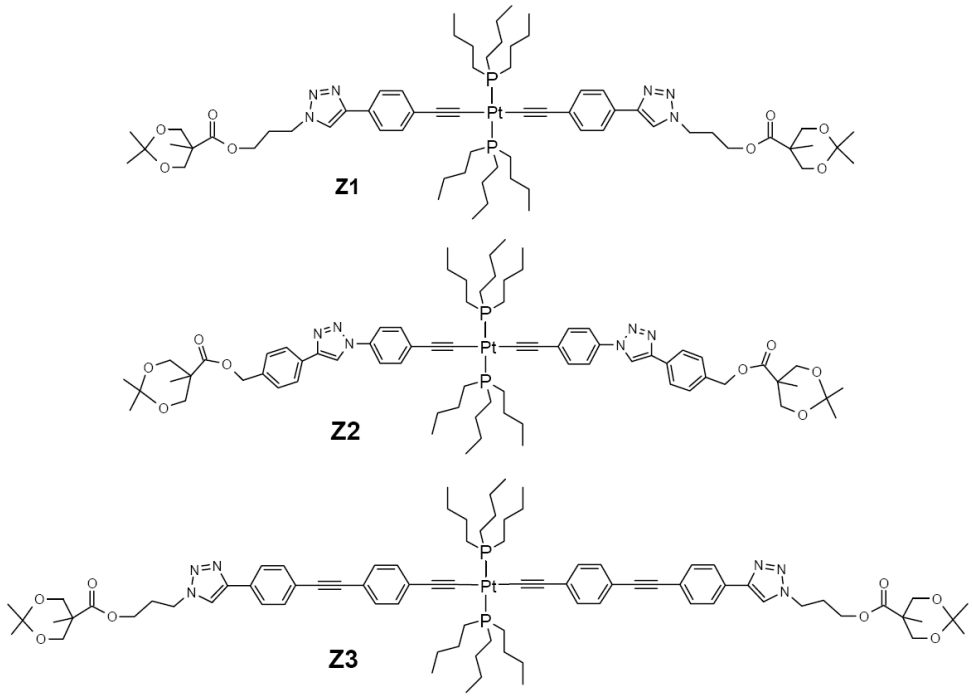

Figure 3.3: Molecular structures of the triazole containing Pt(II)-acetylides Z1, Z2 and Z3.

3.4.3 Solid state PMMA Pt(II)-materials

In Paper V (and related paper 5), the compounds Z1, Z3 and Pt1-G1 were incorporated into solid poly(methyl methacrylate) (PMMA) glasses to obtain a solid-state nonlinear optical device. Two types of materials were prepared (Figure 3.4). In type I glass the Pt-molecules were mixed with liquid MMA, followed by a polymerization of the MMA to PMMA with the dye dispersed inside. In this glass, only secondary forces act between the two components, giving the dye certain mobility within the material. In type II glass, the Pt-molecules were first functionalized with methacrylate groups before mixing with the MMA. In the subsequent polymerization process the Pt-compounds will now covalently bond to the host matrix, and the mobility of the dye becomes very limited. The methacrylate functionalized Pt1-G1 is shown in Figure 3.5.

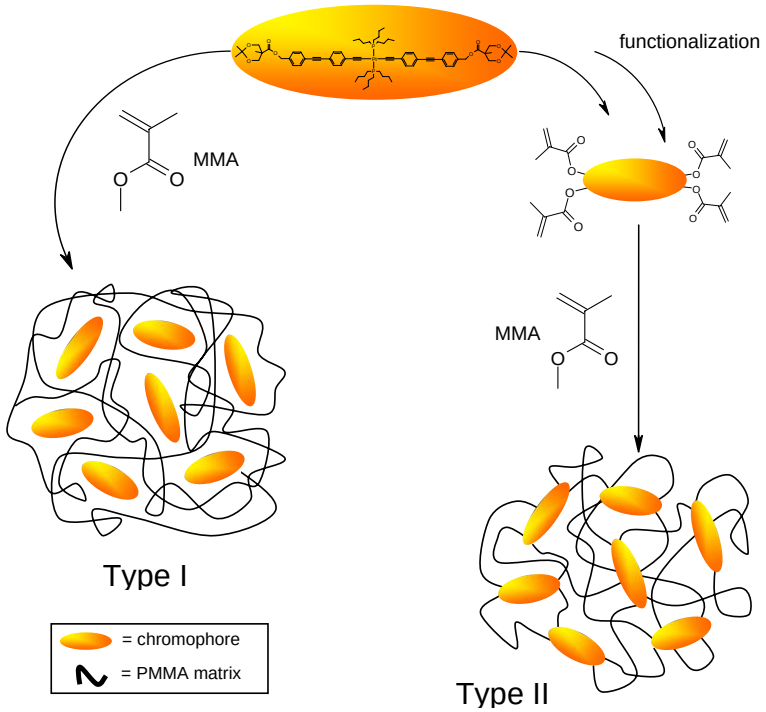

Figure 3.4: Polymerization strategies for Pt(II)-acetylides in PMMA glass. Type I: Dispersed inside the PMMA glass. Type II: Covalently bonded to the PMMA host matrix. (*Figure made by Dr. Robert Westlund, KTH.*)

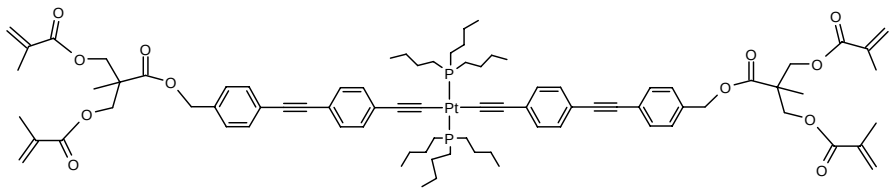

Figure 3.5: Pt1-G1 functionalized with four methacrylate groups on the two bis-MPA units.

Z1, Z3 and Pt1-G1 were prepared in type I PMMA glass. Pt1-G1 functionalized with methacrylate was also prepared in type II PMMA glass. Glasses of both types were prepared with dye concentrations varying from 10 μM up to 50 mM. At 10 μM and 100 μM the glasses were found to be completely colorless, while at higher concentration the glasses became pale yellow at 1 mM and darker yellow/orange at 50 mM, as shown in Figure 3.6. Even though the high concentrated samples have some yellow coloring, they have still quite good transparency in most of the visible region.

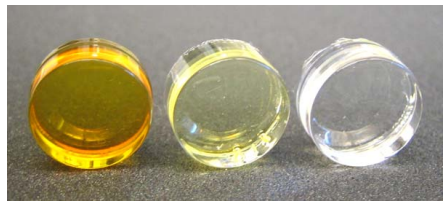

Figure 3.6: Solid state PMMA glasses of Z1 in concentrations of 50 mM (yellow/orange), 1 mM (pale yellow) and 100 μM (colorless). Sample thickness in picture is 8 mm and diameter 13 mm. (*Picture kindly provided by Dr. Robert Westlund.*)

3.4.4 Other compounds: Pt-Star and Pt1-A

In addition to the Platinum(II)-arylalkynyl complexes presented in Section 3.4.1 to 3.4.3, two other compounds were investigated in this study. The first is a three-armed Pt1-compound, called Pt-Star, as shown in Figure 3.7. Here, three Pt1-molecules are linked together by sharing the outer phenyl ring on one side. The new molecule therefore has three Pt-atoms in it.

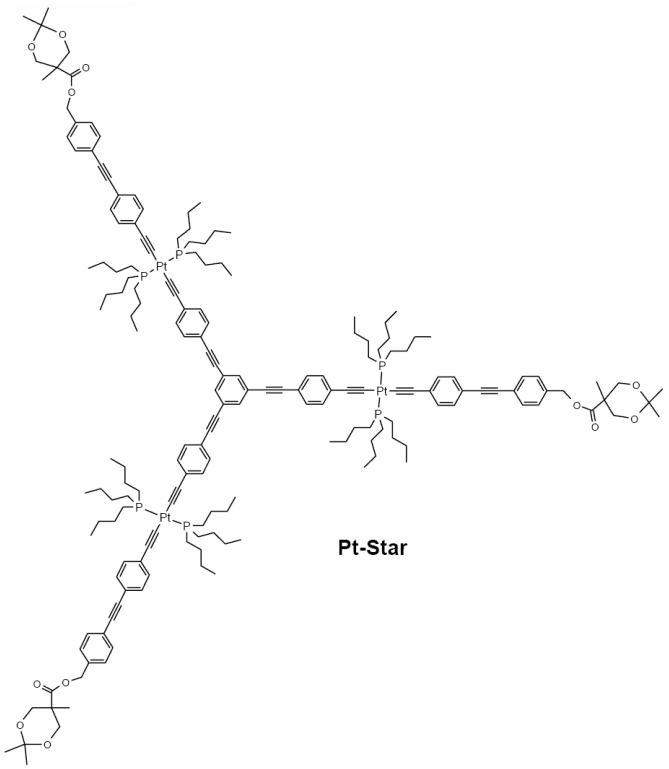

Figure 3.7: Molecular structure of the Pt-Star compound containing three 'Pt1-G1' molecules linked together in a star-shape.

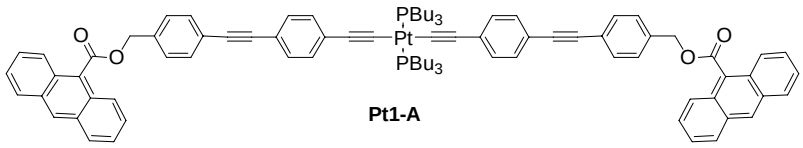

Figure 3.8: Molecular structure of the Pt1-A compound, containing anthracene groups.

The second compound, called Pt1-A, is a Pt1-molecule with an anthracene group attached to each end of the molecule. The molecular structure of the Pt1-A molecule is shown in Figure 3.8. The molecule was synthesized for a possible study of triplet-state transfer from the Pt1-ligand to the anthracene unit, for a possible increase in the excited state absorption properties.

Chapter 4

Methods of spectroscopic characterization

4.1 Absorption spectroscopy

Absorption is usually measured by varying the frequency of the applied radiation and measuring the absorbed energy at each frequency. The absorption spectrum is usually given as a plot of the absorbance, A, or the extinction coefficient, ϵ, as a function of the the wavelength (usually in nm) or the wavenumber.[†] From the $\epsilon(\lambda)$-function, two parameters are often extracted to characterize a molecular absorption band; the position of the maximum ($\lambda_{\max}$) and the value of the extinction coefficient at $\lambda_{\max}$.

In an experimental situation the studied molecules are usually dissolved in some organic or inorganic solvent, such as water, ethanol or tetrahydrofuran (THF) as a few examples, and kept in special glass cells suitable for spectroscopy. Usually the solvent and cell are chosen so that they have low absorption in the measurement region. However, it is impossible for them to be zero, so their effect on the absorption spectrum have to be taken into account. If the cell has an absorption A_c, the solvent A_s and the sample A, the observed absorbance becomes

$$A_{\text{tot}} = A + A_c + A_s. \tag{4.1}$$

[†]Wavenumbers are reciprocal wavelengths and given in units of cm^{-1}. If the wavelength λ is given in nanometers, the wavenumber $\bar{\nu}$ is found from $\bar{\nu} = 10^7/\lambda$. Wavenumbers have the advantage of being proportional to the photon energy ($E = h\nu = hc/\lambda = \hbar\omega$).

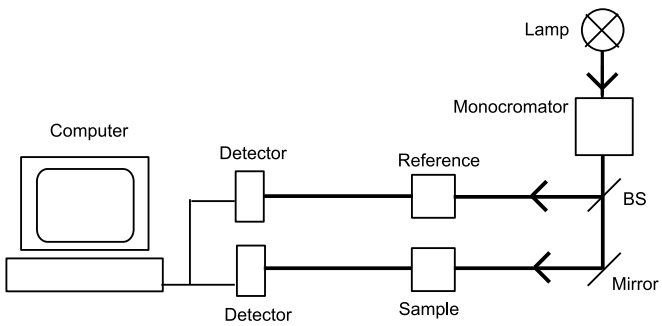

Figure 4.1: Schematic setup of an absorption spectrometer. The monitoring wavelength is selected by a monochromator. A beam splitter (BS) and mirror splits the beam and aligns the two beams onto the reference and sample. Two detectors quantifies the transmitted radiation in each beam-path.

To account for the solvent and cell absorption a reference sample is prepared with an equal glass cell containing pure solvent. A typical absorption measurement setup is shown in Figure 4.1. Here, a measurement of the sample- and the reference-transmittance can be obtained at the same time, and the molecular absorbance calculated from the transmitted intensity collected in the two beam paths.

To account for a difference in beam intensity in the two paths, a baseline needs to be found. Measuring the intensity arriving at both detectors without the reference and sample inserted, two baseline intensity spectra I_0^R and I_0^S are found and stored. Inserting the reference and sample, and again collecting the transmitted intensity, yields two new intensity spectra I^R and I^S, respectively. The molecular absorbance at each wavelength can then be calculated from

$$\begin{aligned} A &= A_{\text{tot}} - A_{\text{ref}} = (A + A_c + A_s) - (A_c + A_s) = \\ &= \log\left(\frac{I_0^S}{I^S}\right) - \log\left(\frac{I_0^R}{I^R}\right) = \log\left(\frac{I_0^S}{I^S}\frac{I^R}{I_0^R}\right). \end{aligned} \tag{4.2}$$

The photon energy needed to excite the molecule into a higher electronic level is typically in the visible ($400-750$ nm) and ultraviolet ($200-400$ nm) region.[29] However, the molecules also possess quantized vibrational energy levels, and for each electronic level there are many such vibrational states.[36] The energy difference of the vibrational levels are much smaller than the electronic ones and hence they will appear as a sort of fine-structure of the electronic levels. The

difference in vibrational energy levels are typically somewhere in the infrared region ($1000 - 4000\ \mathrm{cm}^{-1}$).[29] This means that at room temperature vibrations are in their lowest energy state.

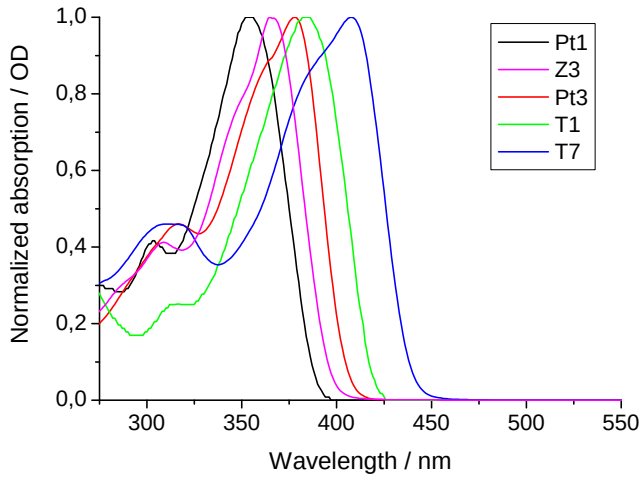

Figure 4.2: Absorption spectra of Pt1 (black), Z3 (magenta), Pt3 (red), T1 (green) and T7 (blue) all dissolved in THF. Data are normalized for spectral comparison.

The existence of the vibrational energy levels gives rise to a vibrational structure and a broadening of the absorption band.[36] With the additional solvent effects and the freedom of the molecules to move in the solvent, the vibrational peaks are smeared out to a broad and nearly structureless absorption band.

Typical absorption spectra of the compounds Pt1, Pt3, T1, T7, Z3 in THF solution are shown in Figure 4.2. These compounds were studied in Papers I to IV. We can see that the different compounds have their absorption at slightly different parts of the UV and blue part of the visible spectrum. All compounds are transparent in the rest of the visible spectrum. Steady state optical absorption spectra were usually recorded in $1 - 10\ \mu$M solutions using a Shimadzu UV-1601PC spectrometer or an Agilent 8453E UV-visible spectroscopy system.

4.2 Emission spectroscopy

As opposed to basic absorption spectroscopy, which is quite simple and generally obtained in steady state, emission spectroscopy opens up new possibilities e.g. by studying the time dependence and polarization properties of the transitions. First of all, it is interesting to collect the emission spectrum of the excited species. That is, at what wavelengths does it emit light, and what's the strength of the emission at the different wavelengths. As noted above, fluorescence emission occur at slightly longer wavelengths than the absorption. In addition, phosphorescence may occur at even longer wavelengths. Since the fluorescence and phosphorescence are collected at other frequencies than the excitation, the background signal is generally low.[29] The collection geometry is also usually at a right angle from the excitation direction, minimizing any background signal.[36] A schematic setup for the emission measurements is shown in Figure 4.3.

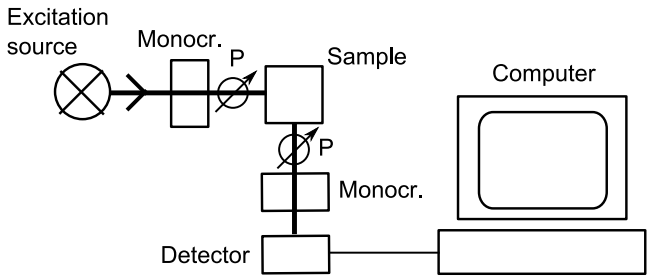

Figure 4.3: Schematic principle of a usual emission spectrometer, with detection angle at 90°. Excitation source can be a laser, lamp, etc. Monochromator and polarizers (P) are shown, and are inserted as desired. Detected emission intensity is collected and monitored using the computer.

The position of the maximum fluorescence intensity (λ_{em}) is a characteristic of the fluorescence spectrum. The same is the case for the phosphorescence with maximum intensity at λ_{ph}. The other two basic characteristics of the fluorescence and phosphorescence, namely the excited state lifetime and the quantum efficiency are discussed in the following sections. It's important to note that the position of the emission maximum is very sensitive to the environment, that is, usually the solvent.[29] Solvent effects, such as the degree of polarity, causes the structure of the excited molecule to adjust its geometry to the surrounding before the emission occur.[36] This will lower the energy of the

excited state. The available vibrational levels of the ground state will now not be optimal and therefore slightly higher in energy than usual. The $v' = 0 \rightarrow v'' = 0$ emission in Figure 2.1 will therefore be of slightly longer wavelength than the $v'' = 0 \rightarrow v' = 0$ absorption transition.[36] This gives rise to a splitting effect between the absorption and emission band. The difference between the maximum of the absorption and emission band is known as the Stokes shift, and the size of the shift is strongly related to the solvent in use.[36]

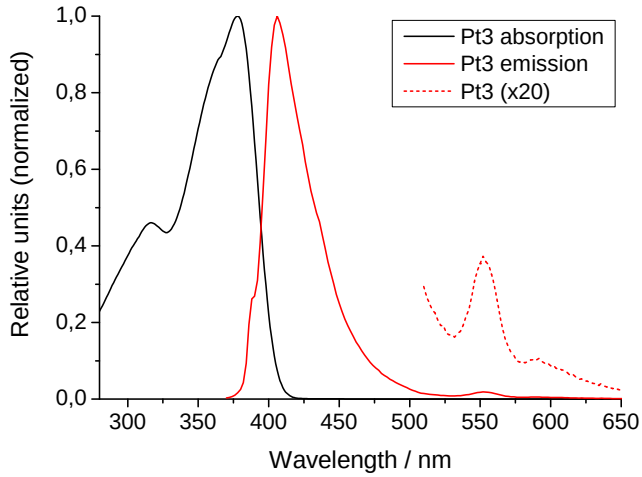

Figure 4.4: Absorption and emission spectra of Pt3 in THF. The black curve is the absorption spectrum with $\lambda_{max} = 378$ nm, and the red curve the emission spectrum excited at 390 nm, with a clear fluorescence band. The fluorescence maximum is at $\lambda_{em} = 406$ nm. The part of the emission spectrum around 550 nm (red dotted line) is magnified to show the weak phosphorescence peak with $\lambda_{ph} = 555$ nm.

The absorption and emission spectra of the Pt3 compound are shown in Figure 4.4. Here we note the Stokes shift between the absorption and fluorescence emission band. The emission spectrum (red) shows two distinct peaks, with a maximum around 400 nm and an additional much weaker band around 550 nm. The two distinct bands are interpreted as fluorescence ($400 - 500$ nm) and phosphorescence ($530 - 650$ nm). In order to do so, one must however, measure the relaxation times of the two bands, where it is found that the left band decays in order of nanoseconds, while the right band decays in the order of microseconds to milliseconds. Lifetime measurements will be discussed in a following section.

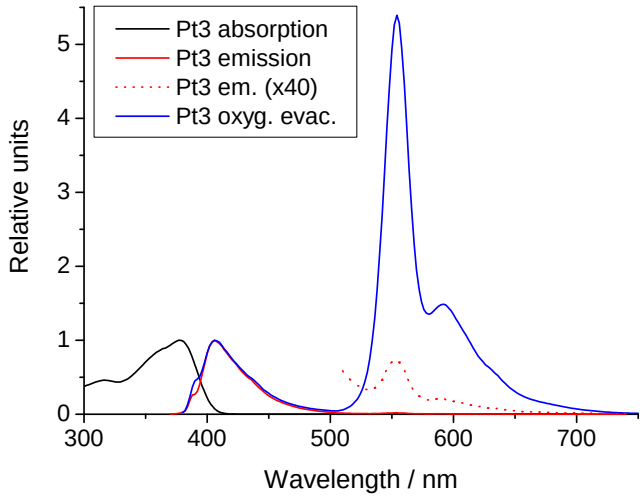

Figure 4.5: Absorption and emission spectra of Pt3 in THF. The red line shows the emission spectrum with oxygen present in the sample. The spectrum is magnified around 550 nm (red dotted). The emission spectrum from an oxygen evacuated solution shows an enhanced phosphorescence emission (blue).

It is known that phosphorescence, originating from a triplet excited state, is efficiently quenched by the presence of oxygen in the solution. (See more below.) In Paper II – IV we showed how this affect the phosphorescence efficiency, and how the phosphorescence increases by several order of magnitudes after the oxygen has been removed from the solutions. As an example, the emission spectrum of Pt3 in an oxygen evacuated sample are shown, together with the spectra of Figure 4.4, in Figure 4.5 (blue). Note the unchanged fluorescence part of the spectrum, essentially independent of oxygen content.

4.3 Deoxygenation of solutions

Oxygen (O_2) is one of a few molecules with a triplet ground state.[33] Oxygen is also easily dissolved in most liquids, and may therefore easily interact with any other triplet states in the solution. Oxygen will efficiently quench other excited triplet states during collisions, and any phosphorescence will be reduced significantly.[37] The reaction equation for the quenching process is given by[35]

$$^3M^* + {}^3O_2 \rightarrow {}^1M + {}^1O_2^*, \tag{4.3}$$

where $^3M^*$ is the excited triplet state being quenched, and ^1M is the corresponding singlet ground state. $^3O_2$ is the triplet ground state of oxygen and $^1O_2^*$ is an oxygen excited singlet state, which could relax by phosphorescence around 1270 nm.[112] The involvement of oxygen quenching on Pt-acetylides has been studied by e.g. Lindgren et al.[107]

Therefore, in order to study the phosphorescence, oxygen must be removed from the solution. Two methods for degassing the samples (in THF solution) were utilized in this study. In the first method samples were purged for 15 minutes with argon gas through a syringe needle. Since argon is a slightly heavier gas than oxygen, it will replace most of the oxygen in the solution. The method is quite fast, but had the disadvantage of oxygen diffusing back into the solution after the purging stops. This limits the time span and consistency of consecutive measurements.

In the other method a custom made vacuum line was build, utilizing a high-vacuum pump ($\sim 10^{-4}$ mBar) to remove the air from the solution. The degassing of the samples was performed by six freeze-pump-thaw cycles. The set-up has both an oil diffusion pump (Leybold Trivac, D1,6B) and an efficient turbo-pump (Varian, Model NW40 H/O) working in series. The experimental setup is shown in Figure 4.6. The samples were placed in 10 mm quartz cells

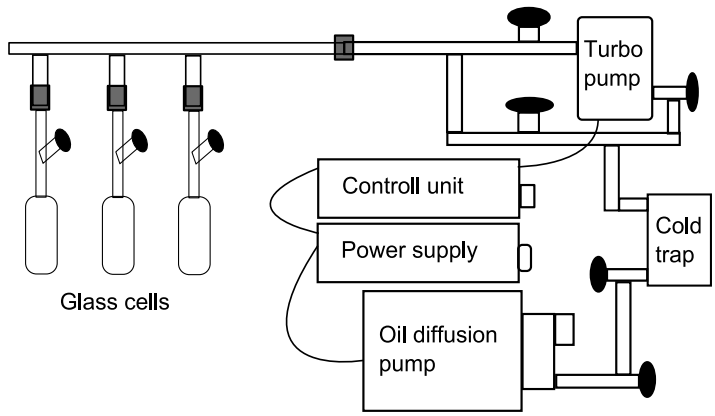

Figure 4.6: Schematic setup for the vacuum line with the pump system. An oil diffusion pump and turbo-pump are working in series. The setup has a control unit for the turbo pump (Turbotronic NT50), power supply (Leybold PT50) and cold trap (ALC TEL, LNT 25S). The glass cells are connected to the vacuum line.

(Hellma Precision) with custom made glass vacuum-line connections with closing valves. Because the measurement cells were custom made to fit the vacuum line, the cell could be directly put into the measurement setup after vacuum pumping, without subsequent transferring the sample to another cell. No air leakage through the valve was detected even several days after degassing.

As we have seen, removing oxygen/air from the sample significantly enhances the phosphorescence part of the emission spectrum. This also results in the lifetimes of the excited triplet state being prolonged by three orders of magnitude. This has been shown in the literature[37] and for several of the platinum complexes in Papers II, III and IV, and related paper 2. In Paper II, we also show the phosphorescence emission from singlet oxygen created by the interaction with the platinum-acetylide triplet state in open air samples.

4.4 Luminescence lifetime measurements

4.4.1 Time-correlated single-photon counting

Time-Correlated Single-Photon Counting (TCSPC) is one of the most widely used methods for time-domain measurements and for other photon counting data acquisition experiments today.[37] The use of this technique was first reported in 1961.[113] The TCSPC technique is based on the principle that the statistical probability distribution for the emission of a single fluorescent photon is equivalent to the actual intensity versus time distribution for all photons emitted.[‡]

TCSPC is a digital technique utilizing a time-to-amplitude converter (TAC). The measurement procedure, described in detail by Lakowicz[37] and Birch[115], follows the schematics of Figure 4.7. In general it goes as follows: A pulsed light source (flashlamp, LED, mode-locked laser) generates a short excitation pulse, which excites the sample. The same pulse triggers the start of the time measurement (TAC Start), or the system controls and triggers the excitation source internally. After being excited, the sample will emit photons according to the probability for spontaneous emission.

The first emitted photon detected by the photomultiplier tube triggers the TAC Stop. The start pulse triggers the charging of a capacitor in the TAC,

[‡]This is known as the ergodic principle of statistics. A process is ergodic if 'time averages' over a single realization of the process converge in mean square to the corresponding 'ensemble averages' over many realizations.[114]

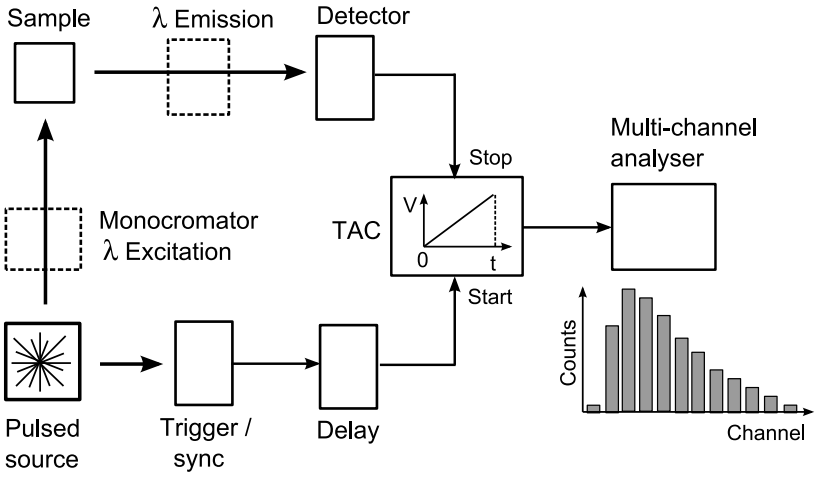

Figure 4.7: Schematic of the TCSPC measurements procedure. See details in text. A delay is introduced due to the different path-lengths of the start and stop signal.

which increases its voltage until a stop-pulse is detected. If no photon is detected in a preselected TAC range the systems resets and awaits the next start pulse.[§] The TAC produces an output pulse whose voltage is proportional to the time between the start and stop signal. The voltage is then converted to a time channel by a multi-channel analyzer (MCA). The sample is repetitively excited and for each excitation pulse a time window is opened waiting for the stop-signal. Summing over many pulses the MCA builds up a histogram of counts versus time channel. The experiment is continued usually until it has collected at least 10,000 counts in the peak channel.[¶]

The nature of the TAC operation is such that it only register the first fluorescent photon after the start pulse. However, if many photons arrive at the detector resulting from the same excitation, only the first will be detected. From the random probability distribution, more photons arrive at early times than at late times. However, if several photons arrive, only the first is detected. Many late photons will be disregarded and the intensity decay time will be shorter than the true value.[37] In order to account for this, the counting

[§]In our system (JobinYvon IBH DataStation Hub) the shortest TAC range is 50 ns over 4096 channels (highest resolution).

[¶]This depends of course on the desired dynamic range and the back-ground 'dark' counts.

rate is limited to below 1-2% of the excitation pulses. Then the likelihood of more than one photon arriving after each excitation pulse is reduced, and it is generally believed that enough late pulses are detected for the correct decay time to be obtained.[115]

4.4.2 Multi-channel scaling

The TCSPC technique enables us to measure short decay times down to $10-100$ ps with great accuracy. Utilizing high repetition rate excitation sources ($\sim$1 MHz) the measurements procedure is quite efficient. At longer decay times, as for those originating from phosphorescence, the pulsed excitation repetition rate must be somewhat slower than the relaxation time to be measured. Then it becomes time consuming, and a waste of the short instrumentation response time, to measure only one photon per excitation pulse.

For decay times in the order of milliseconds and longer, it is more convenient to use another counting method called Multi-Channel Scaling (MCS). This can be thought of as many photon counters working in series, with one counter for each data channel in the decay trace. The total time range is then the number of channels $\times$ time per channel. In our system** the minimum time per channel is 500 ns, and the minimum number of channels is 100, so the shortest time-window in a typical set-up is 50 μs. The excitation source triggers the start of the first channel to be opened, and the number of photons detected in this channel is collected. Then the system progresses to the next channel (time-window), and continues until the last channel is ended. The number of counts in each channel is continuously plotted in a histogram. The measurement is repeated over all channels for each excitation pulse, integrating the counts so that a decay builds up in the histogram.

4.4.3 Data analysis

Even though short pulsed excitation ($\leq$ ns duration) is used, and the system has short response time in the TCSPC mode, the relaxation times are of comparable orders of magnitude and the excitation pulse can not be considered as a δ-function.[37,††] This requires an additional recording of the instrumental

**JobinYvon IBH DataStation Hub.

††This is, however, sometimes possible in the MSC mode, due to the relatively long time per channel, much longer than the instrumental response time and excitation pulse length.

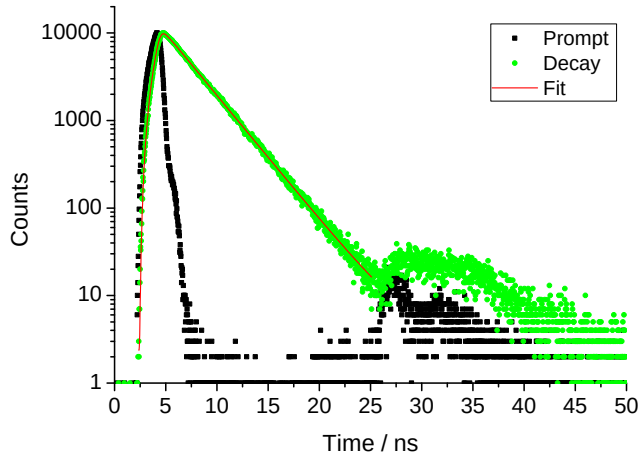

Figure 4.8: Prompt function and relaxation decay of Coumarin 110 in THF, excited at 373 nm using the NanoLED. Emission measured at 420 nm. Single exponential decay with lifetime $\tau = 2.4$ ns.

response function (prompt) of the excitation pulse, prior to any analysis of the decay curve.[‡‡] If the theoretical response function (with δ-function excitation) is $i(t)$, and the instrumental response function is noted as $P(t)$ the actual measured relaxation curve $F(t)$ will be a convolution integral of the instrumental response function and the actual decay. It can be written as[115]

$$F(t) = \int_0^t P(t')\, i(t - t')\, \mathrm{d}t', \tag{4.4}$$

where the integral goes over the excitation response function. In order for the experimental data to be fitted to a decay model (e.g. a single or double exponential) the decay model needs to be convoluted with the prompt. By iterating the values of the decay components until the best fit is obtained, the relaxation time of the studied species is found. An example of a such a decay is shown in Figure 4.8, with the decay curve of the reference compound Coumarin 110 (C110) in THF. The NanoLED, with a pulse FMWH of approx. 1 ns, was used as excitation source, but somewhat shorter response functions can be obtained using the mode-locked laser. (See Section 4.6.) The prompt is of significant size and the need for convolution analysis is clear. The decay is found to be single exponential with a relaxation time of 2.4 ns. Due to

[‡‡]The prompt signal also contain time-uncertainties from other sources in the detector elements.

the logarithmic y-axis in Figure 4.8, the single exponential becomes a straight line. The C110-compound is characterized in paper I and VI, and used as two-photon absorption reference in papers I, II and III.

4.5 Measuring the quantum efficiency

Due to the close relations to the natural properties of the molecule, the fluorescence and phosphorescence lifetime and quantum efficiencies are perhaps some of the most important characteristics of a fluorophore. Measuring the quantum efficiency (QE) is, however, difficult, and requires great care in instrumentation and methodology.[116] Due to this fact, a large number of fluorescence quantum yields reported in the literature are wrong.[117] In principle, two main methods can be used to find the quantum yield; an absolute determination, or relative to another sample with known QE. The second method is the easiest, most commonly used, and probably the most reliable method, therefore we treat only the method of quantum yield comparison with standards in this text. A comprehensive review of the measurement of quantum yields, summarizing the disadvantages and problems with the different measurement methods, are given by Demas and Crosby.[117]

4.5.1 Method

Relative fluorescence quantum yields can be calculated from spectral absorption and fluorescence measurements taken at different concentrations. The absorbance at the excitation wavelength and the corrected integrated fluorescence are collected at each concentration. The gradient of the integrated fluorescence versus absorbance is found from the data points. The relative quantum yield of two samples is given by the equation[118]

$$\frac{\Phi_X}{\Phi_{\mathrm{Ref}}} = \frac{A_{\mathrm{Ref}}}{A_X} \cdot \frac{F_X}{F_{\mathrm{Ref}}} \cdot \frac{n_X^2}{n_{\mathrm{Ref}}^2} \,, \tag{4.5}$$

where indices 'X' and 'Ref' are associated with the two samples – one being the unknown sample (X) and the other the reference sample (Ref). A is the absorbance at the excitation wavelength, F is the corrected integrated fluorescence spectrum, and n is the refractive index of the solvent. Plotting the integrated fluorescence versus the absorbance at different concentrations would give a diagram something like the one shown in Figure 4.9. The gradient

of the straight lines would be

$$\mathrm{Grad}_i = \frac{\Delta F_i}{\Delta A_i} \,. \tag{4.6}$$

and equation (4.5) could be reduced to[119]

$$\frac{\Phi_X}{\Phi_{\mathrm{Ref}}} = \frac{\mathrm{Grad}_X}{\mathrm{Grad}_{\mathrm{Ref}}} \cdot \frac{n_x^2}{n_{\mathrm{Ref}}^2} \,. \tag{4.7}$$

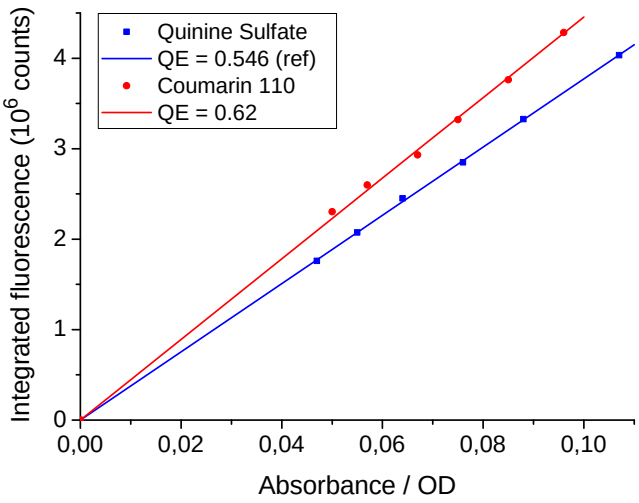

Figure 4.9: Relative quantum efficiency for Quinine Sulfate in 0.5 M H_2SO_4 and Coumarin 110 in THF. Quinine Sulfate is a well known quantum yield standard with known quantum efficiency of 0.546.

In both equations (4.5) and (4.7) it is assumed that both samples are excited at the same wavelengths.[37] In addition, the absorbance (optical density) of the two samples should be kept below 0.1 in 1 cm cells, in order to reduce re-absorption effects and inner filter effects. In a centrally positioned sample the inner filter effects can be accounted for by using

$$F_{\mathrm{corr}} = F_{\mathrm{obs}} \cdot \exp(A/2) \,, \tag{4.8}$$

where F_{corr} and F_{obs} are the corrected and observed integrated fluorescence at absorption A.[37]

Using a reference sample with known quantum efficiency of Φ_{Ref}, the absolute value of the unknown sample, Φ_X, is found from the calculated relative value.

A detailed measurement procedure with experimental considerations are also given in 'A Guide to Recording Fluorescence Quantum Yields' from Jobin Yvon.[119] The quantum efficiency values found from this procedure would be expected to be correct within 5-10% error, depending on the quality of the data.

Due to different sensitivity and efficiency of the emission monochromator and detector as a function of wavelength, the recorded emission spectrum needs to be corrected to account for this difference in sensitivity.[116,117] If this is not done, the integrated fluorescence data would not be correct and comparable between the samples, and the calculated efficiency would be wrong. In order to correct the emission spectra, a sensitivity calibration curve is measured for the whole detection system. The sensitivity curve is then included in the quantum efficiency calculation analysis.

In the determination of the quantum efficiency using eq. (4.7), a series of different solvents were used. It was assumed that the refractive index is not changed by the presence of the solute. The following refractive indices, given at approximately 400 nm at 20 °C, were used:[120] Water (H_2O): $n = 1.34$, Ethanol (C_2H_5OH): $n = 1.37$, Sulfuric Acid (H_2SO_4): $n = 1.43$ and THF (C_4H_8O): $n = 1.41$.

4.5.2 Fluorescent quantum yield standards

In order to calculate absolute quantum efficiencies from relative quantum yield measurements, a standard reference sample with known quantum yield is needed. Several quantum yield standards have been investigated and reported, however, the reported quantum yields differ, sometimes considerable, between the authors.[116–118,121]

In order to characterize the studied samples, and the new standards suitable for other reference purposes, in this work, we have used Fluorescein and Quinine Sulfate as standard quantum efficiency references. Both of these are suitable references in the desired wavelength range. We have used the quantum efficiency values given by Demas and Crosby[117] in this study. They are $\Phi_{QS} = 0.546$ for Quinine Sulfate in 0.5 M H_2SO_4, and $\Phi_F = 0.92$ in 0.1 M NaOH. Similar values are given in the work of e.g. Dawson[122] and Magde[123].

In Paper I and VI the laser dye Coumarin 110 (C110) was fully characterized for its photo-physical properties, using e.g. Quinine Sulfate as quantum yield

reference. There, we reported the QE value for C110 to be $\Phi_{\mathrm{C110}} = 0.62$, as shown in Figure 4.9.

4.5.3 Error calculations

The analysis of the quantum efficiency data is based on the gradient of a straight line starting in the origin and passing through several data points, as shown in Figure 4.9. A straight line, $y = m \cdot x + c$, is fitted to the data points to find the best line which passes as closely as possible through all data points. This is usually done in a standard manner following the method of least squares.[124] If the n data points come in pairs as (x_i, y_i), the best values for m and c are found by taking the minimum of the function

$$S = \sum_n (y_i - mx_i - c)^2. \tag{4.9}$$

It follows that the best values of m and c are found from[124]

$$m = \frac{\sum (x_i - \bar{x}) y_i}{\sum (x_i - \bar{x})^2} \qquad \text{and} \qquad c = \bar{y} - m\bar{x}, \tag{4.10}$$

where $\bar{x} = \frac{1}{n} \sum x_i$ and $\bar{y} = \frac{1}{n} \sum y_i$ notes the center of gravity of all points.

The standard errors, or uncertainties, of the fitted values are given by[124]

$$(\Delta m)^2 = \frac{1}{D} \frac{\sum d_i^2}{(n-2)} \qquad \text{and} \qquad (\Delta c)^2 = \Big(\frac{1}{n} + \frac{\bar{x}^2}{D}\Big) \frac{\sum d_i^2}{(n-2)} \tag{4.11}$$

where $d_i = y_i - mx_i - c$ and $D = \sum (x_i - \bar{x})^2$.

Typical data in a quantum efficiency measurement are shown in Figure 4.10. Measured data are shown as red dots, and the best fit as the red line. The best fit is given by the parameters: $m = 61.27 \pm 0.83$ and $c = 0.025 \pm 0.035$, where the gradient error is 1.3%. Dividing two such numbers would give a total error of approximately 2%. The uncertainty in the line is shown as the green and blue lines in Figure 4.10. Results of some quantum efficiency measurements are discussed in Paper VI and in Section 5.1. The total uncertainty in a new quantum efficiency value is, however, also dependent on the uncertainty in the quantum efficiency of the reference compound.

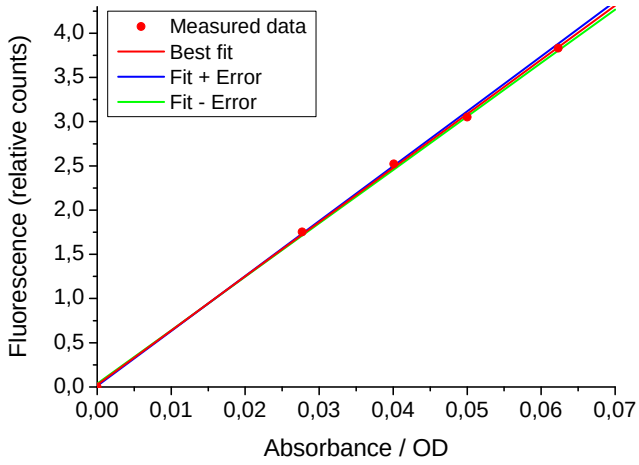

Figure 4.10: Quantum efficiency data for Coumarin 334 (red dots). Best fit (red line) and slope uncertainty (blue and green line) is shown.

4.6 Spectral and time-resolved measurement setup

In all spectrally and time-resolved measurements in Section 4.2 (Emission spectroscopy), Section 4.4 (Luminescence lifetime measurements), Section 4.5 (Measuring the quantum efficiency) and Section 4.9.2 (Two-photon excited fluorescence), essentially the same measurement setup was applied. This setup is shown in Figure 4.11, where different light sources were applied depending on the experimental requirements.

The main radiation source was a 200 fs pulsed Ti:Sapphire laser (Coherent MIRA 900-F). This laser is pumped by a frequency doubled Nd:Vanadate (Nd:YVO_4) laser (Coherent Verdi-V10) at 532 nm with 10 W CW power. The Ti:Sapp laser is wavelength tunable from 700 nm to 1100 nm, however it was mainly used in the $700 - 900$ nm region. The pulse repetition frequency (prf) is 76 MHz with a pulse energy between 7 and 25 nJ, corresponding to an average power of 0.5 to 2 W, depending on the wavelength. To control and reduce the pulse repetition frequency, desirable in some of the experiments, a pulse picker, or Acousto-Optic Modulator, (Coherent 9200 Pulse Picker) was placed after the laser to reduce the prf. to between 9 kHz and 4.75 MHz. Using the external laser system in the luminescence measurements, a pulse reference is needed for the collection system. The IBH TB-01 module (optical trigger) was used as time-reference using a thin glass wedge to take out a small part of

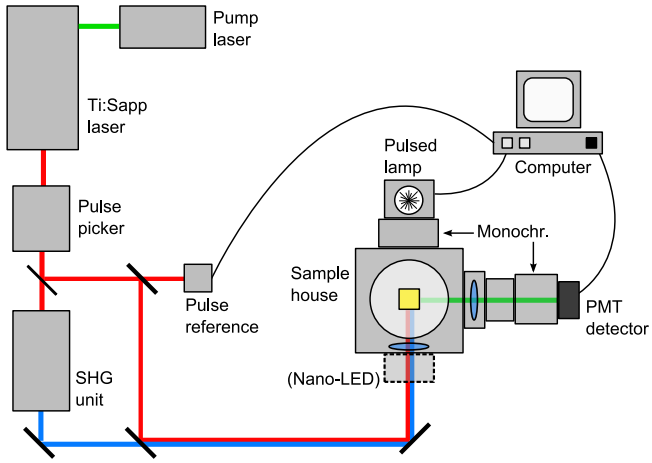

Figure 4.11: Experimental setup for luminescence and time resolved measurements. Possible excitation sources are Ti:S laser, Nano-LED and flash-lamp. See details in text.

the fundamental laser beam. For single photon excitation measurements the fundamental laser beam was frequency doubled using a SHG crystal (Inrad Ultrafast Harmonic Generation System, Model 5-050). We then obtained possible excitation wavelengths in the ultraviolet and blue spectral regions from 350 nm to 450 nm. For two-photon excitation, and in the z-scan experiments treated in Section 4.9.1, the red fundamental beam was used directly as shown in Figures 4.11 and 4.19.

As time and spectrally resolved detection unit, a Jobin Yvon IBH FluoroCube photon-counting spectrometer was used. It consists of a sample cube with entrance and exit ports for emission and excitation. The exit port consists of a collection lens, monochromator (5000M) and photomultiplier tube (PMT) detector (TBX-04 Picosecond photon detection module) working in the 300-850 nm region. The system could switch to a Hamamatsu NIR PMT module (H9170-75) for detection in the range $900-1600$ nm. The monochromator can select the detected light with a resolution of 1 nm. The system also have the possibility to insert polarizers at both entrance and exit ports. All software and hardware are provided by HORIBA Jobin Yvon. Steady state emission spectra in the two detector wavelength regions were recorded by scanning the monochromator in front of the PMT, and collecting the number of detected photons at each wavelength, for a given pulse repetition frequency.

For lifetime measurements, the fluorescence and phosphorescence decay times shorter than approximately 1 μs were measured using the system in time-correlated single photon counting (TC-SPC) mode, with a time resolution down to 0.014 ns. Longer triplet decay times from microseconds to seconds could be measured using the multi-channel scaling mode (MCS), with a time resolution down to 500 ns per channel.

The system was equipped with two internally controlled excitation sources. The NanoLED and a flashlamp. The NanoLED is a laser diode providing pulses with duration < 1 ns at 1 MHz pulse repetition frequency at selected wavelengths. Possible excitation wavelengths in the UV-blue spectral region were 278, 337, 373, 403, 443 and 469 nm for the system in use. Removing the NanoLED opens the possibility for the externally controlled Mira laser to be used, as shown in Figure 4.11.

The third available excitation source was the flashlamp (5000XeF Sub-microsecond Xenon Flashlamp). The lamp emits flashes of 0.1 to 0.8 μs duration with a pulse energy of 5 to 150 mJ with a spectral range covering the UV, visible and near infrared (NIR) regions. A monochromator was used to select the desired excitation wavelength. The system was usually operated at 20 Hz at high pulse energy, making it suitable for measuring long phosphorescence lifetimes. Scanning the excitation monochromator, monitoring at a fixed emission wavelength, also provides the opportunity for recording excitation spectra.

4.7 Transient absorption spectroscopy

Transient absorption spectroscopy is an extension of absorption spectroscopy. In this technique, also called flash photolysis,[27] the absorption of a sample is measured as a function of time after excitation by a flash of light, and therefore against a background of reduced ground state absorption.[35] Typically both the excitation light ('pump') and the light for measuring the absorption ('probe') are generated by pulsed light sources (lasers or flash-lamps). The technique of flash photolysis was introduced by Porter in 1950.[125]

The technique is utilized to study the absorption and dynamics of excited states, that is absorption from the S_1 and T_1 states, and are therefore also referred to as excited state absorption (ESA). Due to short fluorescence lifetimes of the molecules in our study and the efficient inter-system crossing, a large fraction of the initially excited molecules are transferred to the triplet

T_1 state. Now the triplet absorption properties can be observed during the lifetime of the excited state.

A miniaturized flash photolysis equipment, composed of commercial and purpose built units, was used in this investigation.[126] A schematic setup is shown in Figure 4.12. The pump beam is generated by discharging a capacitor (of capacitance $C = 2$ μF) through a linear flash-lamp (EG&G Model FXQ 269-1). The energy ($E = \frac{1}{2}CV^2$) of each flash (of ca. 5 μs duration) was set by applying a voltage V of 3 kV. Only a fraction of the electrical energy is actually converted into light, and only a fraction (amounting to ca. 10 mJ) of the emitted light falls upon the sample, after passing through a pair of lenses. A part of the pump flash is picked up by a photomultiplier, whose output goes to a delay generator (Princeton Instruments, Model PG200) and a digital oscilloscope (LeCroy 9410). The delayed signal (after a variable preset delay) triggers the probe lamp (EG&G Model FX-409U) which has a duration of about 2 μs.

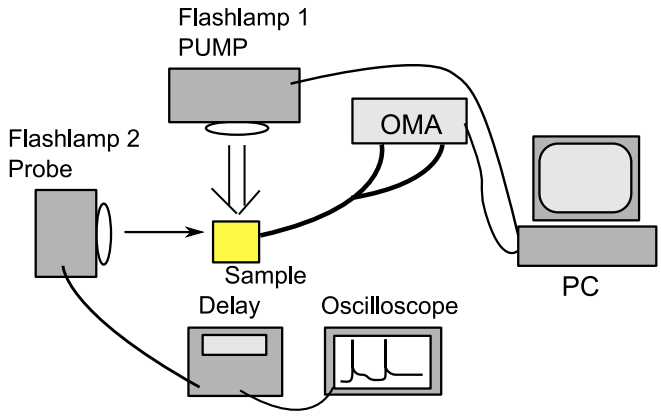

Figure 4.12: Schematic setup of the transient absorption measurement. Flash-lamp 1 (pump) excites the sample. The probe light (flash-lamp 2) hits the sample at 90 degrees angle, with a specified time delay controlled by the delay-box. The actual time difference can be observed on the oscilloscope. Home-made computer software controls the flashes and the readings from the OMA. (Not all wiring is shown in the drawing.)

The probe light, travelling at a right angle to the pump beam, is made to pass through the front portion of the sample (where the excited-state population has the largest density) and is directed, after its emergence from the sample

cell, by an optical fiber to an optical multichannel analyzer (OMA) (Zeiss, MCS 224) controlled by a computer using a home-made software. The time resolution of the system is determined by the temporal width of the probe flash, and the sensing elements receive not only the probe light but also a fraction of the fluorescence and phosphorescence provoked by the pump source. This induced emission therefore has to be corrected for in the transmission spectrum. The detailed calibration and measurement procedure are described in detail in Paper IV.

The transient absorption spectrum $\Delta A(\lambda, t)$ is the change in absorption of a sample when it is struck by the pump flash (at time $t = 0$) followed by the absorption measurement taken later at time t. The ground state absorption (taken at some time $t < 0$), is given by $A_g(\lambda) = \epsilon_g(\lambda) \cdot C \cdot L$, where C is the sample concentration (initially all in the ground state), and L is the sample length (here 10 mm). The absorption at time t after the pump light is given by

$$A(\lambda, t) = \epsilon_T(\lambda) \cdot C_T \cdot L + \epsilon_g(\lambda) \cdot (C - C_T) \cdot L, \tag{4.12}$$

that is; absorption by the excited molecules with concentration C_T, plus the absorption by the molecules still remaining in the ground state. The transient absorption then becomes

$$\Delta A(\lambda, t) = A(\lambda, t) - A_g(\lambda) = (\epsilon_T(\lambda) - \epsilon_g(\lambda)) \cdot C_T \cdot L. \tag{4.13}$$

The reconstruction of the true excited state absorption spectrum $A_T(\lambda, t)$ is done by adding a specific amount of ground state absorption to $\Delta A(\lambda, t)$, corresponding to the amount of molecules removed from the ground state, $\epsilon_g(\lambda) \cdot C_T \cdot L$, such that all the ground state depletion structure is removed from the transient absorption spectrum, as shown in Figure 4.13. From this, the extinction coefficient of the (triplet) excited state $\epsilon_T(\lambda)$ can be determined by comparing it to the corresponding ground state absorption, as done in Paper IV.

Data of triplet absorption decay with increasing pulse delay between pump and probe pulses were analyzed including a triplet-triplet quenching term in the differential equation for the reduced triplet concentration with time:

$$\frac{\mathrm{d}C_T}{\mathrm{d}t} = -k_1 C_T - k_2 C_T^2, \tag{4.14}$$

where k_1 is the first order radiation decay constant, and k_2 is rate constant for triplet-triplet quenching processes. Equation (4.14) can be solved analytically

giving the solution

$$C_T(t) = \frac{\exp(-k_1 t)}{(1/C_T(0) + (1 - \frac{k_2}{k_1} \cdot \exp(-k_1 t)))}\,, \tag{4.15}$$

where $C_T(0)$ is the integration constant equal to the concentration of triplets at time zero (following the pump light). We note that if $k_2 = 0$ (no triplet-triplet quenching), equation (4.15) becomes a single exponential decay, as we should expect.

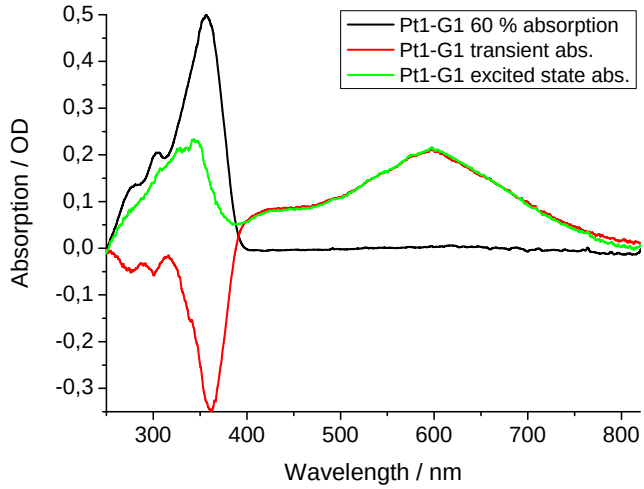

Figure 4.13: 60% absorption (black), transient absorption (red) and triplet excited state absorption (green) of Pt1-G1 in a 10 μM THF solution in a 1 cm cell.

4.8 Optical power limiting measurements

The materials also need to be characterized for their optical limiting capabilities. As stated in Section 1.4 the light needs to be focused down on the sample in order for the nonlinear effects to set in. Therefore a transmission focusing setup was used, as shown in Figure 4.14.[5,127] A Nd:YAG laser at 532 nm, delivering 5 ns pulses at 10 Hz, was used as a radiation source. The laser power was controlled using neutral density (ND) filters to give a pulse energy between $0-300$ μJ. An Optical Parametric Oscillator (OPO) system was used

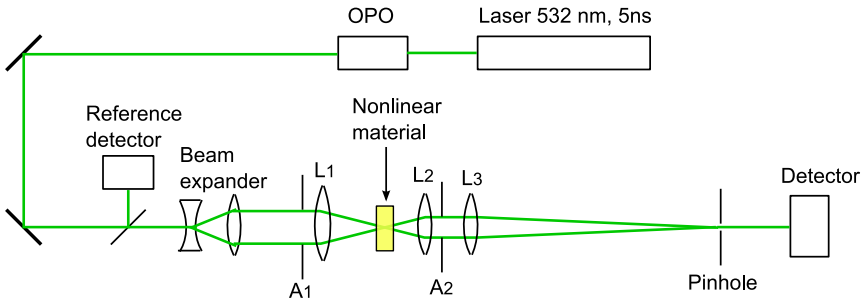

Figure 4.14: Schematic view of the OPL experimental setup. See details in text.

to change the laser wavelength from 532 nm to other wavelengths in the 500 and 600 nm region in some of the experiments.

A beam expanding telescope is used to expand the beam prior to the focusing lenses. An aperture (A_1) limits the diameter of the beam to 20 mm. The focusing and collimating lenses (L_1 and L_2) are chosen for a f/5 optical system with 2.5 times magnification. L_1 has a 100 mm focal length (FL), giving a spot size of approximately 2.7 μm at the focal point. L_2 has a 40 mm FL, and the aperture A_2 is 8 mm in diameter. The lens L_3 focuses the collimated beam, with a focal length of 1.5 meters, to a pinhole of 1.5 mm in diameter. Here, over 90% is transmitted with no sample inserted in the setup.

An energy calibration of the system is performed without any nonlinear material present. Then, after inserting the nonlinear materials, the transmitted pulse energy can be measured as a function of the incoming pulse energy. OPL data were obtained for 0.03 M or 0.05 M THF solutions in 2 mm quartz cells (Hellma Precision) (Paper II and III, and related papers 1 and 3), and for solid state materials PMMA type of similar thickness and concentrations (related paper 5). The OPL set-up, as described above, was located at the laser system lab at the Swedish Defence Research Agency (FOI) in Linköping.

A typical optical power limiting curve is shown in Figure 4.15. Here, the transmitted pulse energy through the nonlinear absorbing material (Pt1-G1 at 50 mM concentration) never exceeds 3 μJ, even though the input power is increased up to above 160 μJ. For comparison, a curve of 80% linear transmission is shown. In the small inset, the data from $0 - 10$ μJ input pulse energy are magnified for clearity.

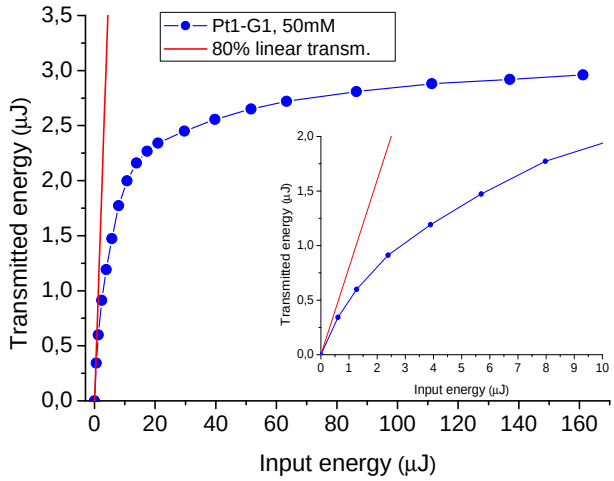

Figure 4.15: Optical power limiting of Pt1-G1 at 532 nm (blue dots). Sample concentration is 50 mM in THF. An 80% linear transmission curve (red) is shown for comparison.

4.9 Measuring the TPA cross section

High power pulsed lasers are today widely used in UV, visible and near-infrared (NIR) multi-photon spectroscopy.[42] Pulsed excitation is necessary to achieve simultaneous two-photon excitation because the two-photon absorption cross sections is in the order of magnitude 10^{-33} smaller than the one-photon cross section,[43] having cross sections in the order of 10^{-49} cm^4 s/photon. The TPA cross section is usually measured in Göppert-Mayer (GM) units, where 1 GM = 10^{-50} cm^4 s/photon.[128] TPA processes also have different selection rules than single-photon absorption, and can therefore reach electronic states forbidden by one-photon absorption.[27] For that reason TPA complements linear absorption spectroscopy in studying the excited states of molecules.

Direct measurement of the two-photon absorption coefficient and cross section, by recording the attenuation of the incident beam, is possible, but difficult for materials with a low numerical value for the cross section.[27] A method for such a direct measurement of the TPA coefficient is the z-scan technique as outlined below. The two-photon absorption cross section can also be found from the observed generated fluorescence following the two-photon excitation, if the fluorescence quantum efficiency of the material is known. This method is described in more detail in section 4.9.2 below.

4.9.1 Z-scan

An absolute determination of the two-photon absorption coefficient can be performed by measuring the attenuation of a focused laser beam as a function of the incoming intensity.[27] Such a method, called the z-scan technique, was first introduced in 1989 by Sheik-Bahae et al.[129] It was introduced as a high sensitivity technique for determining both the sign and the magnitude of the nonlinear refractive index n_2, and for determination of the nonlinear absorption coefficient β.[130] A thin nonlinear absorbing sample is placed in a focused laser beam. The focus creates an intensity variation in the longitudinal direction. As the sample is scanned in the longitudinal z-direction through the laser focus ($z = 0$), and as the transmitted light is simultaneously detected, a characteristic variation of the transmitted intensity as a function of the z-position appears. The schematic principle of the method is shown in Figure 4.16.

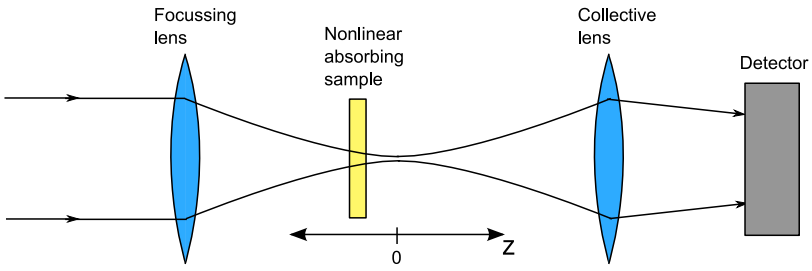

Figure 4.16: Schematic principle of the z-scan method. The transmitted light is detected as the sample is moved in the z-direction through the focus.

When the sample is far from the focus the intensity is quite low and the nonlinear absorption is weak. As the sample moves closer to the focal point the intensity increases and the nonlinear absorption becomes larger. The detected transmission will now be reduced. As the sample passes the focus, it passes the point of maximum intensity, and the transmitted power is at its lowest point. Continuing away from the focus, decreasing the intensity, the nonlinear effects will again become weaker, and the transmitted power increases again. A typical z-scan transmission curve is shown in Figure 4.17.

The lens focal length and size of the beam determines the Rayleigh length of

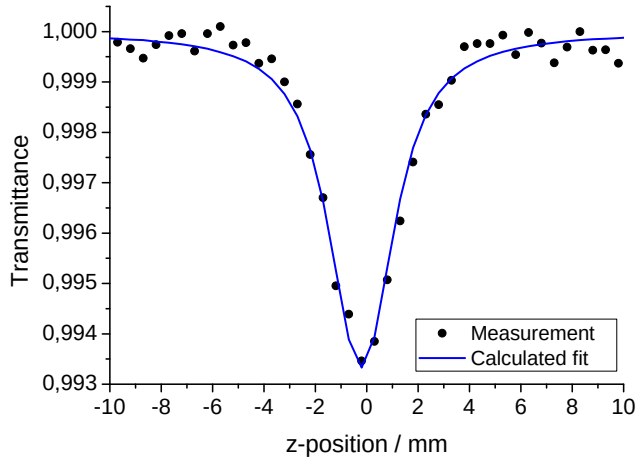

Figure 4.17: Typical normalized transmitted power as a function of z-position in a z-scan measurement. Measurement data are for Pt1-G1 in a 30 mM solution. A calculated fit using eq. (4.18) are shown, giving a TPA cross section of approximately 16 GM.

the focus. For a Gaussian beam the Rayleigh length in air is given by[13]

$$z_R = \frac{\pi\, w_0^2}{\lambda_0} = \frac{\lambda_0\, f^2}{\pi w_1^2}\,, \tag{4.16}$$

where w_0 is the $1/e$ radius of the beam at focus, f is the focal length and w_1 is the $1/e$ radius of the incoming beam. For a top-hat beam the minimum spot size if found from $w_0 = \lambda\, f/d$, where d is the diameter of the incoming beam.[131] The Rayleigh-length is still calculated from eq. (4.16).

In the thin sample limit, where the sample thickness L is smaller than the Rayleigh length, equation (2.16) is integrated to give the transmitted intensity[130]

$$I_t(z,r,t) = \frac{I(z,r,t)\, e^{-\alpha L}}{1 + \beta\, I(z,r,t)\, L_{\text{eff}}}\,. \tag{4.17}$$

Here, $I(z,r,t)$ is the incident intensity and $L_{\text{eff}} = (1 - \exp(-\alpha L))/\alpha$. For a Gaussian radial and temporal pulse the transmittance of the pulse at sample position z is found to be[130]

$$T(z) = \frac{\int_{\infty}^{\infty} \ln\!\left[1 + q_0(z,0) e^{-\tau^2}\right] \mathrm{d}\tau}{\sqrt{\pi}\, q_0(z,0)} = \sum_{m=0}^{\infty} \frac{\left[-q_0(z,0)\right]^m}{(m+1)^{3/2}}\,, \tag{4.18}$$

where $q_0(z,0) = \beta\, I_0(0)\, L_{\text{eff}}/(1+z^2/z_R^2)$, and $I_0(0)$ is the peak on axis intensity at the focus. In the last equality the integral is expressed as a sum, making it suitable for numerical evaluation, when $q_0(z,0) < 1$.

In the thick sample limit where $L > z_R$, the expression in eq. (4.17) is no longer valid because $I(z,r,t)$ varies significantly through the sample. This is desirable when for instance a tighter focus is needed to achieve a detectable signal.

Nonlinear absorption in the thick sample limit has been studied by e.g. A. Eriksson et al.[132–134] by use of a numerical mode expansion method, and by J. A. Hermann et al.[135,136] using a more analytical approach to the weakly nonlinear regime in the paraxial approximation. In the latter case, the instantaneous transmitted power through a nonlinear absorber with thickness L at position z away from the focus is[136]

$$\wp(z,L) = \frac{P_{\text{trans}}}{P_{\text{in}}} = 1 - \frac{Q_{0\text{R}}}{2}\left\{\left(1+\widehat{\alpha}_0\zeta\right)\left[\tan^{-1}(\zeta+\zeta_L) - \tan^{-1}(\zeta)\right] - \frac{\widehat{\alpha}_0}{2}\,\ln\left[\frac{1+(\zeta+\zeta_L)^2}{1+\zeta^2}\right]\right\}, \tag{4.19}$$

when linear absorption is sufficiently small. Here, $\zeta_L = L/(n_0 z_R)$, ζ is the distance z of the front interface from the waist position divided by z_R. $\widehat{\alpha}_0 = \alpha_0 n_0 z_R$ and $Q_{0\text{R}}$ contains the nonlinear parameter and is defined as $Q_{0\text{R}} = \beta\, I(0,z)\, n_0 z_R$. $I(0,z)$ is the on-axis (peak) intensity at a distance z from the focus. n_0 is the refractive index of the medium, z_R the Rayleigh length, β the two-photon absorption coefficient, α_0 the linear absorption coefficient.

The instantaneous transmitted power in equation (4.19) may be integrated over the temporal pulse profile (assumed Gaussian) to obtain the transmitted pulse energy. This introduces an extra factor $1/\sqrt{2}$ in the expression for $Q_{0\text{R}}$. The expressions in equation (4.18) and (4.19) are compared in the paper by Hermann.[135] Figure 4.18 shows a comparison of the two expressions in a $z_R = L$ setup, with less than 5% difference in analysys of the σ_2 vaule.

The analysis based on equation (4.19) was compared with the model based on the Crank-Nicholson approach to numerically solve the beam propagation and nonlinear absorption.[132] The two techniques were found to give identical results in simulations, as noted in Paper I.

In the experimental work reported in this thesis, the thick-sample analysis was applied since z_R was between $0.2 - 1.0$ mm, depending on the experiment,

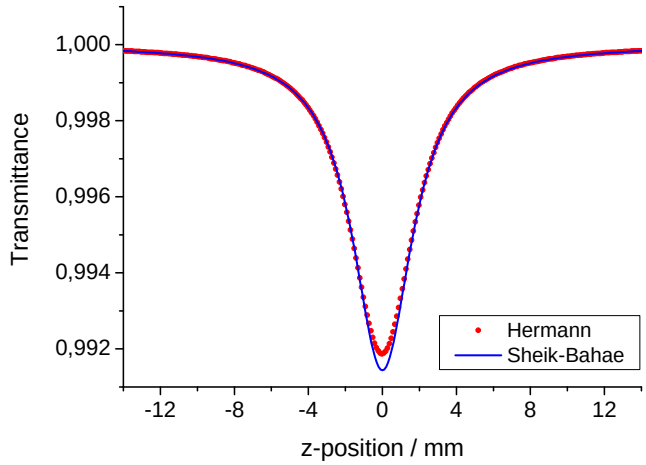

Figure 4.18: Theoretical transmittance of a 50 mM sample with $\sigma_2 = 20$ GM in a focusing setup with $z_R = L = 2$ mm ($I_0 = 5$ GW/cm^2 and $w_0 = 22$ μm), using equation (4.18) and (4.19). The curves would differ within 5% in an experimental analysis.

whereas the sample thickness was held constant at $L = 2$ mm. The focal length was 100 mm or 150 mm, with beam widths of 5-10 mm in diameter, and wavelengths varied between 700 and 800 nm.

The femtosecond Titanium:Sapphire laser was used as radiation source in the z-scan experiments. The laser and pulse picker set-up is identical as in the time-resolved spectroscopic measurements, as outlined in Section 4.6. To align the laser beam into the z-scan setup two mirrors were used (Newport Ultrafast BB with Rs $> 99\%$ at 45° and $700 - 930$ nm). The beam was expanded using two lenses with focal length -25 mm and +75.6 mm (Newport PCC UVFS -25 FL, and PCX UVFS +75.6 FL with BBAR coat $0.050 - 1.00$ μm). The focusing and collimating lenses were; Newport BCX UVFS 50.8 Dia x 150 FL, and PCX UVFS 25.4 Dia x 100 FL, respectively, both with BBAR coating between $0.65 - 1.00$ μm.

To detect the transmitted light a Newport 918-SL Low Power Photo Detector, connected to a Newport Power Meter Model 2930C, was used. The sample was placed in a sample holder upon a linear translation stage (Newport (M-)ILS Travel Linear Stage) connected to a Newport Universal Motion Controller/Driver Model ESP300. By connecting the detector and travel stage to a computer, both the power reading and sample position could be controlled

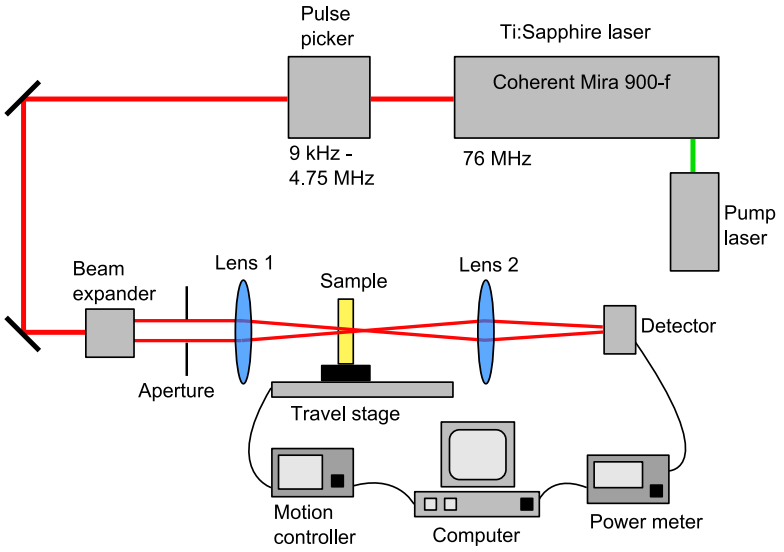

Figure 4.19: Experimental setup for the z-scan with laser, pulse picker, lenses, travel stage and collection hardware. See details in text.

simultaneously. To do this, an operation program was written in LabView 7.0 (National Instruments). A long pass filter (Melles Griot) with cut off at 590 nm was placed in front of the detector to remove any stray light due to luminescence. The z-scan experimental setup is shown in Figure 4.19.

4.9.2 Two-photon excited fluorescence

The two-photon absorption cross section can also be determined from the amount of emitted fluorescence. This is a relative technique, with procedures similar to the quantum efficiency technique outlined in Section 4.5. Therefore, a reference sample with known TPA cross section needs to be included. In addition, the analysis requires the knowledge of the quantum efficiency of both the sample and reference.[137]

The idea is that the molecules are being excited in a simultaneous two-photon process from the high intensity laser beam, and the regular fluorescence emission intensity is collected.[128] This is done both for the unknown and reference sample at the same excitation wavelength, focusing optics and collection geometry.

In general, the number of absorbed photons per unit time by a two-photon process, $N^{(2)}_{\mathrm{abs}}(t)$, is given by the expression[43]

$$N^{(2)}_{\mathrm{abs}}(t) = \int_V \mathrm{d}\vec{r}\,\sigma_2\, C(\vec{r},t)\, I^2(\vec{r},t) \tag{4.20}$$

where σ_2 is the TPA cross section, C is the sample concentration in number of molecules/cm^3, I is the number intensity of the incident beam (number of photons/(cm^2 sec)), and the integral goes over the spatial distribution of the excitation light pulse. The square power dependence of absorbed photons is clearly shown here. Furthermore, the number of detected fluorescence photons per unit time, $F(t)$, following a two-photon absorption process, is given by[137]

$$F(t) = \frac{1}{2}\,\phi\,\eta\, N^{(2)}_{\mathrm{abs}}(t), \tag{4.21}$$

where ϕ and η are the fluorescence quantum efficiency of the material and the collection efficiency of the measurement system, respectively. The factor 1/2 reflects the fact that 2 absorbing photons are needed for each emitted photon.

The ratio of the experimentally measured fluorescence signals then becomes[128]

$$\frac{\langle F(t)\rangle_{\mathrm{new}}}{\langle F(t)\rangle_{\mathrm{ref}}} = \frac{\phi_{\mathrm{new}}\,\eta_{\mathrm{new}}\,\sigma_{2\,\mathrm{new}}\,C_{\mathrm{new}}\,\langle P_{\mathrm{new}}(t)\rangle^2\,n_{\mathrm{new}}}{\phi_{\mathrm{ref}}\,\eta_{\mathrm{ref}}\,\sigma_{2\,\mathrm{ref}}\,C_{\mathrm{ref}}\,\langle P_{\mathrm{ref}}(t)\rangle^2\,n_{\mathrm{ref}}}\,, \tag{4.22}$$

where $\langle F(t)\rangle$ is the time averaged integrated fluorescence counts for the unknown and reference sample, n_i is the regular index of refraction of the solvents, and $\langle P(t)\rangle$ is the average incident power. Usually, the focusing and collection geometry and the radiation source are identical in both situations. The unknown TPA cross section can therefore be calculated from the simpler expression

$$\sigma_{2\,\mathrm{new}}(\lambda) = \frac{\langle F(t)\rangle_{\mathrm{new}}}{\langle F(t)\rangle_{\mathrm{ref}}} \cdot \frac{\phi_{\mathrm{ref}}\,C_{\mathrm{ref}}\,n_{\mathrm{ref}}\,\sigma_{2\,\mathrm{ref}}}{\phi_{\mathrm{new}}\,C_{\mathrm{new}}\,n_{\mathrm{new}}}\,. \tag{4.23}$$

Sometimes, the sample concentration and the solvent are also the same for sample and reference, and the expression in eq. (4.23) simplifies further. Xu and Webb[137] also derived an expression for the absolute number of fluorescent photons following a general multi-photon absorption process. However, an accurate determination of the cross section from such an expression, requires detailed knowledge of the temporal and spatial dependence of the light used for excitation,[137] which are usually difficult to analyze with great precision for confined focal volumes.[128]

The experimental setup for two-photon excited fluorescence measurements is the same as for the other spectral and time-resolved measurements, as shown in Figure 4.11 of Section 4.6.

Chapter 5

Summary and discussions of spectroscopic results

5.1 Characterizing reference materials

A series of highly fluorescent molecules were characterized in order to be used as reference compounds in determination of the quantum efficiency and two-photon absorption cross section from fluorescence. Three Coumarin fluorophores were chosen to cover the intermediate wavelength region between the two well-known fluorescence standards Fluorescein and Quinine Sulfate.[117,128] The coumarines were Coumarin 110 (abbreviated C110), Coumarin 314 (C314)

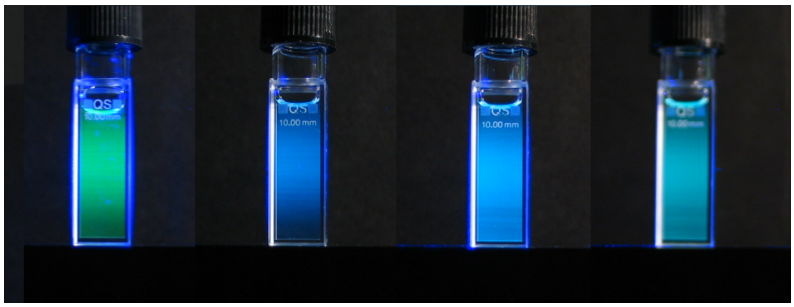

Figure 5.1: Picture of the fluorescence emission of Fluorescein, C110, C314 and C334, respectively. The samples show different emission colors in the blue-green region.

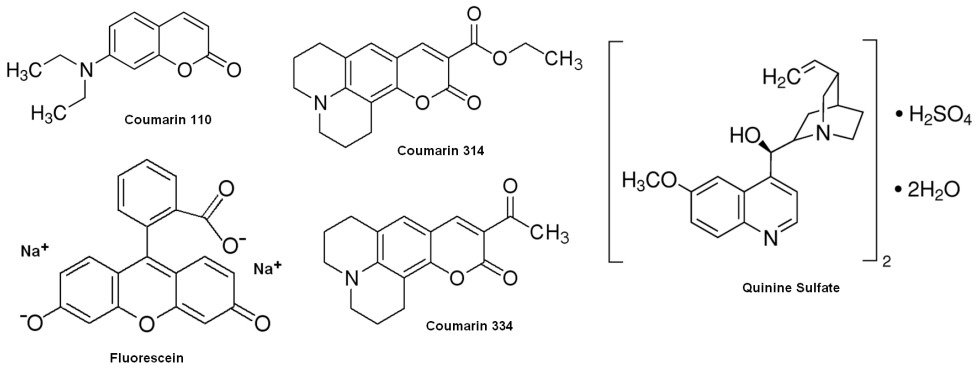

Figure 5.2: Structural formula of the studied reference chromophores.

and Coumarin 334 (C334) (Figure 5.2). The fluorescence emission in the blue−green part of the spectrum (400 to 550 nm) from four of the samples are shown in the picture of Figure 5.1, following absorption in the $300 - 500$ nm region. All compounds have fluorescence quantum yields between 0.62 and 0.93, and TPA cross sections in the range from $5 - 75$ GM. The fluorescence quantum efficiencies and TPA cross sections were found using the fluorescence methods as outlined in Section 4.5 and 4.9.2, using Quinine Sulfate and Fluorescein as fluorescence references.[117,121–123,128,138] Details of the photo-physical characterization and results are given in Paper VI.

In Paper I, the TPA cross section of C110 was determined using the absolute z-scan technique of Section 4.9.1. Results of both fluorescence and z-scan measurements are shown in Figure 5.3. It's clear from the TPA cross section data of C110 in the two panels that the results differ between the two methods in use. The cross sections given in Paper I were later found to be underestimated with approximately 35% due to the use of a too short pulse length in the analysis.* This comes as a systematic error in addition to the measurement error of approx. 35%, given in Paper I. Corrected data are given in Figure 5.3, where the right panel can be compared to Figure 4b in Paper I. However, still, the data from the z-scan method and the fluorescence method differ with a factor close to 5. We note that the cross section spectral shape, with a peak around 740 nm and a reduced cross section towards 800 nm, is the same in both panels.

*A more correct FWHM pulse length is 240 fs instead of 180 fs used in Paper I. The pulse length was measured using the APE Autocorrelator Pulse Check.

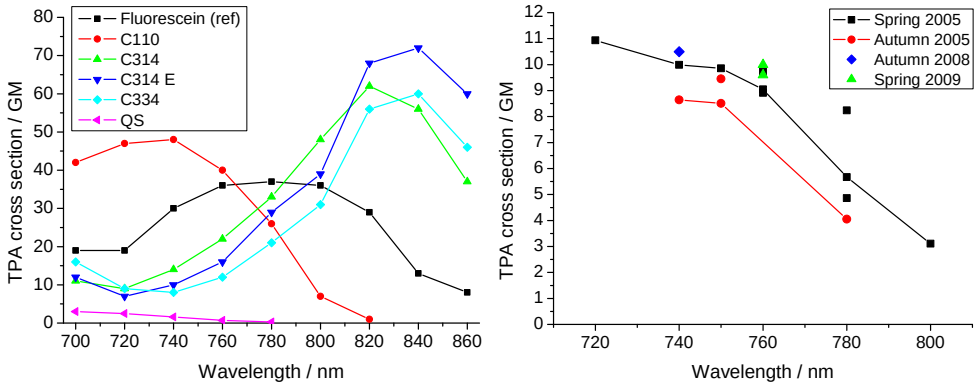

Figure 5.3: *Left:* TPA cross section of the reference materials measured against Fluorescein using the relative fluorescence emission technique. *Right:* TPA cross section of C110, measured at several occasions, using the z-scan technique.

The reason for this discrepancy in data has not yet fully been understood. However, we note the following points in the discussion. i) The analysis of the z-scan data using eq. (4.19) is based on a transversal Gaussian beam profile. The real beam profile might have been somewhat different than this, causing the assumed focus of the beam, and peak on-axis intensity around the focal spot to be reduced. ii) The z-scan method was utilized on the well studied fluorophore Rhodamine B in methanol.[117,137,139] The TPA cross section at 800 nm was measured to be in the range $115 - 130$ GM in a series of experiments. The TPA cross sections between 720 and 800 nm were also determined using the relative fluorescence technique with the result: 95 GM (720 nm), 60 GM (740 nm), 70 GM (760 nm), 110 GM (780 nm) and 135 GM (800 nm).[†] The results of the z-scan were here only found to be slightly lower than the fluorescence measurements, and both numbers are within the experimental errors of $30 - 35\%$. The measurement data from the fluorescence series also fits well with the results given by Xu and Webb[137] and Makarov et al.[139] iii) The samples used for z-scans were usually higly concentrated (30 mM), compared to the case of using the relative fluorescence technique ($50 - 100$ μM). In the high concentration solutions, interactions between the molecules are more probable and the formation of molecular complexes is possible. This could affect the measured transmittance at high input intensities.

[†]The fluorescence quantum efficiency of Rhodamine B in methanol is taken to be 0.66 as given by Demas and Crosby.[117]

Some authors have explained the lower cross section in the nonlinear transmission (z-scan), compared to the two-photon induced fluorescence method, by the presence of other intensity dependent effects, such as stimulated emission or Raman scattering, which may lead to an underestimation of the TPA cross section.[140]

We note at the end, that the two-photon induced fluorescence of all standards follow the power-square dependence, as one should expect from a pure two-photon absorbing sample from equation (2.18). This is shown in Figure 5.4 for three of the Coumarin samples in this investigation, where the integrated fluorescence counts vs. the pulse energy follow a straight line with a gradient of 2 in a logarithmic plot.

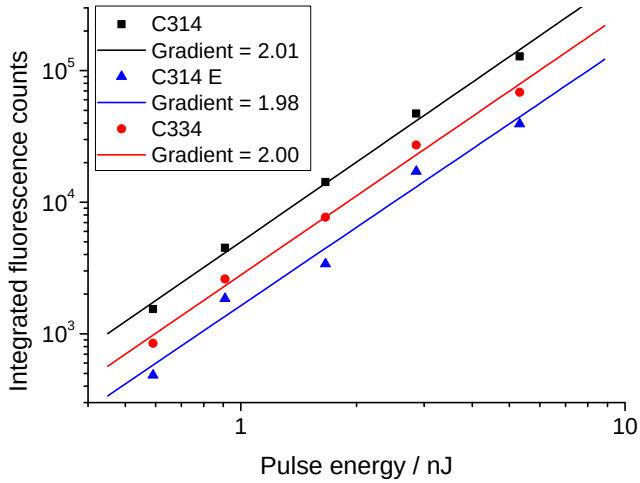

Figure 5.4: Two-photon induced fluorescence vs. input pulse energy.

5.2 Photo-physical properties of Pt(II)-acetylides

5.2.1 Thiophenyl-containing Pt-arylalkynyls

The thiophenyl-containing Pt(II)-arylalkynyl complexes were studied in Paper I, II and IV. The introduced thiophene rings were substituted into the structure at different positions in the molecular ligands. In addition, methoxy and methyl substituents were added to the structures, as shown in Figure 3.2

of Section 3.4.1. The introduction of the thiophene rings into the structure clearly changes the photo-physical properties of the molecules. It's also clear that when the thiophene rings are placed closest to the Pt-atom, the interaction between the ligand and Pt-atom is strongest, yielding e.g. a red-shifted absorption and emission spectrum, and a shorter phosphorescence decay time.

The two-photon absorption properties of T1, T2 and Pt1-G1 were measured using the z-scan technique. Figure 5.5 shows z-scan transmission curves of Pt1-G1 at different pulse repetition frequencies (prf). During the z-scan measurements at high prf, it was observed bright green phosphorescence with the naked eye. At high prf, the triplet state may not have been fully relaxed before the next pulse strikes the sample. Therefore, it is believed that excited state absorption from the triplet state also comes into account at high prf. To reduce the unwanted excited state absorption, lower prf's (longer time between pulses) were used. Then, the apparent TPA cross section values are believed to approach the true TPA cross section. This is further discussed also for T1 and T2 in Paper I.

It was found that the thiophenes (and triazoles) were not particularly good two-photon absorbers in the $700 - 800$ nm region. Therefore, a thorough investigation of the TPA cross sections in this region was not performed, and only a few values of the TPA cross sections of the chromophores at selected wavelengths appear in this study. A more interesting region to investigate the

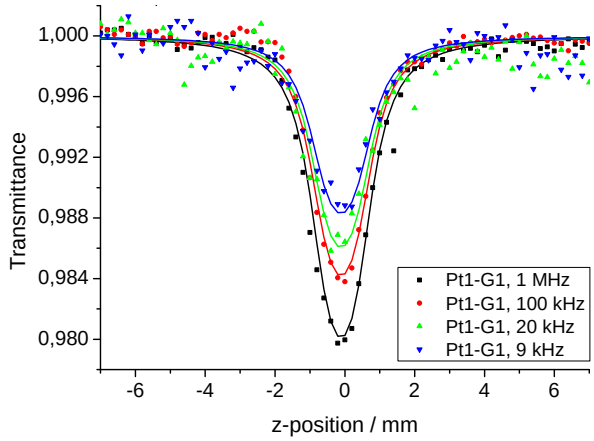

Figure 5.5: Z-scan curves of Pt1-G1 at 740 nm at four different pulse repetition frequencies from 1 MHz to 9 kHz.

TPA properties, as indicated by some other studies, are the 500 – 700 nm region.[28,141] However, the experimental equipment prevented us from performing such investigations at this time.

Due to the somewhat low TPA cross sections in the selected wavelength region, two-photon absorption itself can not give any strong nonlinear behavior for OPL performance for these molecules. However, two-photon absorption in the whole 500 – 800 nm region, acts as an important 'triggering mechanism' in this wavelength region, exciting the chromophores. Then, strong absorption in the same wavelength region appear from the triplet states, providing the strong excited state absorption nonlinear behavior suitable for good OPL performance.

The transient absorption properties of the thiophene (and triazole) samples are discussed in Paper IV. Interestingly, the introduction of the thiophene ring in the T3-, T4-, T5- and T7-compound results in a blue shift of the transient absorption peak, in opposite to the red-shift observed in the ground state absorption. However, the methoxy-substituted T6-compound was the most red-shifted in this molecular series in both cases. The ground state and transient absorption spectra of the 'long' thiophenes are shown in Figure 5.6. Numerical data are found in Paper IV, and summarized for all studied chromophores in Table 5.1 below. The triplet state properties and phosphorescence decay of the non-symmetrical Pt1-T4 molecule are thoroughly discussed in Paper IV.

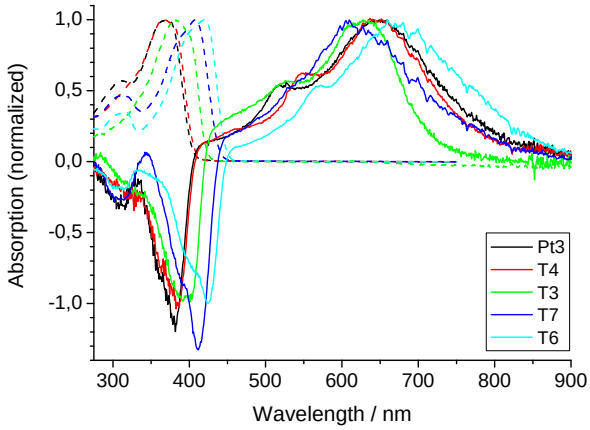

Figure 5.6: Normalized ground state and triplet state absorption of the T3, T4, T6, T7 and Pt3 chromophores in THF solution.

If the delay between pump and probe pulse in the transient absorption measurements were increased, a reduced triplet state absorption was found. This is expected due to a less number of molecules remaining in the excited triplet state as the time after the pump light increases. The decay of this spectrum is expected to follow the same decay behavior as the decay measured from phosphorescence. However, the analysis of the data showed a two-component decay of the triplet state measured from the decay in triplet absorption. This is shown for Pt1-G1 in Figure 5.7. The data were fitted to equation (4.15). The long component of the decay was equal to the decay time measured from phosphorescence (0.19 ms), whereas the short component was found to be diffusion limited triplet-triplet quenching due to a strong flash light and a high concentration of excited molecules.

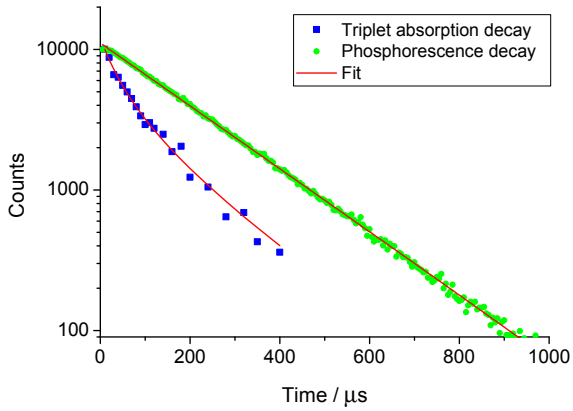

Figure 5.7: Triplet state decay measured from phosphorescence and triplet absorption.

5.2.2 Triazole-containing Pt-acetylides

The triazole-containing Pt(II)-acetylides were studied in Paper III, IV and V. The triazole units were incorporated into the structure from the click-chemistry process. The triazole rings were placed at different positions in the molecular structure to investigate the effect on the photo-physical properties. The three triazole compounds are shown in Figure 3.3 of Section 3.4.2.

Absorption measurements indicated that the electron transfer and conjugation is somehow interrupted by the triazole unit, due to a blue shifted and almost

Table 5.1: Spectroscopic characteristics of all platinum(II)-arylalkynyls investigated in this thesis.

Sample	λ_{abs} (nm)	ϵ (¶)	λ_{em} / λ_{ph} (nm)	τ_{ph}* (μs)	λ_T (nm)	ϵ_T (¶)	Paper
Pt1	354	9	384 / 525	156	585	3.1	I, IV
Pt1-G1	357	9	390 / 525	190	596	2.9	I, IV
Pt3	378	9	404 / 555	166	650	3.3	II, IV
Pt-Star	364	34	396 / 532	100§	-	-	(6)
T1	378	9	420 / 610	0.19†	-	-	I
T2	362	11	392 / 550	0.33†	-	-	I
T3	385	11	424 / 625	280	630	6.8	II, IV
T4	382	10.1	412 / 566	140	645	4.3	II, IV
T7	408	10.4	440 / 628	28	610	5.6	II, IV
T6	419	12.7	446 / 625	300	660	8.9	II, IV
T5	386	12.5	424 / 650	11	510	3.1	IV
Pt1-Me	353	11.8	396 / 528	310	540	3.3	IV
Pt1-OMe	388	9.3	388 / 566	190	575	4.5	IV
Pt1-T4	363	11.1	402 / 562	480/85	654	5.4	IV
Pt1-A	362	9.7	440 / (530)	35	426	1.2	-
Z1	342	7.1	388 / 486	0.6	600	1.5	III, IV
Z2	342	8.5	388 / 488	-	-	-	III
Z3	365	14.3	396 / 535	310	605	4.7	III, IV
Solid state PMMA glasses:							
Z1	< 400	-	- / 482	52	600	1.3	V
Z3	< 400	-	- / 534	86	570	3.6	V
Pt1-G1	< 400	-	- / 522	66	580	2.7	V
Pt1(m)‡	< 400	-	- / 522	66	570	2.7	V

¶ $= 10^4$ $M^{-1}cm^{-1}$.

* Phosphorescence emission lifetimes measured in oxygen evacuated samples. Average decay times for the PMMA samples.

§ Argon purged sample. Uncertain value due to oxygen evacuation procedure.

† Measured only in oxygen saturated / open air samples. Corresponding value for Pt1-G1 is approximately 0.50 μs.

‡ Pt1-G1-methacrylate/PMMA glass (type II).

equal absorption spectrum of Z1 and Z2 compared to Pt1-G1 and Z3. Emission spectra were found to be blue- and red-shifted in similar ways as the absorption,

with e.g. phosphorescence emission bands around 490 nm for Z1 and Z2 and 535 nm for Z3 (525 nm for Pt1-G1). Oxygen evacuation was performed with argon purging, giving a large increase in phosphorescence emission for Z3 and Pt1-G1, but not to the same extent for Z1 and Z2, as shown in Figure 5 of Paper III. As the oxygen was removed, the phosphorescence lifetime increased by one order of magnitude for Z1 and Z2 to approximately 0.6 μs,[‡] while the phosphorescence emission and lifetimes increased by three orders of magnitude to 0.31 ms and 0.19 ms for Z3 and Pt1-G1, respectively.

Just as for some of the thiophenes (Paper II), oxygen evacuation did not give the same increase in phosphorescence emission for all compounds. It is therefore found that the introduction and position of the introduced triazole and thiophene units are of great importance for the ISC process and probability for triplet quenching of these molecules. A summary of the basic photo-physical properties are found in Table 5.1. Further excitation and emission properties of Pt1-G1 and Z3 in high and low concentrated samples are discussed in Paper V.

5.2.3 Solid PMMA materials

In paper V, Pt1-G1 and the triazole compounds Z1 and Z3 were incorporated into solid PMMA glasses. The basic photo-physical properties found in the liquid state were found to be maintained also in the solid state. Importantly, the phosphorescence emission decay times were found to be in the order of 10-100 μs, just slightly shorter than in oxygen evacuated liquid samples. We therefore believe that the reduced mobility of the chromophores inside the PMMA matrix, prevents efficient oxygen quenching as found in the liquid state.

The photo-physical properties were measured at different concentrations ranging from 10 μM to 50 mM. All glass materials showed good optical transparency in the visible region. As noted in Section 3.4.3, this is maintained even at high concentration. Transmission spectra are shown in Figure 2 in Paper V. Interestingly, at higher concentrations – both in liquid and solid state – new spectral substructures at 380-500 nm appears in the excitation spectrum, monitoring at the phosphorescence emission (Figure 5 in Paper V). The new peaks also become more and more prominent as the concentration increases. Transient absorption, and extinction coefficients of the excited triplet states, were found to be approximately the same as those found in solution (within the experimental errors given in Paper IV). (Table 5.1.)

[‡]In Paper III, the erroneous value of 6 μs was given.

5.3 Results for Pt-Star and Pt1-A

Two more Pt(II)-acetylides were investigated in this work. They are presented in Section 3.4.4 with structural formulas. The Pt-Star molecule was synthesized in order to investigate how the photo-physical properties is affected by a branched structure, and if this may result in a better clamping level for optical power limiting. The results are described in detail in related paper 6 and in reference 105 (Westlund, PhD thesis). Here, a short summary of the photo-physical properties is given.

The linear absorption was found to be much stronger for Pt-Star than for Pt1-G1, with an extinction coefficient of approximately $\epsilon = 34 \cdot 10^4$ $M^{-1}cm^{-1}$ at 364 nm, three and a half times stronger than that of for Pt1-G1 at 357 nm (Table 5.1). Absorption and emission spectra are shown in Figure 5.8. Emission spectrum in open air samples displays a fluorescence emission peak at 396 nm, and small phosphorescence peak at 532 nm. Phosphorescence decay time in open air sample was found to be 217 ns. After air evacuation by argon purging, the phosphorescence emission were increased by three orders of magnitude (Figure 5.8, right), just as for the phosphorescence decay time.

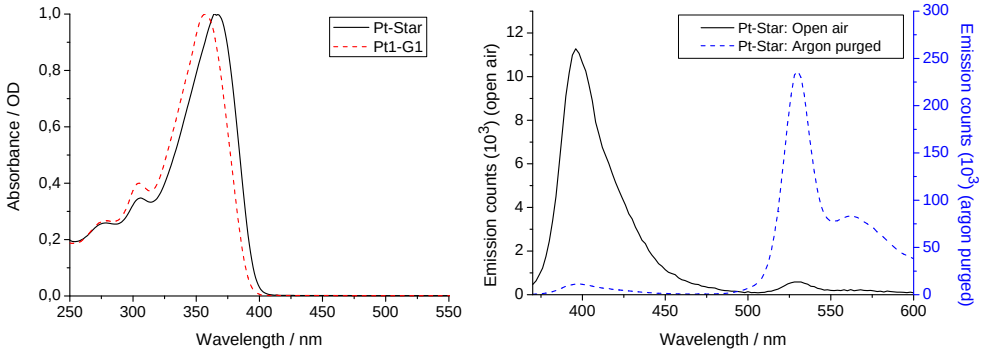

Figure 5.8: *Left:* Absorption spectrum of Pt-Star compared to Pt1-G1. Absorption maximum for Pt-Star at 364 nm. *Right:* Emission in open air and air evacuated samples. Emission maximum at 396 nm and 532 nm, respectively.

Two-photon excited fluorescence of Pt-Star, excited at 720 nm, gave a much more intense fluorescence signal than that of Pt1-G1. Both compounds have an emission quantum efficiency in the order of 10^{-3}. This gives an estimation of the TPA cross section of Pt-Star to be approximately 5 times that of Pt1-G1. Optical power limiting performance of Pt-Star is discussed in a following section.

The Pt1-A molecule (see Section 3.4.4) was prepared as a Pt1-molecule with an additional anthracene group attached to the end of each ligand, as shown in Figure 3.8. The purpose was to investigate the influence of this group on the photo-physical properties of the Pt1-molecule, with the possibility of any energy transfer channels to and from the anthracene group. Anthracene has previously been found to have some triplet absorption,[142] and we were curious to see how this would influence the triplet absorption of the Pt1-molecule.

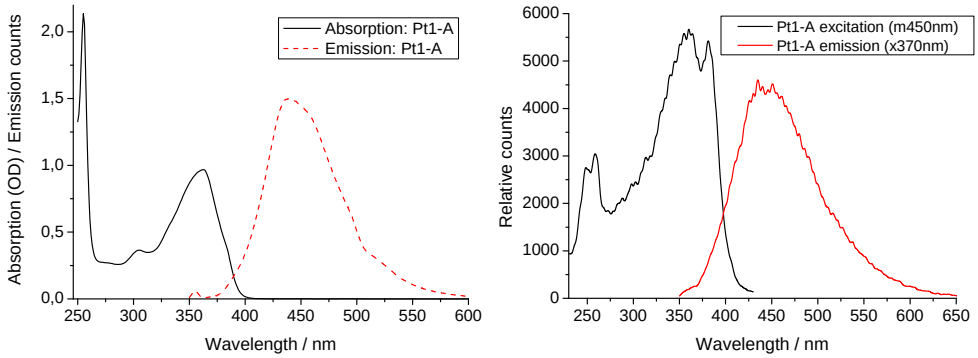

Figure 5.9: *Left:* Absorption and emission spectrum of Pt1-A in THF solution. *Right:* Excitation and emission spectrum taken at emission wavelength 450 nm and excitation wavelength 370 nm, respectively.

Absorption and emission spectra of Pt1-A are shown in Figure 5.9. The absorption shows a structure that above 280 nm resembles that of Pt1, with a peak at 262 nm (ϵ = 9700 $M^{-1}cm^{-1}$). The spectrum has also an additional peak at 255 nm (ϵ = 21300 $M^{-1}cm^{-1}$), which can be attributed to the anthracene unit.[143] The emission spectrum (Figure 5.9) is found to be strong, broad and red-shifted compared to the regular emission spectrum of Pt1/Pt1-G1, with an emission maximum at 440 nm. The same emission is also found from a molecule being just the phenyl-ethynyl ligand of Pt1-A. This might indicate that the plane of the anthracene unit has a twisted configuration, relative to the Pt1-ligand plane, in the ground state of Pt1-A as shown in Figure 5.10, while the structure in the excited state is more planar. The (fluorescence) emission therefore comes from a more conjugated ligand structure on one side of the Pt1-A molecule.

The enhanced emission yield of Pt1-A indicates more efficient fluorescence channels in Pt1-A than in Pt1/Pt1-G1, and lower inter-system crossing efficiency to the triplet state. Excitation spectra (Figure 5.9) were found to be independent on monitoring wavelength in the emission band, and vice versa.

Figure 5.10: Twisted (*left*) and planar (*right*) structure of the anthracene unit compared to the Pt1-ligand plane.

Also, the excitation peak at 255 nm is not found to be the main excitation channel for emission, compared to excitation between 300 and 400 nm. Fluorescence emission decay curves (Figure 5.11, left) show a clear two-component decay with lifetimes of $\tau_1 = 1.7$ ns (90%) and $\tau_2 = 5 - 6$ ns (10%) (where the latter slightly varies with emission wavelength).

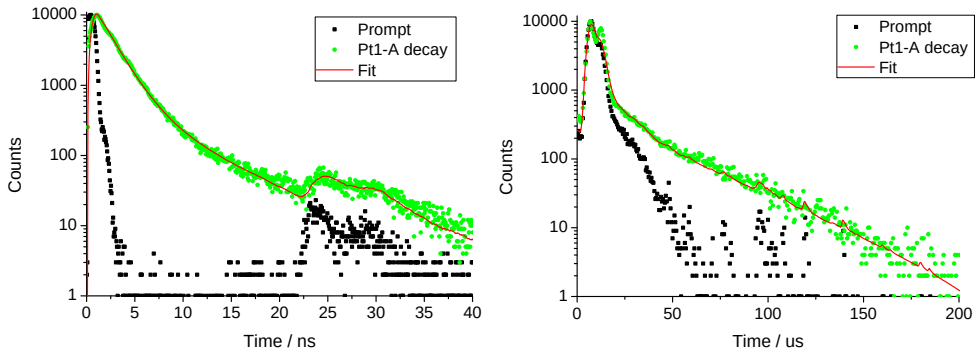

Figure 5.11: *Left:* Fluorescence emission decay curve at 440 nm, excited at 337 nm using the NanoLED. *Right:* Phosphorescence decay trace at 530 nm using flash-lamp excitation at 360 nm.

Solutions were also oxygen evacuated using the vacuum pump. Excitation with the laser or NanoLED, gave no difference in emission spectrum after pumping, while excitation with the flash-lamp (with same instrumental settings) yielded a slightly broader spectrum and an additional emission peak at 530 nm (Figure 5.12). Emission decay traces were found to have a decay component of 35 μs at and above 510 nm, while at lower emission wavelength, the emission signal could not be resolved from the μs-long pulse prompt. (Figure 5.11, right.) The new phosphorescence emission peak at 530 nm resembles that of a small

contribution from regular phosphorescence from Pt1, with a much shorter decay time than for regular vacuum pumped Pt1/Pt1-G1. The phosphorescence peak disappeared when exciting at the anthracene band at 255 nm (Figure 5.12, left). Therefore, we believe that at excitation at 360 nm (using the long μs-pulses), a triplet state in Pt1 is reached with an efficient energy transfer channel to a localized triplet state at the anthracene unit. The interpretation was further supported by measurements of the triplet state absorption.

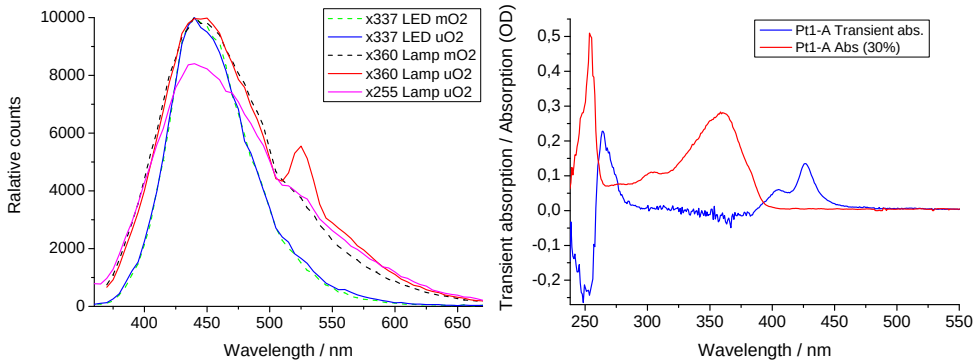

Figure 5.12: *Left:* Emission spectra of Pt1-A before (mO2) and after (uO2) oxygen evacuation, excited at 337 nm using NanoLED and at 360 and 255 nm using flash-lamp. *Right:* Transient absorption spectrum of Pt1-A in 10 μM, 10 mm long samples. 30% normal absorption is shown for comparison.

A transient absorption measurement is shown to the right in Figure 5.12. The transient spectrum shows a large depletion valley around 250 nm, close to the strong ground state absorption. A 30% absorption spectrum is shown in Figure 5.12 for comparison. After 5 μs, the transient absorption spectrum shows two new absorption bands with peaks at 405 nm and 426 nm, and yet another peak at 265 nm. The spectrum also shows some depletion in the $300-400$ nm region. This means that the sample has almost the same absorption in this region 5 μs after excitation with the pump, as before the excitation. The anthracene excitation at 255 nm is, however, strongly depleted. This support the findings above that the excited triplet state has been transferred to the anthracene unit, and that the rest of the molecule (resembeling that of Pt1), is almost recovered to its ground state electron configuration. The new structure in the $400-450$ nm region is believed to be absorption from the triplet state localized at the anthracene unit. Conclusively, the introduction of the anthracene unit clearly quenches the triplet state of the Pt1-structure by 'stealing' the triplet excitation. This might have crucial influence on OPL and related properties.

5.4 Optical power limiting

Optical power limiting performance has been measured for most of the materials presented in this thesis. Results are presented in Paper II (T3-T7) and III (triazoles), and in related papers 1 (Pt1-G1), 3 (T1,T2), 5 (solid PMMA) and 6 (Pt1-Star). Results of two OPL measurement series at 532 nm are shown in Figure 5.13. To the left are some of the compounds in the T-series compared to Pt3 in 30 mM THF solutions. Here, only T6 shows a better clamping level than Pt3 at 532 nm with a clamping level at approximately 4 μJ. More details are discussed in Paper II.

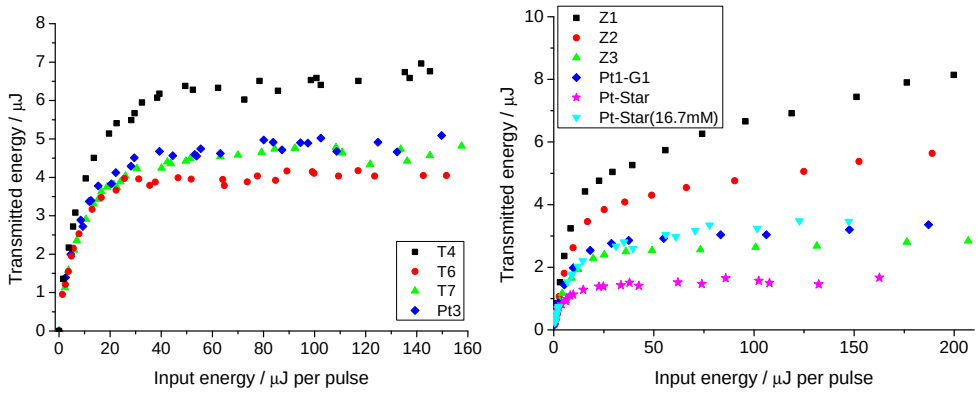

Figure 5.13: *Left:* OPL spectra of 30 mM THF samples of T4, T6, T7 and Pt3 for 5 ns pulses at input energies up to 160 μJ. *Right:* OPL performance at 532 nm of Z1, Z2, Z3, Pt1-G1 and Pt-Star at 50 mM concentrations and Pt-Star at 16.7 mM at input energies up to 200 μJ.

Some of the OPL measurements of the triazoles, discussed in Paper III, are reproduced to the right in Figure 5.13 together with those of Pt1-G1 and Pt-Star, all taken at 50 mM concentration. We here note the higher clamping levels of Z1 and Z2, compared to Pt1-G1, and the slightly lower clamping level of Z3. We also note that Pt1-Star is clearly superior in optical limiting performance than the others. However, correcting for the star-shape of Pt1-Star, containing three Pt1-G1 molecules, we see that at 16.7 mM concentration (1/3 of 50 mM), the clamping level equals that of Pt1-G1. The increased OPL performance at 50 mM at 532 nm, pays the price of a reduced linear transmission of only $60 - 70\%$ compared to that of approximately 90% for Pt1-G1 at the same concentration. Hence, Pt1-G1 is superior in application performance.

Optical power limiting at 532 nm were also measured on the platinum-acetylide doped PMMA glasses presented in Paper V (and related papers 5 and 12). Results of OPL measurements are reproduced from related paper 5 in Figure 5.14. Here, we see that the clamping level of Pt1-G1 in type I glass (dispersed dopant), remain its clamping levels of 3-4 μJ at input pulse energies up to 120 μJ. However, for Pt1-G1 in type II glass (covalently bonded dopant) the clamping level was found to reach 8.5 μJ at input energies up to 90 μJ, followed by a reduction of the transmitted power at higher pulse energies due to laser induced damages on the polymer glass-material.

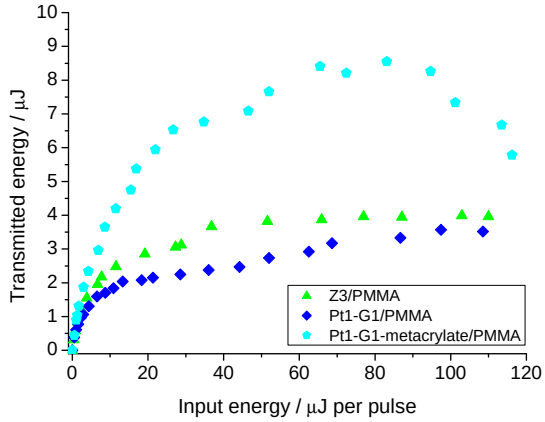

Figure 5.14: OPL data for 50 mM doped PMMA glasses with Z3 and Pt1-G1 in type I glass (dispersed dopant), and Pt1-G1-methacrylate in type II glass (covalently bonded dopant).

It is therefore concluded that the cross-linked glass has a lower damage threshold than the type I glass. The higher clamping level of Pt1-G1 type II glass might also indicate that the bonding of the platinum acetylide molecule to the PMMA matrix negatively affects the nonlinear response of the chromophore. This could be explained from a more pronounced rigidity experienced by the Pt-molecule, thus limiting structural rearrangements and relaxation to particular states important for good OPL performance. However, photo-physical characterization, presented in Paper V, did not display any particular differences between type I and type II doped glasses.

5.5 Simulations of OPL properties

In this PhD-project we have studied several nonlinear absorbing Pt-molecules for optical power limiting, and characterized their photo-physical properties. Based on previous studies of these material, the nonlinear absorption is interpreted as linear and two-photon absorption, followed by excited state absorption in the relatively long lived triplet manifold.[28] As the spectroscopic investigations gave new experimental data in terms of the excited state dynamics and absorption of triplet states, it is interesting to further elucidate how these contribute in the OPL process.

In order to test the importance of the individual processes, such as TPA and ESA, it is desirable to study the OPL performance under a controllable situation. This can be done using theoretical modeling of the propagation of radiation through optically nonlinear media. Such an analysis was performed by A. Eriksson in his PhD-thesis from 2001.[5,144] Here, a theoretical model based on the Cranck-Nicholson method was utilized to numerically solve the propagation problem and the dynamic differential equations associated with the population of electronic states in a three- and five-level molecular system.[66,144] The numerical pulse propagation was performed by dividing the pulse into a number of temporal slices. Each slice was then propagated through the sample divided into many thin layers. After each layer, the new population of the molecular states in that layer are calculated at each radial point, by numerically solving the population differential equations using the absorption cross sections and the field intensity. The state populations are saved and used as a modified 'material parameter' for the next temporal slice.

In the work by Eriksson et al.[5,132,133] the OPL performance was mainly modeled from pure two-photon absorption, or a combination of one-photon absorption with excited state absorption (reverse saturable absorption). In order to fit the theoretical model to the experimental data, huge TPA cross sections were needed. Later, Staromlynska et al. explained the nonlinear absorption as excited state absorption from the triplet state, initialized by two-photon absorption in the singlet manifold followed by efficient ISC to the triplet states.[28] They also emphasized the contribution of some direct absorption from the ground state to the triplet state in the $500 - 540$ nm region.[28,83]

The pulse propagation model initiated by A. Eriksson, is here further developed to simulate a combination of two-photon absorption in the singlet manifold followed by triplet excited state absorption. In addition, a direct absorption channel into the triplet state was added to the model. The model was ap-

plied with the same basic numerical pulse and focusing parameters as used by Eriksson et al.[5,144] A longer pulse length of 5 ns FWHM was applied to simulate the pulse used in the real OPL measurements, however, in order for the underlying approximation to be valid, the same focusing parameters were used.** The numerical pulse and material parameters used in this study are summarized in Table 5.2.

Table 5.2: Parameters used in the numerical pulse propagation model.

Pulse propagation		Material	
Parameter	Value	Parameter	Value
Wavelength, λ	532 nm	S_1-lifetime	0.1 ns
Rayleigh length, z_R	0.5 mm	ISC efficiency	90%
Sample length, z	2 mm	T_1-lifetime	500 ns
Sample step, Δz	50 μm	S_2-lifetime	1 ps
Radius, r	100 μm	T_2-lifetime	1 ps
Radial step, Δr	1 μm	$\sigma_{S0\rightarrow S1}$	0–3.7·10^{-24} m^2 †
Time span, t	12 ns	$\sigma_{S0\rightarrow T1}$	0–3.7·10^{-24} m^2 †
Time step, Δt	0.5 ns	$\sigma_{S1\rightarrow S2}$	0
Temporal pulse-shape	Gaussian	$\sigma_{T1\rightarrow T2}$	$1 - 10^5 \times \sigma_{S0\rightarrow T1}$
Pulse length, (FWHM)	5 ns	σ_{TPA}	1200 GM †
Pulse energies	$0.1 - 250$ μJ	Concentration	50 mM

† Some different cross sections were applied in the various individual simulations, see text for details.

Only a few calculations and simulations of OPL are presented here, in order to estimate the role of TPA in comparison with other absorption processes involving the triplet state. It is anticipated that further development and use of this theoretical modeling tool could provide new and important information on the optical limiting process and mechanisms in the future.

5.5.1 OPL from two-photon absorption

Applying only 'pure' two-photon absorption, OPL curves using different TPA cross sections from $10-10.000$ GM are shown to the left in Figure 5.15. Here, a TPA cross section of 100.000 GM must be applied before an OPL clamping level

**The same focusing parameters as in the OPL measurements could not be applied due to a numerical 'break-down' using such a tight focused pulse.

of 1.5% transmission of the input pulse is reached. The high TPA cross section of 10^5 GM is in the order of the highest TPA cross sections ever observed.[145,146] As the TPA cross-sections of the investigated molecules, in the range $700-800$ nm, was a few tenths of GM, it is unlikely that only TPA can account for the observed OPL performance.

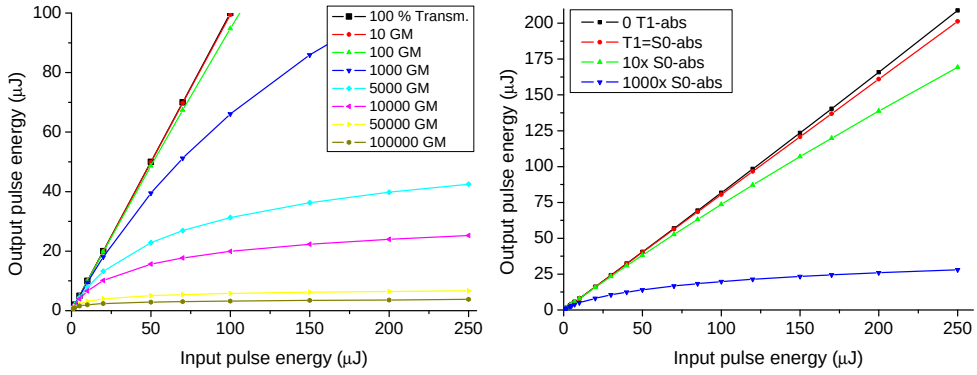

Figure 5.15: *Left:* Simulations of pure two-photon absorbing OPL performance from 5 ns pulses through a 2 mm long two-photon absorbing sample with TPA cross section from 10-100.000 GM. *Right:* OPL performance of a triplet excited state absorption system with different T_1 absorption.

The influence of linear absorption on the two-photon absorption OPL performance was also investigated. Applying for instance 80% linear ground state absorption in addition to the TPA, the inclination of the OPL curve was reduced accordingly and never exceeded 80%, at low input power. The clamping level was also reduced by a similar amount. However, when the lifetime of the excited state was increased (e.g., by adding linear absortion from the ground state into the long lived triplet state), the effect of the linear absorption on the clamping level was reduced. This could be explained by the fact that for long excited state lifetimes (much longer than the pulse length), a substantial amount of molecules are 'trapped' in the excited state, reducing the amount of molecules available for two-photon absorption.

5.5.2 OPL from reverse saturable absorption

Next, reverse saturable absorption in a five-level system similar to Figure 2.2 was studied to investigate the importance of ESA in the system. 20% linear

ground state absorption[††] in the sample was applied to populate the first excited singlet state (S_1). Excited state lifetimes and ISC efficiency typical for Pt-acetylides, were applied. These parameters are summarized in Table 5.2. The short ISC time gives, corresponding to the spectroscopic data, an almost instantaneous population of the T_1-state, and the long T_1 lifetime leads to essentially no relaxation from this state during the excitation pulse.

By applying different amounts of $T_1 \rightarrow T_2$ absorption, relative to the ground state absorption, the effect of the ESA process was investigated. With no absorption in the T_1 state, the absorption remains close to 20%, but at high pulse energies a slight increase in the transmission was observed, as shown in the black curve to the right in Figure 5.15. This is explained by, as in the TPA-case above, that a significant amount of populated excited states are reached during the pulse, bleaching the ground state absorption. When the same absorption cross section as that of the ground state also was applied to the T_1 state (the red 'T1=S0-abs' cruve in Figure 5.15, right) the transmission at 80% remained constant, independent of input pulse energy, eliminating the bleaching of the sample. Then, further increasing the T_1 absorption cross section by 10 and 1000 times (where the latter is similar to the absorption cross section measured for the Pt-acetylides in Paper IV, corresponding to $\varepsilon = 10^4$ $M^{-1}cm^{-1}$), the total transmission of the pulse decreased towards 11% at the highest input pulse energy. The corresponding OPL transmission curves are shown to the right in Figure 5.15. Obviously, the typical experimental T_1-absorption gives a substantial OPL performance in the simulations. To obtain the same level of OPL from only TPA, a cross-section of approx. 10^4 GM is needed (compare with Figure 5.15, left).

5.5.3 TPA combined with triplet state ESA

The next stage was to combine ESA from the first triplet state together with ground state two-photon absorption. A two-photon absorption cross section of $\sigma_{TPA} = 1200$ GM was applied together with a varying amount of ESA. By increasing the amount of ESA in the triplet manifold, in a similar way as above, reaching extinction coefficients of $\varepsilon = 10^4$ $M^{-1}cm^{-1}$ (1000x) and $\varepsilon = 10^5$ $M^{-1}cm^{-1}$ (10000x), clamping levels of approximately 15% transmission ($E_{out} = 37$ μJ) and 5.5% transmission ($E_{out} = 14$ μJ) at the highest input pulse energy, were reached. The corresponding OPL curves are shown to the left in Figure 5.16.

[††]Corresponding to an absorbance of 0.1 in the 2 mm long 50 mM sample.

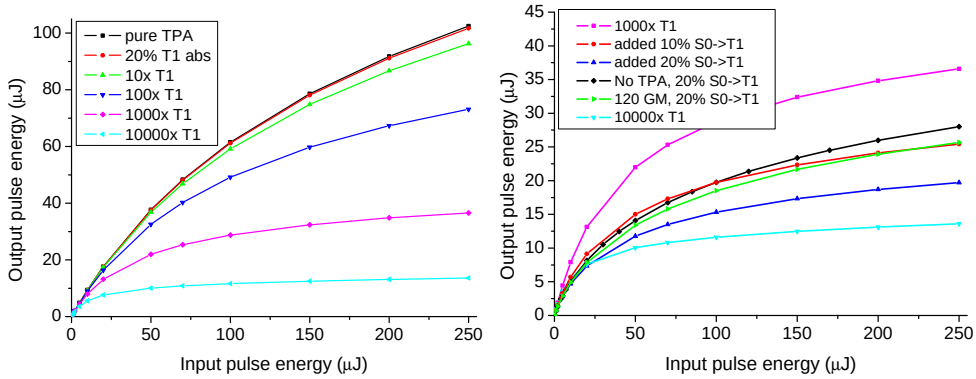

Figure 5.16: *Left:* Simulations of two-photon absorption combined with excited triplet state absorption. *Right:* A combination of TPA, ESA and $S_0 \rightarrow T_1$ absorption directly into the triplet state. See more details in the text.

As noted above, the possibility for direct $S_0 \rightarrow T_1$ absorption into the triplet manifold was also included in the model. This was observed for samples at high concentration in Paper V. Adding a possibility for 10% and 20% (A=0.1) absorption directly into the triplet state (using $\varepsilon = 10^4$ $M^{-1}cm^{-1}$ as ESA coefficient), this had a considerable effect on the OPL performance, lowering the clamping level from 15% to 10% and 8%, respectively. This is shown as the red and blue curves to the right in Figure 5.16, compared to the pink curve without any such direct $S_0 \rightarrow T_1$ absorption. The OPL curve for TPA and ESA with $\varepsilon = 10^5$ $M^{-1}cm^{-1}$ (light blue), are also added in the right panel for comparison. (The pink and light blue curves are therefore the same in the two panels of Figure 5.16.) Taking the blue curve (with $\sigma_{\mathrm{TPA}} = 1200$ GM, 20% $S_0 \rightarrow T_1$ and 1000x T_1-absorption), and reducing the TPA cross section to 120 GM and 0 GM, the OPL clamping level was reduced. This is shown as the green (120 GM) and black (0 GM) curves to the right in Figure 5.16, with clamping levels of 10% and 11% of the input pulse energy, respectively. Thus, using a typical experimental triplet excited state absorption, this is the dominating process, also combined with TPA cross sections in the range $0 - 1200$ GM.

The highest applied TPA cross section is, however, approximately 10 times greater than the real TPA cross section expected in the $500 - 700$ nm wavelength region for these compounds.[28,84] However, we note that in the real OPL measurements, the tighter focus may result in a larger TPA absorption probability, giving stronger population of the triplet state via this route. We also note that increasing the extinction coefficient of the T_1-state to $\varepsilon = 10^5$

$M^{-1}cm^{-1}$ gave a strong reduction of the clamping level. The ε-value is here still in the order of the observed values from Paper IV.

Taking together the results of the spectroscopic investigations and the OPL simulations, we have found that population of the triplet state is efficient, either by singlet absorption and ISC, or direct $S_0 \rightarrow T_1$ absorption. (Recall that the linear transmission of the high concentrated samples was typically $80-90\%$ at 532 nm.) In addition, by considering the ESA of the T_1 state, using experimental $T_1 \rightarrow T_n$ extinction coefficients, we observe a substantial OPL performance, emphasizing the importance of strong T_1-absorption to reach a low OPL clamping level. We also found that for two-photon absorption to be a substantional T_1-poulating process, TPA cross sections of at least $120-1200$ GM were needed with our focusing geometry. At OPL wavelengths above 550 nm, the linear absorption becomes weaker, and the TPA process becomes more and more important for population of the triplet states. The 'strength' of the TPA cross section between $550-800$ nm therefore becomes an important issue searching for low OPL clamping levels in this wavelength region.

It is anticipated that further work along these lines can provide new and important information about the OPL mechanisms of these and related materials. We also note that other simulations of the OPL clamping levels of different Pt-acetylides using quantum chemistry calculations, combined with electrodynamic models of the pulse propagation, have been performed.[87,147,148] However, whilst the quantum chemical modeling is based on the linear and two-photon absorption properties being calculated for a given molecule, our simulations are based on applying experimental parameters directly into the model having the freedom for a controllable variation of these parameters. We note that the excited triplet absorption spectra used in the previous simulations, for 10 ns pulses at 532 nm,[148] are blue shifted and have more detailed substructure than the ones experimentally found, as reported in Paper IV.

Chapter 6

Conclusions and future perspectives

The work presented in this thesis has focused on the spectroscopic characterization of a series of platinum(II) acetylide molecules. These molecules have been found to have good optical power limiting capabilities due to their special photo-physical properties suitable for this application. Low linear absorption and relatively good two-photon absorption in the visible region, fast and efficient inter-system crossing to long lived triplet states and strong excited state absorption from these states, are the desired properties. This results in optical power limiting clamping levels approaching 1 μJ for 5 ns pulses with approximately 200 μJ input pulse energy.

Several structural modifications have been made on a square planar *trans*-diarylalkynyl-bis(tributyl-phosphine) platinum(II) complex, introducing thiophenyl and triazole groups, and methyl and methoxy substituents, in the ligands. The effect on the photo-physical properties and the optical power limiting performance, following these modifications, were investigated. Several different spectroscopic methods have been utilized for this purpose. Even though, no particular large improvement of the optical limiting capabilities was found for these new compounds (compared to the previously studied analogues), some important general knowledge of the photo-physical properties and structure-to-property relationships of this family of compounds have been found for a better understanding of the OPL mechanisms.

The new introduced thiophene and triazole rings, and the methyl and methoxy substituents were in general found to give spectral shifts (usually red-shifts) in

absorption and emission spectra, together with shorter or longer triplet decay times and some reduced inter-system crossing efficiency. No particular conclusions could be drawn to explain the different OPL performances based on the intrinsic properties. However, strong excited state absorption and good ISC efficiency still holds as the most important general properties. We also believe that the increased direct absorption into the triplet states at high concentrations, as discussed in Paper V, are of importance for the good OPL performance of these molecules. These findings are also supported by numerical simulations of the OPL performance, as discussed in Section 5.5.

Interesting new results were obtained for the Pt1-A-molecule with the attached anthracene groups, as outlined in Section 5.3. Here, the anthracene group was found to 'steal' the triplet excitation from the Pt1-ligand. An interesting route to follow in further studies, is to attach other groups with known large triplet excitation cross sections to the ligands, to possibly increase the probability for excited state absorption. Also interesting would be to follow up a study of the TPA cross section in the $500 - 700$ nm region, which is important for population of the triplet states outside the linear absorption wavelength region. Also lacking are more detailed studies on the important ISC process of these new compounds.

Further studies of the molecules inserted into solid state hosts would also be of great interest to continue in the future, because only such materials could serve as a real practical protecting device. In addition, continuation of the work with numerical simulations could be interesting. Here, a further development of the numerical procedure to simulate OPL with the same focusing geometry as in the measurements, and to fit the simulations to experimental data, would be possible. This could lead to a better understanding of the individual processes contributing in the OPL mechanisms. Particularly, the triplet states showed a large variation in spectral shifts in absorption and emission, with phosphorescence decay times very sensitive to the environment of the dye molecules. Interestingly, quenching of the triplet state by oxygen in the solvent gives rise to singlet oxygen emission (Paper II). As the singlet oxygen is important in medical applications based on photo-dynamic therapy, there is a possibility to exploit and further develop similar organometallic systems towards such use.

My contribution to the papers

Paper I:
In this paper, I was responsible for all photo-physical characterization, all experiments, and for writing the paper. The z-scan experimental setup for femto-second laser pulses was built, and hardware control and data collection software was developed in LabView. Boris Minaev performed the quantum chemistry calculations, and wrote the corresponding text. Bertil Eliasson and Mikael Lindgren contributed to the writing process and the presentation of the paper. Marcus Carlsson synthesized the chromophores.

Paper II:
Here, I was responsible for all photo-physical characterization and experiments, except some of the OPL experiments performed by Cesar Lopes. The quantum efficiency method was further developed to better suite the experimental setup and needs. Analysis software for this was developed using Matlab. Bertil Eliasson wrote the paper in cooperation with me and Mikael Lindgren. Marcus Carlsson synthesized the chromophores, and Tomas Kindahl and Bertil Eliasson performed the chemical calculations.

Paper III:
I was responsible for all photo-physical characterization and for writing of the corresponding parts in the paper. The argon purging method was set up and utilized to remove oxygen from the solutions. Robert Westlund wrote the chemical synthesis part and other general parts of the paper. Anders Eriksson performed the OPL measurements and the other authors contributed in the synthesis, discussions and the presentation of the paper.

Paper IV:
In this paper, I was responsible for all photo-physical characterization, all experiments, and for writing the paper. A vacuum pump and a new glass sample cell system was build to remove the air from the liquid solutions using

the freeze-pump-thaw technique. A previously build in-house transient absorption set-up was utilized and Thor Bernt Melø contributed with help and discussions regarding these experiments. Ingunn Dragland contributed on the photo-physical experiments on the four 'new' samples.

Paper V:
I was responsible for all experiments and writing of the corresponding parts in cooperation with Mikael Lindgren. The absorption, excitation and emission experiments were modified to be performed on the solid state samples. Patrick Norman performed the quantum chemistry calculations and wrote the corresponding parts. Robert Westlund synthesized the chromophores and prepared the solid PMMA-based materials.

Paper VI:
I was responsible for all experiments and writing of this paper. The two-photon excitation fluorescence method was utilized in a systematic way to develop two-photon absorption wavelength spectra. Mikael Lindgren helped with discussions and presentation of the paper.

List of related papers not included in thesis

1. "Dendron Decorated Platinum(II) Acetylides for Optical Power Limiting", Robert Vestberg, Robert Westlund, Anders Eriksson, Cesar Lopes, Marcus Carlsson, Bertil Eliasson, **Eirik Glimsdal**, Mikael Lindgren and Eva Malmström,
Macromolecules 39, p. 2238-2246, 2006.

2. "Electronic states and phosphorescence of dendron functionalized platinum(II) acetylides", Mikael Lindgren, Boris Minaev, **Eirik Glimsdal**, Robert Vestberg, Robert Westlund and Eva Malmström.
Journal of Luminescence 124, p. 302-310, 2007.

3. "Structural, Photophysical, and Nonlinear Optical Properties of trans-di-arylalkynyl Platinum (II) Complexes with Phenyl and Thiophenyl Groups", Per Lind, Dan Boström, Marcus Carlsson, **Eirik Glimsdal**, Mikael Lindgren, Cesar Lopes and Bertil Eliasson,
Journal of Physical Chemistry A 111, p. 1598-1609, 2007.

4. "A theoretical and experimental study of non-linear absorption properties of substituted 2,5-di-(phenylethynyl)thiophenes and structurally related compounds",
Per Lind, Marcus Carlsson, Bertil Eliasson, **Eirik Glimsdal**, Mikael Lindgren, Cesar Lopes, Linus Boman and Patrick Norman,
Molecular Physics 107, p. 629-641, 2009.

5. "Efficient Nonlinear Absorbing Platinum(II) Acetylide Chromophores in Solid PMMA Matrices", Robert Westlund, Eva Malmström, Cesar Lopes, Johan Öhgren, T. Rodgers, Y. Saito, S. Kawata, **Eirik Glimsdal** and Mikael Lindgren,
Advanced Functional Materials 18, p. 1939-1948, 2008.

6. "Synthesis and Characterization of a 3-Arm Star Platinum(II) Acetylide Chromophore targeted for Optical Limiting Applications", Robert Westlund, Robert Vestberg, **Eirik Glimsdal**, Mikael Lindgren, Cesar Lopes and Eva Malmström,
Manuscript.

7. "Novel pentameric thiophene derivatives for in vitro and in vivo optical imaging of a plethora of protein aggregates in cerebral amyloidoses", A. Åslund, C. J. Sigurdson, T. Klingstedt, S. Grathwohl, T. Bolmont, D. L. Dickstein, **Eirik Glimsdal**, S. Prokop, M. Lindgren, P. Konradsson, D. M. Holtzman, P. R. Hof, F. L. Heppner, S. Gandy, M. Jucker, A. Aguzzi, Per Hammarström and K. Peter R. Nilsson, Accepted in *ACS Chemical Biology*, July 2009. (doi: 10.1021/cb900112v)

Conference proceedings

8. "Two-photon absorption cross section and triplet states of dendritic Pt-acetylides for OPL applications",
Eirik Glimsdal, Anders Eriksson, Robert Vestberg, Eva Malmström and Mikael Lindgren, *Proceedings of SPIE* 5934, 59340N, 2005. (SPIE Optics and Photonics, 31.7.-4.8.2005, SanDiego, CA, USA)

9. "Photo-physical properties and OPL of some novel thiophenyl Pt(II)-ethynyl derivatives", **Eirik Glimsdal**, Marcus Carlsson, Bertil Eliasson and Mikael Lindgren, *Proceedings of SPIE* 6401, 64010J, 2006. (SPIE Optics/Photonics in Security & Defence, 11.-14.9.2006 Stockholm, Sweden)

10. "Multi-functionalized Platinum(II) Acetylides for Optical Power Limiting", Robert Westlund, Eva Malmström, Markus Hoffmann, Robert Vestberg, Craig Hawker, **Eirik Glimsdal**, Mikael Lindgren, Patrick Norman, Anders Eriksson and Cesar Lopes,
Proceedings of SPIE 6401, 64010H, 2006. (SPIE Optics/Photonics in Security & Defence, 11.-14.9.2006 Stockholm, Sweden)

11. "Photo-physical properties and OPL of some new longer thiophenyl-containing Pt(II)-arylalkynyl compounds", **Eirik Glimsdal**, Marcus Carlsson, Bertil Eliasson, Robert Westlund and Mikael Lindgren, *Proceedings of SPIE* 6740, 67400M, 2007. (SPIE Optics/Photonics in Security & Defence, 17.-20.9.2007 Florence, Italy.)

12. "Photo-physical properties and triplet-triplet absorption of platinum(II) acetylides in solid PMMA matrices",
Eirik Glimsdal, Robert Westlund and Mikael Lindgren,
Proceedings of SPIE 7354, 73540H, 2009. (SPIE Europe Optics + Optoelectronics, 20.-23.4.2009 Prague, Czech Republic.)

Bibliography

1. M. Csele, *Fundamentals of Light Sources and Lasers*, Wiley-Interscience, 2004.

2. R. Henderson and K. Schulmeister, *Laser safety*, Institute of Physics Publishing, 2004.

3. Nettavisen, 12.10.2008: "http://www.nettavisen.no/innenriks/ioslo/article2293343.ece" Adressa.no, 05.02.2009: "http://stjordal.adressa.no/index.php?option=com_content_lokal&task=view&id=1566&Itemid=1".

4. L. Matthews and G. Garcia, *Laser and eye safety in the laboratory*, IEEE Press and SPIE Press, 1995.

5. A. Eriksson, *Modeling and Characterization of Nonlinear Materials for Protection of Optical Sensors.* PhD thesis, Linköpings Universitet, Linköping, Sweden, 2001.

6. M. J. Miller, A. G. Mott, and B. P. Ketchel, "General optical limiting requirements," *SPIE* **3472**, pp. 24–29, 1998.

7. J. Hecht, *Beam Weapons*, New York, Plenum Press, 1984.

8. M. P. Cifuentes and M. G. Humphrey, "Alkynyl compounds and nonlinear optics," *Journal of Organometallic Chemistry* **689**, pp. 3969–3981, 2004.

9. W.-Y. Wong, "Luminescent organometallic poly(aryleneethylene)s: functional properties towards implications in molecular optoelectronics," *Dalton Transactions* (40), pp. 4495–4510, 2007.

10. E. Hecht, *Optics*, Addison Wesley, 4 ed., 2002.

11. R. E. Slusher, "Laser technology," *Reviews of Modern Physics* **71**, p. S471, 1999.

12. A. E. Siegman, *Lasers*, University Science Books, 1986.

13. J. T. Verdeyen, *Laser Electronics*, Prentice Hall, 2 ed., 1989.

14. M. Bertolotti, *Masers and Lasers*, Adam Higler, 1983.

15. A. L. Schawlow, "Lasers in historical perspective," *IEEE Journal of quantum electronics* **20**, pp. 558–561, 1984.

16. T. H. Maiman, "Stimulated optical radiation in ruby," *Nature* **187**, p. 493, 1960.

17. A. L. Schawlow and C. H. Townes, "Infrared and optical masers," *Physical Review* **112**, pp. 1940–1949, 1958.

18. J. L. Bromberg, "The birth of the laser," *Physics Today* **41**, pp. 26–33, 1988.

19. A. Javan, W. R. Bennett, and D. R. Herriott, "Population inversion and continuous optical maser oscillation in a gas discharge containing a He-Ne mixture," *Physical Review Letters* **6**, pp. 106–110, 1961.

20. R. W. Seidel, "How the military responded to the laser," *Physics Today* **41**, pp. 36–43, 1988.

21. J. Marshall, "Blinding laser weapons," *BMJ* **315**, p. 1392, 1997.

22. Y. Barkana and M. Belkin, "Laser eye injuries," *Survey of Ophthalmology* **44**, pp. 459–478, 2000.

23. G. E. Forden, "The airborn laser," *IEEE Spectrum* **34**, pp. 40–49, 1997.

24. R. J. Dunn, "Operational implications of laser weapons," *Northorp Grumman, Analysis Center Papers* , pp. 1–26, September 2005.

25. L. Doswald-Beck, "New protocol on blinding laser weapons," *Review of the Red Cross* **312**, pp. 272–299, 1996.

26. S. J. Hudson, "Eye injuries from laser exposure: A review," *Aviation, Space and Environmental Medicine* **69**, pp. 519–524, 1998.

27. R. L. Sutherland, *Handbook of Nonlinear Optics*, Marcel Dekker, Inc., 2nd ed., 2003. Revised and Expanded.

28. J. Staromlynska, T. J. McKay, and P. Wilson, "Broadband optical limiting based on excited state absorption in Pt:ethynyl," *Journal of Applied Physics* **88**, pp. 1726–1732, 2000.

29. I. D. Campbell and R. A. Dwek, *Biological Spectroscopy*, Benjamin/Cummings, Inc., 1984.

30. P. C. Hemmer, *Kvantemekanikk*, Tapir akademisk forlag, 2000.

31. M. Fox, *Quantum Optics*, Oxford University Press, 2006.

32. W. Heitler, *The Quantum Theory of Radiation*, Oxford, 3rd ed., 1957.

33. P. W. Atkins and R. S. Friedman, *Molecular Quantum Mechanics*, Oxford University Press, 1997.

34. E. Merzbacher, *Quantum Mechanics*, John Wiley & Sons, Inc., 1998.

35. J. B. Birks, *Photophysics of Aromatic Molecules*, Wiley-Interscience, 1970.

36. D. Rendell, *Fluorescence and Phosphorescence Spectroscopy*, John Wiley & Sons, 1987.

37. J. R. Lakowicz, *Principles of Fluorescence Spectroscopy*, Kluwer Academic/Plenum Publishers, 2nd ed., 1999.

38. M. Göppert, "Über die wahrscheinlichkeit des zusammenwirkens zweier lichtquanten in einem elemetarakt," *Naturwissenschaften* **17**, p. 932, 1929.

39. M. Göppert-Mayer, "Über elementarakte mit zwei quantensprüngen," *Annalen der Physik* **401**, pp. 273–294, 1931.

40. W. Kaiser and C. G. B. Garrett, "Two-photon excitation in CaF_2:Eu^{2+}," *Physical Review Letters* **7**, pp. 229–231, 1961.

41. P. A. Franken, A. E. Hill, C. W. Peters, and G. Weinreich, "Generation of optical harmonics," *Physical Review Letters* **7**, pp. 118–119, 1961.

42. S. H. Lin, Y. Fujimura, H. J. Neusser, and E. W. Schlag, *Multiphoton Spectroscopy of Molecules*, Academic Press, Inc., 1984.

43. C. Xu and W. W. Webb, *Multiphoton Excitation of Molecular Fluorophores and Nonlinear Laser Microscopy*, vol. 5 of *Topics in Fluorescence Spectroscopy*, ch. 11, pp. 471–537. Plenum Press, 1997. Ed. by: Joseph R. Lakowicz.

44. Y. R. Shen, *The Principles of Nonlinear Optics*, Wiley Interscience, 2003.

45. D. J. Griffiths, *Introduction to Electrodynamics*, Prentice Hall, 3rd ed., 1999.

46. C. R. Giuliano and L. D. Hess, "Nonlinear absorption of light: Optical saturation of electronic transitions in organic molecules with high intensity laser radiation," *IEEE Journal of Quantum Electronics* **QE-3**, pp. 358–369, 1967.

47. I. R. Whittall, A. M. McDonagh, M. G. Humphrey, and M. Samoc, "Organometallic complexes in nonlinear optics II: Third-order nonlinearities and optical limiting studies," *Advances in Organometallic Chemistry* **43**, pp. 349–405, 1999.

48. H. S. Nalwa, "Organometallic materials for nonlinear optics," *Applied Organometallic Chemistry* **5**, pp. 349–377, 1991.

49. I. R. Whittall, A. M. McDonagh, M. G. Humphrey, and M. Samoc, "Organometallic complexes in nonlinear optics I: Second-order nonlinearities," *Advances in Organometallic Chemistry* **42**, pp. 291–362, 1998.

50. D. S. Chemla and J. Zyss, *Nonlinear Optical Properties of Organic Molecules and Crystals*, Academic Press, Inc., 1987.

51. A. Vlček Jr., "The life and times of excited states of organometallic and coordination compounds," *Coordination Chemistry Reviews* **200-202**, pp. 933–977, 2000.

52. M. Thompson, "The evolution of organometallic complexes in organic light-emitting devices," *MRS Bulletin* **32**, pp. 694–701, 2007.

53. R. P. Kingsborough and T. M. Swager, *Transition metals in polymeric π-conjuagted organic framework*, vol. 48 of *Progress in Inorganic Chemistry*, pp. 123–231. John Wiley & Sons Inc., 1999. Ed. by Kenneth D. Karlin.

54. D. Riehl, N. Izard, L. Vivien, E. Anglaret, E. Doris, C. Ménard, M. Mioskowski, L. Porrès, O. Mongin, M. Charlot, M. Blanchard-Desce, R. Anémian, J. Mulatier, C. Barsu, and C. Andraud, "Broadband optical limiting optimisation by combination of carbon nanotubes and two-photon absorbing chromophores in liquids," *Proceedings of SPIE* **5211**, pp. 124–134, 2003.

55. N. Venkatram and D. N. Rao, "Nonlinear absorption, scattering an optical limiting studies of CdS nanoparticles," *Optics Express* **13**, pp. 867–872, 2005.

56. M. Cha, N. S. Sariciftci, A. J. Heeger, and J. C. Hummelen, "Enhanced nonlinear absorption and optical limiting in semiconducting polymer/metallofullerene charge transfer films," *Applied Physics Letters* **67**, pp. 3850–3852, 1995.

57. J. Hua, W. Yang, Y. Zhu, Z. Guo, H. Yang, L. Xu, and D. Chen, "Optical-limiting effect of C_{60} bonded poly(*N*-vinylcarbazole) initiated with $C_{60}Cl_n$/CuCl/Bpy catalyst system," *Materials Letters* **59**, pp. 644–647, 2004.

58. S. R. Mishra, H. S. Rawat, and M. Laghate, "Nonlinear absorption and optical limiting in metalloporphyrins," *Optics Communications* **147**, pp. 328–332, 1998.

59. P. P. Kiran, D. R. Reddy, B. G. Maiya, A. K. Dharmadhikari, G. R. Kumar, and N. R. Desai, "Enhanced optical limiting and nonlinear absorption properties of azoarene-appended phosphorus (V) tetratolylporphyrins," *Applied Optics* **41**, pp. 7631–7636, 2002.

60. K. Sendhil, C. Vijayan, and M. P. Kothiyal, "Low-treshold optical power limiting of cw laser illumination based on nonlinear refraction in zinc tetraphenyl porphyrin," *Optics & Laser Technology* **38**, pp. 512–515, 2005.

61. T. Ceyhan, M. Yüksek, H. G. Yaglioglu, B. Salih, M. K. Erbil, A. Elmali, and Ö. Bekaroglu, "Synthesis, characterization and nonlinear absorption of novel octakis-POSS substituted metallophthalocyanines and strong optical limiting of CuPc," *Dalton Transactions* (18), pp. 2407–2113, 2008.

62. P. Wang, S. Zhang, P. Wu, C. Ye, H. Liu, and F. Xi, "Optical limiting properties of optically active phthalocyanine derivatives," *Chemical Physics Letters* **340**, pp. 261–266, 2001.

63. C. Desroches, C. Lopes, V. Kessler, and S. Parola, "Design and synthesis of multifunctional thiacalixarenes and related metal derivatives for the preparation of sol-gel hybrid materials with non-linear optical properties," *Dalton Transactions* (10), pp. 2085–2092, 2003.

64. C. Desroches, S. Parola, F. Vocanson, N. Ehlinger, P. Miele, R. Lamartine, J. Bouix, A. Eriksson, M. Lindgren, and C. Lopes, "Synthesis, characterization and optical power limiting behaviour of phenylazo- and 4-nitrophenylazo-tetrahydroxytetrathiacalix[4]arene," *Journal of Materials Chemistry* **11**, pp. 3014–3017, 2001.

65. N. Chawdhury, A. Köhler, R. H. Friend, M. Younus, N. J. Long, P. R. Raithby, and J. Lewis, "Synthesis and electronic structure of platinum-containing poly-ynes with aromatic and heteroaromatic rings," *Macromolecules* **31**, pp. 722–727, 1998.

66. L. W. Tutt and T. F. Boggess, "A review of optical limiting mechanisms and devices using organics, fullerenes, semiconductors and other materials," *Progress in Quantum Electronics* **17**, pp. 299–338, 1993.

67. C. W. Spangler, "Recent development in the design of organic materials for optical power limiting," *Journal of Materials Chemistry* **9**, pp. 2013–2020, 1999.

68. R. C. Hollins, "Materials for optical limiters," *Current Opinion in Solid State and Materials Science* **4**, pp. 189–196, 1999.

69. C. E. Powell and M. G. Humphrey, "Nonlinear optical properties of transition metal acetylides and their derivatives," *Coordination Chemistry Reviews* **248**, pp. 725–756, 2004.

70. A. S. Abd-El-Aziz, "Organometallic polymers of the transition metals," *Macromolecular Rapid Communication* **23**, pp. 995–1031, 2002.

71. G.-J. Zhou, W.-Y. Wong, Z. Lin, and C. Ye, "White metallopolyynes for optical limiting/transparency trade-off optimization," *Angewandte Chemie Int. Ed.* **45**, pp. 6189–6193, 2006.

72. K. Sonogashira, Y. Fujikura, T. Yatake, N. Toyoshima, S. Takahashi, and N. Hagihara, "Syntheses and properties of cis- and trans-dialkynyl complexes of platinum(II)," *Journal of Organometallic Chemistry* **145**, pp. 101–108, 1978.

73. H. Masai, K. Sonogashira, and N. Hagihara, "Electronic spectra of square-planar bis-(tertiary phosphine)dialkynyl complexes of Nickel(II), Palladium(II) and Platinum(II)," *Bulletin of the Chemical Society of Japan* **44**, pp. 2226–2230, 1971.

74. B. Minaev, E. Jansson, and M. Lindgren, "Application of density functional theory for studies of excited states and phosphorescence of platinum(II) acetylides," *The Journal of Chemical Physics* **125**, p. 094306, 2006.

75. J. Staromlynska, T. J. McKay, J. A. Bolger, and J. R. Davy, "Evidence for broadband optical limiting in a Pt:ethynyl compound," *Journal of the Optical Society of America B* **15**, pp. 1731–1736, 1998.

76. J. E. Rogers, T. M. Cooper, P. A. Fleitz, D. J. Glass, and D. G. McLean, "Photophysical characterization of a series of platinum(II)-containing phenyl-ethynyl oligomers," *Journal of Physical Chemistry A* **106**, pp. 10108–10115, 2002.

77. T. M. Cooper, D. M. Krein, A. R. Burke, D. G. McLean, J. E. Rogers, and J. E. Slagle, "Asymmetry in platinum acetylide complexes: Confinement of the triplet exciton to the lowest energy ligand," *Journal of Physical Chemistry A* **110**, pp. 13370–13378, 2006.

78. R. Vestberg, R. Westlund, A. Eriksson, C. Lopes, M. Carlsson, B. Eliasson, E. Glimsdal, M. Lindgren, and E. Malmström, "Dendron decorated platinum(II) acetylides for optical power limiting," *Macromolecules* **39**, pp. 2238–2246, 2006.

79. K. Glusac, M. E. Köse, H. Jiang, and K. S. Schanze, "Triplet excited state in platinum-acetylide oligomers: Triplet localization and effects of conformation," *Journal of Physical Chemistry B* **111**, pp. 929–940, 2007.

80. S. P. McGlynn, T. Azumi, and M. Kinoshita, *Molecular spectroscopy of the triplet state*, Prentice-Hall Inc., 1969.

81. D. S. McClure, "Spin-orbit interaction in aromatic molecules," *The Journal of Chemical Physics* **20**, pp. 682–686, 1952.

82. J. Staromlynska, P. B. Chapple, J. R. Davy, and T. J. McKay, "Platinum ethynyl compound for optical limiting," *Proceedings of SPIE* **2229**, pp. 59–66, 1994.

83. T. J. McKay, J. A. Bolger, J. Staromlynska, and J. R. Davy, "Linear and nonlinear optical properties of platinum-ethynyl," *Journal of Chemical Physics* **108**, pp. 5537–5541, 1998.

84. T. J. McKay, J. Staromlynska, P. Wilson, and J. R. Davy, "Nonlinear luminescence spectroscopy in a Pt:ethynyl compound," *Journal of Applied Physics* **85**, pp. 1337–1341, 1999.

85. T. J. McKay, J. Staromlynska, J. R. Davy, and J. A. Bolger, "Cross sections for excited state absorption in a Pt:ethynyl complex," *Journal of the Optical Society of America B* **18**, pp. 358–362, 2001.

86. S. Guha, K. Kang, P. Porter, J. F. Roach, D. E. Remy, F. J. Aranda, and D. V. G. L. N. Rao, "Third-order optical nonlinearities of metallotetrabenzoporphyrines and a platinum poly-yne," *Optics Letters* **17**, pp. 264–266, 1992.

87. A. Baev, P. Norman, J. Henriksson, and H. Ågren, "Theoretical simulations of clamping levels in optical power limiting," *Journal of Physical Chemistry B* **110**, pp. 20912–20916, 2006.

88. T. M. Cooper, D. G. McLean, and J. E. Rogers, "Molecular structure-spectroscopic property relationships in a series of transition metal-containing phenylacetylene oligomers," *Chemical Physics Letters* **349**, pp. 31–36, 2001.

89. T. M. Cooper, J.-P. Blaudeau, B. C. Hall, J. E. Rogers, D. G. McLean, Y. Liu, and J. P. Toscano, "The triplet state of a Platinum acetylide chromophore examined by time-resolved infrared spectroscopy and density functional theory," *Chemical Physics Letters* **400**, pp. 239–244, 2004.

90. J. E. Rogers, B. C. Hall, D. C. Hufnagle, J. E. Slagle, A. P. Ault, D. G. McLean, P. A. Fleitz, and T. M. Cooper, "Effect of platinum on the photophysical properties of a series of phenyl-ethynyl oligomers," *The Journal of Chemical Physics* **122**, p. 214708, 2005.

91. T. M. Cooper, D. M. Krein, A. R. Burke, D. G. McLean, J. E. Rogers, J. E. Slagle, and P. A. Fleitz, "Spectroscopic characterization of a series of platinum acetylide complexes having a localized triplet exciton," *Journal of Physical Chemistry A* **110**, pp. 4369–4375, 2006.

92. J. E. Slagle, T. M. Cooper, D. M. Krein, J. E. Rogers, D. G. McLean, and A. M. Urbas, "Triplet excimer formation in a platinum acetylide," *Chemical Physics Letters* **447**, pp. 65–68, 2007.

93. G. Ramakrishna, T. Goodson III, J. E. Rogers-Haley, T. M. Cooper, D. G. McLean, and A. Urbas, "Ultrafast intersystem crossing: Excited state dynamics of platinum acetylide complexes," *Journal of Physical Chemistry C* **113**, pp. 1060–1066, 2009.

94. Y. Liu, S. Jiang, K. Glusac, D. H. Powell, D. F. Anderson, and K. S. Schanze, "Photophysics of monodisperse platinum-acetylide oligomers: Delocalization in the singlet and triplet excited states," *Journal of the American Chemical Society* **124**, pp. 12412–12413, 2002.

95. E. E. Silverman, T. Cardolaccia, X. Zhao, K.-Y. Kim, K. Haskins-Glusac, and K. S. Schanze, "The triplet state in Pt-acetylide oligomers, polymers and copolymers," *Coordination Chemistry Reviews* **249**, pp. 1491–1500, 2005.

96. L. A. Emmert, W. Choi, J. A. Marshall, J. Yang, L. A. Mayer, and J. A. Brozik, "The excited state symmertry characteristics of platinum phenylacetylene compounds," *Journal of Physical Chemistry A* **107**, pp. 11340–11346, 2003.

97. E. R. Batista and R. L. Martin, "Exciton localization in a Pt-acetylide complex," *Journal of Physical Chemistry A* **109**, pp. 9856–9859, 2005.

98. T. M. Cooper, B. C. Hall, D. G. McLean, J. E. Rogers, A. R. Burke, K. Turnbull, A. Weisner, A. Fratini, Y. Liu, and K. S. Schanze, "Structure-optical property relationships in organometallic sydnones," *Journal of Physical Chemistry A* **109**, pp. 999–1007, 2005.

99. T. M. Cooper, B. C. Hall, A. R. Burke, J. E. Rogers, D. G. McLean, J. E. Slagle, and P. A. Fleitz, "Glass-forming liquid platinum acetylides," *Chemistry of Materials* **16**, pp. 3215–3217, 2004.

100. J. E. Rogers, J. E. Slagle, D. M. Krein, A. R. Burke, B. C. Hall, A. Fratini, D. G. McLean, P. A. Fleitz, T. M. Cooper, M. Drobizhev, N. S. Makarov, A. Rebane, K.-Y. Kim, R. Farley, and K. S. Schanze, "Platinum acetylide two-photon chromophores," *Inorganic Chemistry* **46**, pp. 6483–6494, 2007.

101. K. Haskins-Glusac, I. Ghiviriga, K. A. Abboud, and K. S. Schanze, "Photophysics and photochemistry of stilbene-containing platinum acetylides," *Journal of Physical Chemistry B* **108**, pp. 4969–4978, 2004.

102. R. Vestberg, *Dendron Decorated Chromophores for Optical Power Limiting Applications*. PhD thesis, Royal Institute of Technology, KTH, Stockholm, Sweden, 2004.

103. P. Lind, *Organic and Organometallic Compounds for Nonlinear Absorption of Light*. PhD thesis, Umeå University, Umeå, Sweden, 2007.

104. M. Carlsson, *Synthesis and Optical Characterization of Optical Power Limiting Platinum(II) Acetylides*. PhD thesis, Umeå University, Umeå, Sweden, 2007.

105. R. Westlund, *Nonlinear Absorpbing Platinum(II) Acetylides for Optical Power Limiting Applications*. PhD thesis, Royal Institute of Technology, KTH, Stockholm, Sweden, 2008.

106. R. Vestberg, E. Malmström, A. Eriksson, C. Lopes, and M. Lindgren, "Novel dendrimer-capped Pt-acetylides for optical power limiting," *Proceedings of SPIE* **5621**, pp. 31–45, 2004.

107. M. Lindgren, B. Minaev, E. Glimsdal, R. Vestberg, R. Westlund, and E. Malmström, "Electronic states and phosphorescence of dendron functionalized platinum(II) acetylides," *Journal of Luminescence* **124**, pp. 302–310, 2007.

108. R. Vestberg, A. Nyström, M. Lindgren, E. Malmström, and A. Hult, "Porphyrin-cored 2,2-bis(methylol)propionic acid dendrimers," *Chemistry of Materials* **16**, pp. 2794–2804, 2004.

109. R. Vestberg, C. Nilsson, C. Lopes, P. Lind, B. Eliasson, and E. Malmström, "Thiophene-cored 2,2-bis(methylol)propionic acid dendrimers for optical-power-limiting applications," *Journal of Polymer Science: Part A: Polymer Chemistry* **43**, pp. 1177–1187, 2005.

110. P. N. Prasad and B. A. Reinhardt, "Is there a role for organic materials chemistry in nonlinear optics and photonics?," *Chemistry of Materials* **2**, pp. 660–669, 1990.

111. P. Wu, A. K. Feldman, A. K. Nugent, C. J. Hawker, A. Scheel, B. Voit, J. Pyun, J. M. J. Fréchet, K. B. Sharpless, and V. V. Fokin, "Efficiency and fidelity in a click-chemistry route to triazole dendrimers by the copper(I)-catalyzed ligation of azides and alkynes," *Angewandte Chemie - Int. Ed.* **43**, pp. 3928–3932, 2004.

112. C. Schweitzer and R. Schmidt, "Physical mechanisms of generation and deactivation of singlet oxygen," *Chemical Reviews* **103**, pp. 1685–1757, 2003.

113. L. M. Bollinger and G. E. Thomas, "Measurement of the time dependence of scintillation intensity by a delayed-coincidence method," *The Review of Scientific Instruments* **32**, pp. 1044–1050, 1961.

114. M. B. Priestley, *Spectral Analysis and Time Series*, vol. 1, Academic Press, 1981.

115. D. J. S. Birch and R. E. Imhof, *Time-Domain Fluorescence Spectroscopy Using Time-Correlated Single Photon Counting*, vol. 1 of *Topics in Fluorescence Spectroscopy*, ch. 1. Kluwer Academic Publishers, 2002. Ed. by: Joseph R. Lakowicz.

116. D. F. Eaton, "Reference materials for fluorescence measurements," *Pure and Applied Chemistry* **60**, pp. 1107–1114, 1988.

117. J. N. Demas and G. A. Crosby, "The measurement of photoluminescence quantum yields," *Journal of Physical Chemistry* **75**, pp. 991–1024, 1971.

118. A. T. R. Williams, S. A. Winfield, and J. N. Miller, "Relative fluorescence quantum yields using a computer-controlled luminescence spectrometer," *Analyst* **108**, pp. 1067–1071, 1983.

119. "A guide to recording fluorescent quantum yields." HORIBA JobinYvon. http://www.jobinyvon.com/Fluorescence/Applications/Quantum-Yield.

120. C. Wohlfart and B. Wohlfart, *Optical Constants*, vol. 38 (Group III) of *Landolt-Börnstein: Numerical Data and Functional Relationships in Science and Technology*, Springer, 1996. Ed. by: M. D. Lechner.

121. W. H. Melhuish, "Quantum efficiencies for fluorescence of organic substances: Effect of solvent and concentration of the fluorescent solute," *Journal of Physical Chemistry* **65**, pp. 229–235, 1961.

122. W. R. Dawson and M. W. Windson, "Fluorescence yields of aromatic compounds," *Journal of Physical Chemistry* **72**, pp. 3251–3260, 1968.

123. D. Magde, R. Wong, and P. G. Seybold, "Fluorescence quantum yields and their relation to lifetime of Rhodamine 6G and Fluorescein in nine solvents: Improved absolute standards for quantum yields," *Photochemistry and Photobiology* **75**, pp. 327–334, 2002.

124. G. L. Squires, *Practical Physics*, Cambridge University Press, 4th ed., 2001.

125. G. Porter, "Flash photolysis and spectroscopy. A new method for the study of free radical reactions," *Proceedings of the Royal Society of London A* **200**, pp. 284–300, 1950.

126. T. B. Melø, M. A. Ionescu, G. W. Haggquist, and K. R. Naqvi, "Hydrogen abstraction by triplet flavins. I: time-resolved multi-channel absorption spectra of flash-irradiated riboflavin solutions in water," *Spectrochimica Acta Part A* **55**, pp. 2299–2307, 1999.

127. J. Robertson, P. Milsom, J. Duignan, and G. Bourhill, "Spatial redistribution of energy in a nanosecond lases pulse by an organic optical limiter," *Opticsl Letters* **25**, pp. 1258–1260, 2000.

128. M. A. Albota, C. Xu, and W. W. Webb, "Two-photon fluorescence excitation cross sections of biomolecular probes from 690 to 960 nm," *Applied Optics* **37**, pp. 7352–7356, 1998.

129. M. Sheik-Bahae, A. A. Said, and E. W. V. Stryland, "High-sensitivity, single-beam n_2 measurements," *Optics Letters* **14**, pp. 955–957, 1989.

130. M. Sheik-Bahae, A. A. Said, T. Wei, D. J. Hagan, and E. W. V. Stryland, "Sensitive measurements of optical nonlinearities using a single beam," *IEEE Journal of Quantum Electronics* **26**, pp. 760–769, 1990.

131. W. Zhao and P. Palffy-Muhoray, "Z-scan technique using top-hat beams," *Applied Physics Letters* **63**, pp. 1613–1615, 1993.

132. A. Eriksson, M. Lindgren, S. Svenson, and P.-O. Arntsen, "Numerical analysis of z-scan experiments by use of a mode expansion," *Journal of the Optical Society of America B* **15**, pp. 810–816, 1998.

133. A. Eriksson, M. Lindgren, S. Svenson, and P.-O. Arntsen, "Complex optical limiting devices based on the z-scan technique: modeling using a numerical expansion," *Optical Materials* **9**, pp. 342–346, 1998.

134. A. Eriksson, M. Lindgren, S. Svenson, T. Baubner, T. McKay, and J. Staromlynska, "Numerical modeling of z-scans of thick nonlinear absorbers," *Proceedings of SPIE* **3472**, pp. 144–150, 1998.

135. J. A. Hermann, "Nonlinear optical absorption in thick media," *Journal of the Optical Society of America B* **14**, pp. 814–823, 1997.

136. J. A. Hermann, T. Baubner, T. J. McKay, P. J. Wilson, J. Staromlynska, A. Eriksson, M. Lindgren, and S. Svensson, "Optical limiting capability of thick nonlinear absorbers," *Journal of Nonlinear Optical Physysics & Materials* **8**, pp. 235–275, 1999.

137. C. Xu and W. W. Webb, "Measurement of two-photon excitation cross sections of molecular fluorophores with data from 690 to 1050 nm," *Journal of the Optical Society of America B* **13**, pp. 481–491, 1996.

138. P. G. Seybold, M. Gouterman, and J. Callis, "Calorimetric, photometric and lifetime determinations of fluorescence yields of fluorescein dyes," *Photochemistry and Photobiology* **9**, pp. 229–242, 1969.

139. N. S. Makarov, M. Drobizhev, and A. Rebane, "Two-photon absorption standards in the 550-1600 nm excitation wavelength range," *Optics Express* **16**, pp. 4029–4047, 2008.

140. D. A. Oulianov, I. V. Tomov, A. S. Dvornikov, and P. M. Rentzepis, "Observations of the measurement of two-photon absorption cross-section," *Optics Communications* **191**, pp. 235–243, 2001.

141. P. Norman, P. Cronstrand, and J. Ericsson, "Theoretical study of linear and nonlinear absorption in platinum-organic compounds," *Chemical Physics* **285**, pp. 207–220, 2002.

142. T. Wismontski-Knittel and P. K. Das, "Laser flash photolysis study of (2-anthryl)ethylenes. Triplet-related photophysical behaviors," *Journal of Physical Chemistry* **88**, pp. 1168–1173, 1984.

143. H. Du, R.-C. A. Fuh, J. Li, L. A. Corkan, and J. S. Lindsey, "Photochemcad: A computer-aided design and research tool in photochemistry," *Photochemistry and photobiology* **68**, pp. 141–142, 1998.

144. A. Eriksson, K. Bertilsson, and M. Lindgren, "Simulations of beam propagation with time-dependent nonlinear processes in optical limiting applications," *Synthetic Metals* **127**, pp. 147–150, 2002.

145. G. S. He, L.-S. Tan, Q. Zheng, and P. N. Prasad, "Miltiphoton absorbing materials: Molecular designs, characterizations, and applications," *Chemical Reviews* **108**, pp. 1245–1330, 2008.

146. S. Chakrabarti and K. Ruud, "Large two-photon absorption cross section: molecular tweezer as a new promising class of compounds for nonlinear optics," *Physical Chemistry Chemical Physics* **11**, pp. 2592–2596, 2009.

147. A. Baev, O. Rubio-Pons, F. Gel'mukhanov, and H. Ågren, "Optical limiting properties of zinc- and platinum-based organometallic compounds," *Journal of Physical Chemistry A* **108**, pp. 7406–7416, 2004.

148. A. Baev, P. Welinder, R. Erlandsson, J. Henriksson, P. Norman, and H. Ågren, "A quantum mechanical – electrodynamical approach to nonlinear properties: Application to optical power limiting with platinum-organic compounds," *Journal of Nonlinear Optical Physics & Materials* **16**, pp. 157–169, 2007.

Paper I

Excited states and two-photon absorption of some novel thiophenyl Pt(II)-ethynyl derivatives

Eirik Glimsdal, Marcus Carlsson, Bertil Eliasson,
Boris Minaev and Mikael Lindgren

Journal of Physical Chemistry A 111, p. 244-250, 2007

Is not included due to copyright

Paper II

Luminescence, singlet oxygen production and optical power limiting of some novel diacetylide platinum(II) diphosphine complexes

Eirik Glimsdal, Marcus Carlsson, Tomas Kindahl, Mikael Lindgren, Cesar Lopes and Bertil Eliasson

Manuscript submitted for publication in *Physical Chemistry Chemical Physics*, June 2009.

Is not included due to copyright

Paper III

Click chemistry for photonic applications: triazole-functionalized platinum(II) acetylides for optical power limiting

Robert Westlund, Eirik Glimsdal, Mikael Lindgren, Robert Vestberg, Craig Hawker, Cesar Lopes and Eva Malmström

Journal of Materials Chemistry 18, p. 166-175, 2008

Is not included due to copyright

Paper IV

Triplet excited states of some thiophene and triazole substituted platinum(II) acetylide chromophores

Eirik Glimsdal, Ingunn Dragland, Marcus Carlsson,
Bertil Eliasson, Thor Bernt Melø and Mikael Lindgren

Journal of Physical Chemistry A 113, p. 3311-3320, 2009

Is not included due to copyright

Paper V

Excitation and emission properties of platinum(II) acetylides at high and low concentrations

Eirik Glimsdal, Patrick Norman and Mikael Lindgren

Manuscript submitted for publication in
Journal of Physical Chemistry A, June 2009.

Is not included due to copyright

Paper VI

Two-photon absorption cross-section and quantum efficiency of molecular fluorophores for spectroscopic reference purposes

Eirik Glimsdal and Mikael Lindgren

Manuscript.

Two-photon absorption cross-section and quantum efficiency of molecular fluorophores for spectroscopic reference purposes

Eirik Glimsdal* and Mikael Lindgren
Department of Physics, Norwegian University of Science and Technology (NTNU), NO-7491 Trondheim, Norway

A series of highly fluorescent molecules were characterized for the use as reference compounds in quantum efficiency and two-photon absorption (TPA) cross-section measurements from two-photon excited fluorescence. Three commercial coumarin fluorophores, Coumarin 110, Coumarin 314 and Coumarin 334, were chosen to cover the wavelength region between the well known fluorescence quantum yield standards Fluorescein Sodium Salt and Quinine Sulfate. All coumarins show high quantum efficiency (QE), with values from 0.62 to 0.93, and useful TPA cross-section typically from 5 to 75 GM in the wavelength range between 700 to 860 nm. [1 GM = 10^{-50} cm^4 s/photon.] In addition to QE and TPA cross sections, the absorption and emission spectra and fluorescence decay times, are presented.

I. INTRODUCTION

During the last decades the nonlinear optical properties of materials have found an increasing amount of interest for several laser based applications. In particular, the two-photon absorption (TPA) process is utilized in for instance fluorescence microscopy and spectroscopy,[1,2] optical power limiting,[3,4] singlet oxygen production in photo-dynamic therapy,[5,6] two-photon light harvesting,[7] and many other.

In the process of characterizing new chromophores for their two-photon absorption properties it is an advantage to utilize the two-photon excited fluorescence technique, due to the difficulties of absolute determination of the TPA cross-section.[8,9] In such a measurement, both the TPA cross-section and the fluorescence quantum efficiency (QE) of the reference compound need to be known.[9] In addition, it is desirable for the reference and unknown sample to have overlapping absorption bands for the quantum efficiency determination. Therefore, there is a need for well characterized molecules with known TPA cross-section and quantum efficiency.

Several chromophores have been studied for their two-photon absorption properties by e.g. Xu and Webb,[9] Albota,[10] and Makarov.[8] Here, we report on the quantum efficiency and TPA cross-section of three commercial Coumarin fluorophores in tetrahydrofuran (THF) and ethanol solution, suitable for TPA characterization using the indirect fluorescence technique. The chromophores are Coumarin 110 (abbreviated C110), Coumarin 314 (C314) and Coumarin 334 (C334). Molecular structures of the chromophores are shown in Figure 1. Fluorescein Sodium Salt (Fluor) and Quinine Sulfate (QS) were used as QE references, and Fluorescein was used as the TPA reference in the measurements.

II. METHODS

All samples were purchased from Sigma Aldrich. Fluorescein sodium salt was dissolved in 0.1 M NaOH in water (pH13), Quinine Sulfate was dissolved in 0.5M H_2SO_4, and all Coumarins were dissolved in tetrahydrofuran (THF). C314 was also dissolved in pure ethanol solution (C314E).

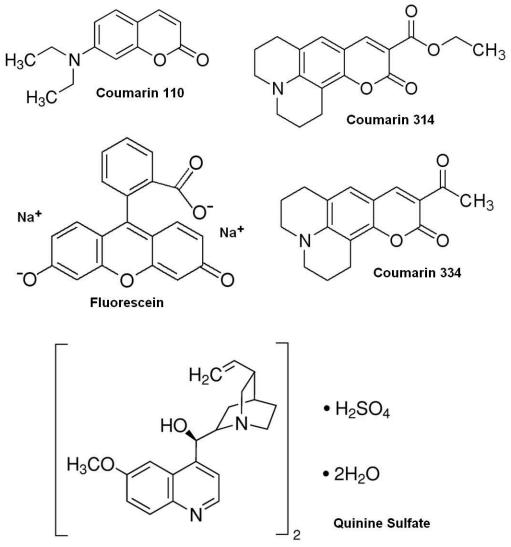

FIG. 1: Structural formula of the studied chromophores.

Measurements of steady state optical absorption spectra were recorded for 10 μM solutions using an Agilent 8456E UV-vis spectroscopic system. Luminescence and time-resolved measurements were performed on a Jobin Yvon IBH FluoroCube photon-counting spectrometer. A 200 fs pulsed Ti:Sapphire laser (Coherent MIRA 900-F) was used as radiation source. The experimental setup is shown in Figure 2. For two-photon excitation measurements the laser was tuned in the $700 - 860$ nm range, and taken out before the SHG unit. For single photon excitations the laser beam was frequency doubled using a SHG crystal (Inrad Ultrafast Harmonic Generation System, Model 5-050). A pulse picker (Coherent 9200) is placed after the laser (76 MHz) to control the pulse rep-

etition frequency (prf). This is especially important if long lived excited states are present.[4] For the measurements reported here 4.75 MHz prf was found appropriate.

Fluorescence decay times were measured in time-correlated single photon counting (TC-SPC) mode, with a time resolution down to 0.014 ns. An optical trigger (IBH TB-01) was used as time-reference using a thin glass wedge to take out a small part of the fundamental. Emission spectra were recorded by scanning the monochromator in front of the PMT. Fluorescence quantum yields were calculated from absorption and fluorescence measurements at five different concentrations with peak absorbance below 0.1 OD. The absorbance at the excitation wavelength and the spectrally corrected integrated fluorescence is collected at each concentration. The relative quantum yield of two samples is then calculated from the equation given by Williams et al.[11] Using a reference sample with known quantum yield, the absolute quantum efficiency of the new sample is determined.

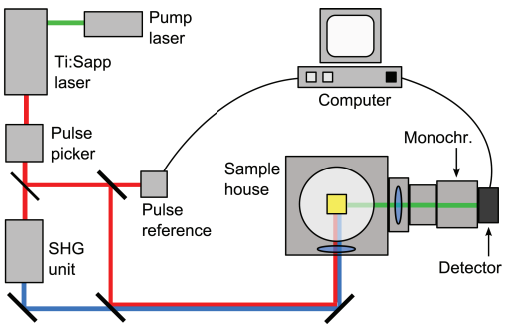

FIG. 2: Experimental setup for the luminescence measurements.

TABLE I: Absorption (λ_{max}) and emission maximum (λ_{em}), extinction coefficient (ϵ), fluorescence emission lifetime (τ) and fluorescence quantum efficiency (Φ) for all chromophores.

Sample	λ_{max}(nm)	λ_{em}(nm)	ϵ (10^4 $M^{-1}cm^{-1}$)	τ(ns)	Φ
Fluor	490	514	8.8[a]	4.2	0.92[b]
QS	347	442	5.5	19.5	0.55[c]
C110	370	423	2.4	2.9	0.62
C334	444	476	3.6	3.0	0.83
C314	427	458	3.5	2.8	0.93
C314E	437	474	4.5[d]	3.3	0.85

[a]References Demas[12] and Seybold.[13]
[b]References Demas,[12] Dawson[14] and Magde.[15]
[c]References Demas[12] and Melhuish.[16]
[d]References Reynolds[17] and Fletcher.[18]

The two-photon absorption (TPA) cross-section can be found from two-photon excitation induced fluorescence as outlined by Xu and Webb.[9] The relative amount of fluorescence collected by two-photon excitation of 50 μM samples were collected. The relative TPA cross section

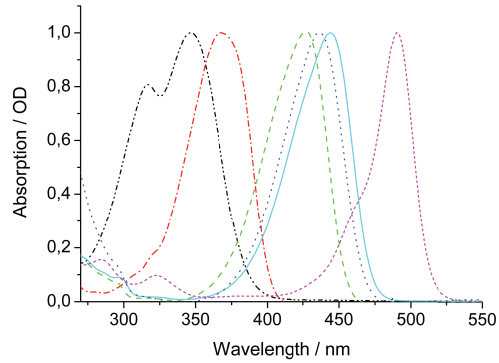

FIG. 3: Absorption spectrum of QS (black dash dot dot), C110 (red dash dot), C314 (green dash), C314E (blue dot), C334 (cyan solid line) and Fluor (magenta short dash).

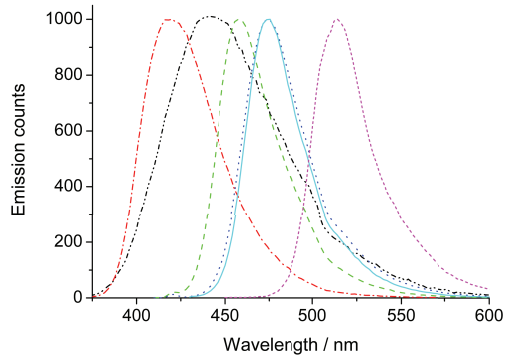

FIG. 4: Emission spectrum of QS (black dash dot dot), C110 (red dash dot), C314 (green dash), C314E (blue dot), C334 (cyan solid line) and Fluor (magenta short dash).

can be found when the quantum efficiency of both samples are known, and other experimental parameters either are determined, or identical. Albota et al.[10] derived expressions suitable for numerical calculation. Utilizing one sample with known quantum efficiency and TPA cross section, the absolute value of the cross section for the new sample is calculated. Fluorescein was used as reference material due to its high quantum yield and suitable TPA cross section, as previously determined.[10]

III. RESULTS AND DISCUSSIONS

The absorption spectrum of all chromophores are shown in Figure 3, covering the $300-500$ nm region. The corresponding emission spectra, exciting close to the absorption peak, are shown in Figure 4. Numerical values of absorption maximum (λ_{max}), extinction coefficient at absorption maximum (ϵ), emission maximum (λ_{em}), and

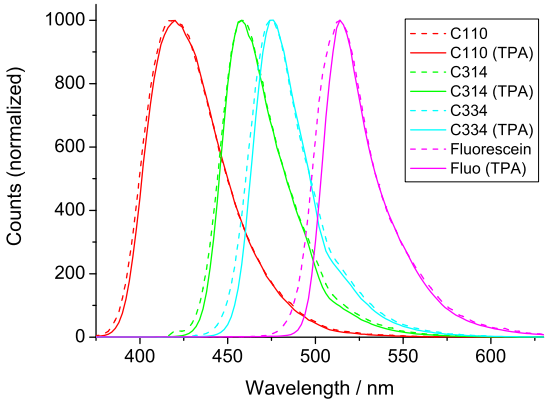

FIG. 5: One-photon excited (dashed) and two-photon excited (solid) fluorescence emission spectra of C110 (red), C314 (green), C334 (cyan) and Fluorescein (magenta).

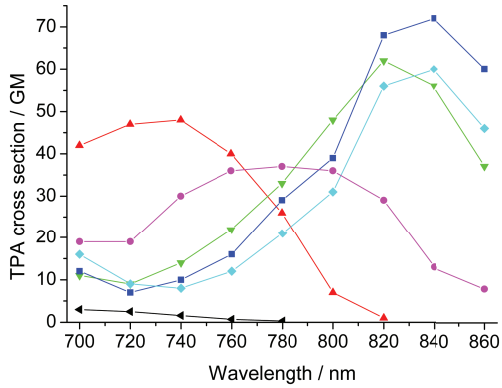

FIG. 6: Two-photon absorption cross section of Fluorescein[10] (magenta circles), C110 (red triangles up), C314 (green triangles down), C314E (blue squares), C334 (cyan diamonds) and QS (black triangles left).

TABLE II: Two-photon absorption cross section of Fluorescein,[10] C110, C334, C314 and C314E and Quinine Sulfate at 700 − 860 nm. TPA cross sections are given in GM units. [1 GM = 10^{-50} cm^4 s/photon.]

Wavelength	Fluor	C110	C334	C314	C314E	QS
700 nm	19	42	16	11	12	3
720 nm	19	47	9	9	7	2.5
740 nm	30	48	8	14	10	1.5
760 nm	36	40	12	22	16	<1
780 nm	37	26	21	33	29	<0.1
800 nm	36	7	31	48	39	–
820 nm	29	1	56	62	68	–
840 nm	13	<1	60	56	72	–
860 nm	8	–	46	37	60	–

fluorescence quantum efficiency (Φ) for all compounds are collected in Table I. Fluorescence emission lifetimes (τ) of all chromophores were also measured, and the numerical values are given in Table I.

The two-photon induced fluorescence emission spectra were also collected with excitation between 700 and 860 nm. The two-photon excited emission spectra of all samples were found to be essentially identical as the ones emitted upon one-photon excitation, except for small distortions in the two-photon emission spectra on the short wavelength side, due to the higher concentrated samples and the small overlap with the absorption band. This is shown in Figure 5. Moreover, the measured emission decay time was the same for one- and the corresponding two-photon excitation. Hence, we conclude that the emission occur from the same excited state in the molecules, independent of excitation method. Measured TPA cross-sections of the coumarins are given in Table II. The TPA cross-sections are also plotted in Figure 6 as a function of wavelength. Quinine Sulfate was found to have low TPA cross-section, and is not suitable as a TPA reference chromophore in this wavelength region.

An important issue concerning TPA excitation is that it were found to follow the power-square dependence, as expected for an instantaneous two-photon processes. The integrated fluorescence intensity as a function of the pulse energy of the pump beam is plotted in Figure 7 for some of the molecules. For all samples a liner fit of the log-log plot was found to give a slope varying from 1.98 to 2.01 ± 10%. The uncertainty in the TPA cross-sections of the Fluorescein reference is 25%, as determined by Xu and Webb.[9] The total uncertainty of our determined TPA cross-sections is then approximately 30%, taking an uncertainty of 10% in the quantum yields and 5% for the integrated fluorescence counts.

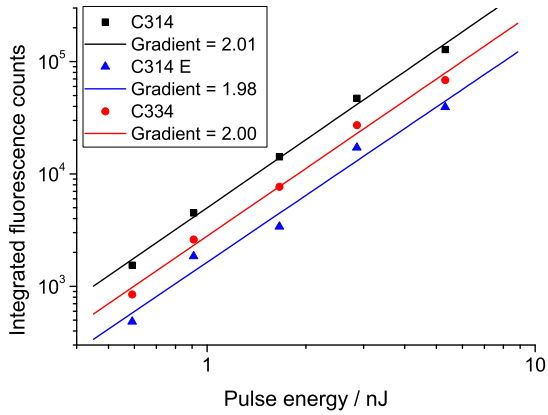

FIG. 7: Log-log plot of integrated fluorescence counts versus input pulse power for C314, C314E and C334.

IV. CONCLUSIONS

Fluorescein Sodium Salt and Quinine Sulfate are well known standards for quantum efficiency measurements, with high emission yield. Fluorescein is also a suitable reference for two-photon excited fluorescence. The fluorophores Coumarin 110, 334 and 314 in THF (and ethanol) solutions were characterized and found to be suitable compounds as reference materials when measuring the quantum efficiency in the $330-460$ nm region, and two-photon absorption cross-section in the $700-860$ nm region, using the relative fluorescence techniques. Useful TPA cross-sections were found to be in the range of 5 to 75 GM, with fluorescence quantum efficiencies ranging from 0.62 to 0.93.

* eirik.glimsdal@ntnu.no

[1] W. R. Zipfel, R. M. Williams, and W. W. Webb, Nature biotech. **21**, 1369 (2003).

[2] F. Stabo-Eeg, M. Lindgren, K. P. R. Nilsson, O. Inganäs, and P. Hammarström, Chem. Phys. **336**, 121 (2007).

[3] C. W. Spangler, J. Mater. Chem. **9**, 2013 (1999).

[4] E. Glimsdal, M. Carlsson, B. Eliasson, B. Minaev, and M. Lindgren, J. Phys. Chem. A **111**, 244 (2007).

[5] P. K. Frederiksen, S. P. McIlroy, C. B. Nielsen, L. Nikolajsen, E. Skovsen, M. Jørgensen, K. V. Mikkelsen, and P. R. Ogilby, J. Am. Chem. Soc **127**, 255 (2005).

[6] S. P. McIlroy, E. Cló, L. Nikolajsen, P. K. Frederiksen, C. B. Nielsen, K. V. Mikkelsen, K. V. Gothelf, and P. R. Ogilby, J. Org. Chem. **70**, 1134 (2005).

[7] A. Picot, F. Malvolti, B. Le Guennic, P. L. Baldeck, J. A. G. Williams, C. Andraud, and O. Maury, Inorg. Chem. **46**, 2659 (2007).

[8] N. S. Makarov, M. Drobizhev, and A. Rebane, Opt. Express **16**, 4029 (2008).

[9] C. Xu and W. W. Webb, J. Opt. Soc. Am. B **13**, 481 (1996).

[10] M. A. Albota, C. Xu, and W. W. Webb, Appl. Opt. **37**, 7352 (1998).

[11] A. T. R. Williams, S. A. Winfield, and J. N. Miller, Analyst **108**, 1067 (1983).

[12] J. N. Demas and G. A. Crosby, J. Phys. Chem. **75**, 991 (1971).

[13] P. G. Seybold, M. Gouterman, and J. Callis, Photochem. and Photobiol. **9**, 229 (1969).

[14] W. R. Dawson and M. W. Windson, J. Phys. Chem. **72**, 3251 (1968).

[15] D. Magde, R. Wong, and P. G. Seybold, Photochem. and Photobiol. **75**, 327 (2002).

[16] W. H. Melhuish, J. Phys. Chem. **65**, 229 (1961).

[17] G. A. Reynolds and K. H. Drexhage, Opt. Commun. **13**, 222 (1975).

[18] A. N. Fletcher and D. E. Bliss, Appl. Phys. **16**, 289 (1978).